Multi-Area Architecture for Real-Time Feedback-Based Optimization of Distribution Grids

by

Ilyas Farhat

A thesis
presented to the University of Waterloo
in fulfillment of the
thesis requirement for the degree of
Doctor of Philosophy
in
Electrical and Computer Engineering

Waterloo, Ontario, Canada, 2024

Examining Committee Membership

The following served on the Examining Committee for this thesis. The decision of the Examining Committee is by majority vote.

External Examiner: Emiliano Dall'Anese
                              Professor,
                              Dept. of Electrical, Computer, and Energy Engineering
                              University of Colorado Boulder

Supervisor: John W. Simpson-Porco
                              Professor,
                              Dept. of Electrical and Computer Engineering,
                              University of Toronto

Internal Member: Kankar Bhattacharya
                              Professor
                              Dept. of Electrical and Computer Engineering,
                              University of Waterloo

Internal Member: Mehrdad Kazerani
                              Professor,
                              Dept. of Electrical and Computer Engineering,
                              University of Waterloo

Internal-External Member: Mehrdad Pirnia
                              Professor,
                              Dept. of Management Science and Engineering,
                              University of Waterloo

Author's Declaration

I hereby declare that I am the sole author of this thesis. This is a true copy of the thesis, including any required final revisions, as accepted by my examiners.

I understand that my thesis may be made electronically available to the public.

Abstract

The transition to a more environmentally-friendly power system, predominantly driven by Distributed Energy Resources (DERs) such as smart loads, Electric Vehicles (EVs), and Photovoltaics (PVs) systems, signals a shift towards a new structural paradigm. Significant challenges have emerged as more DERs, particularly those interfaced through inverters, are integrated into the grid. These challenges include variability in power supply and reduced rotational inertia, which contribute to more frequent frequency events and grid instabilities globally. Despite these challenges, DERs offer potential solutions by participating in ancillary service provision.

This thesis aims to harness the potential of DERs at the distribution network (DN) as their integration increases. We focus on overcoming coordination challenges between distribution and transmission networks to integrate DN-DERs in frequency support. To achieve this goal, we develop a coordination framework for distribution networks to manage the DERs. Subsequently, we integrate this DN framework with a recently proposed fast frequency control scheme at the transmission network (TN) level.

In the first stage, we develop a hierarchical feedback-based control architecture for DN-DER coordination. This architecture enables DNs to swiftly respond to power set-point requests from the Transmission System Operator (TSO) while adhering to local operational constraints and ensuring data privacy. The scheme minimizes inter-area communication needs by leveraging physically adjacent areas within the DN control hierarchy. Rigorous stability analysis establishes intuitive closed-loop stability conditions, accompanied by detailed tuning recommendations. Case studies on multiple feeders, including IEEE-123 and IEEE-8500, validate the architecture using a custom MATLAB®-based application integrated with OpenDSS©. Results demonstrate scalability and effective coordination of DERs in response to TSO commands while managing local DN disturbances and operational limits.

In the second stage, we integrate the developed DN control framework into a TN fast frequency control scheme by incorporating a simplified linear model of DN dynamics into the TN control design framework. This integrated approach aims to enhance system responsiveness and performance. To validate this approach, we conducted case studies using the IEEE 9-bus TN system, incorporating IEEE-123 DNs structured according to the hierarchical control framework developed in stage 1. The TN controller, designed with the integrated DN dynamic model, demonstrated improved performance across various DN feeder configurations and tuning scenarios.

Combining these stages yields a comprehensive solution that enhances overall system stability and performance. By optimally utilizing DN-DERs to respond to the TN controller,

which is designed with awareness of DN-DERs dynamics, the integrated solution resulted in improved response times and reduced oscillations.

Acknowledgments

I would like to express my sincere gratitude to my supervisor, Professor John Simpson-Porco, for his invaluable guidance, support, and encouragement throughout my doctoral journey. His expertise and insightful feedback have been instrumental in shaping this thesis.

I am deeply thankful to my PhD committee members:

Professor Emiliano Dall'Anese from Boston University, whose constructive feedback has greatly enriched this work. Professor Mehrdad Kazerani, Professor Kankar Bhattacharya and Professor Mehrdad Pirnia from the University of Waterloo for their thoughtful guidance and scholarly insights.

To my beloved wife, Sara, thank you for your unwavering support, patience, and encouragement throughout this challenging endeavor. Your belief in me has been a constant source of strength.

To my beloved kids, Omar and Joury, your love and joy have kept me motivated every day. You mean the world to me.

I extend my heartfelt appreciation to my parents, Abdul-Hafiz and Subhiah, for their unconditional love, sacrifices, prayers, and unwavering belief in my aspirations.

I am grateful to my siblings, Salman, Hajar, Haroun, Omran, Aalaa, and Ali, for their support and encouragement throughout my academic journey.

Special thanks to my parents-in-law, Bashir and Sawsan, and their family for their support and encouragement.

I would also like to acknowledge the support of my friends and relatives, including Abdul-Bary Farhat, Hassan Qazi, Etinosa Ekomwenrenren, and others who have supported me along the way.

Their unwavering support and encouragement have made this journey possible.

Dedication

to my beloved parents,
Abdul-Hafiz Farhat and Subhiah Farhat

to my beloved wife,
Sara Timraz

to my adorable kids,
Omar and Joury

to my brothers and sisters,
Salman, Hajar, Haroun, Omran, Aalaa, and Ali

Table of Contents

List of Figures

List of Tables

List of Acronyms

ADMM Alternating Direction Method of Multipliers

ADN Active Distribution Network

ADPMs Adaptive Dynamic Participation Matrices

BESS Battery Energy Storage System

CA Control Area

DER Distributed Energy Resource

DERMS Distributed Energy Resource Management System

DMS Distribution Management System

DN Distribution Network

DOPF Distribution Optimal Power Flow

DSO Distribution System Operator

DVPP Dynamic Virtual Power Plant

EV Electric Vehicle

FFC Fast Frequency Control

GNE Generalized Nash Equilibrium

IBR Inverter-Based Resource

ICT Information and Communication Technology

IMPC Integral Model Predictive Control

LC Local-Controller

LOOD Lyapunov Optimization-Based Online Distributed

LP Linear Programming

LPF Low-pass Filter

MIMO Multi-Input Multi-Output

MPC Model Predictive Control

PV Photovoltaic

SOCP Second-Order Cone Programming

TSO Transmission System Operator

TN Transmission Network

VDER Virtual DER

VPP Virtual Power Plant

وَقُل رَّبِّ زِدْنِي عِلْمًا [سُورَةُ طه: ١١٤]

"My Lord, increase me in knowledge."

[Surah Ta-ha 20:114]

Chapter 1

Introduction

1.1 Motivation

The world is shifting towards renewable energy to combat climate change and achieve a sustainable energy future. Countries worldwide are striving to reduce their carbon footprints by relying on renewable energy sources such as solar, wind and hydro. Advancements in power electronics, manufacturing, and Information and Communication Technology (ICT) are accelerating the transition from traditional power grids, which are predominantly driven by fossil-fuel-based synchronous generators, to modern power systems that integrate a diverse mix of resources [1, 2].

Ontario's Provincial Government *Clean Energy Plan*, for example, outlines ambitious targets to ensure a reliable, affordable, and clean energy supply to support economic growth and the construction of over one million new homes by 2030 [3]. Central to the plan is the acknowledgment of Ontario's diverse energy mix, which includes hydroelectric, nuclear, natural gas, solar, wind and bio-energy sources. However, the transition towards clean energy poses significant challenges for grid stability and reliability. The increasing penetration of Distributed Energy Resources (DERs), including smart loads and Electric Vehicles (EVs), introduces complexities that traditional grid infrastructure struggles to accommodate [4–9]. As the integration of DERs increases, particularly Inverter-Based Resources (IBRs), system stability is affected due to decreased overall system inertia, making the grid more sensitive to load imbalances [8, 10].

In conventional power systems, generators preserve kinetic potential energy in their rotating parts, which can be utilized in the event of a disturbance, enhancing system

robustness [11]. However, as more DERs replace conventional generators, system robustness is weakened since DERs are integrated through inertialess power converters and system stability is compromised [12]. Various blackout incidents related to voltage instability or large frequency deviations due to the increased penetration of DERs have been reported [8, 13, 14].

The transition to a more environmentally-friendly grid, predominantly driven by DERs, signals a shift towards a new structural paradigm. This evolution adds complexity to the operational strategies crucial for the reliable management of the bulk grid. Research conducted by the California ISO (CAISO) highlights the uncertainties and variabilities associated with these DERs, emphasizing the need for the implementation of faster and more flexible regulation services to maintain system reliability [15].

Coordinated control of DERs — including battery/thermal storage, distributed generation, flexible load, and EVs — is one of the promising solutions to address these challenges [16–19]. Indeed, DERs (or aggregations thereof) offer unique advantages for fast regulation services, including low capital costs, integration within existing load centers, and, depending on the resource, fast response to commands [16–19]. As DERs are primarily distribution-connected [20, 21], and are owned and operated by a variety of stakeholders (or consumers/individuals), harnessing their full collective flexibility for emergency and ancillary services to the bulk grid requires further advances in Transmission Network–Distribution Network (TN–DN) coordination [19–21]. This work aims to develop a hierarchical framework that enables safe and fast coordination of DERs and DER aggregates behind the substation, while respecting operational boundaries and stakeholder privacy.

1.2   Power Grid Structure Overview

A general power grid structure incorporates DERs integrated at both TN & DN levels. The DERs at the TN are usually larger in scale and capacity compared to those at the DN, and the Transmission System Operator (TSO) can (in principle) directly control and utilize them for ancillary services [22]. In today's network, most DERs are integrated through the DN [22].

If DN-DERs can be effectively utilized to respond to TSO requests in a manner similar to TN-DERs, it would significantly enhance grid flexibility and reliability. However, this is challenging due to the decentralized nature of DN-DERs. Despite these challenges, the potential benefits are substantial. In the US, a rapid expansion of DERs is projected, with the DER capacity predicted to reach 387 GW by 2025. This expansion is driven

by a dynamic mix of resources, including Photovoltaic (PV) systems, EV infrastructure and units, and residential load management (including smart loads) [23, 24]. This example underscores that DN-DERs are not insignificant when collectively utilized, highlighting the potential benefits of an effective utilization scheme.

As the power system landscape evolves, the traditional boundary between the TN and DN is increasingly blurred by the integration of DERs [25]. Historically, the TN and DN operated independently, with the TN responsible for large-scale power generation and bulk energy transmission, while the DN passively delivered power to end-users. However, the proliferation of DERs, including distributed generation, flexible demand, and energy storage, is challenging this conventional separation, making the TN-DN boundary more fluid and dynamic [25].

To address the complexities introduced by this shift, various coordination schemes between the TN and DN have been investigated and proposed [26–28]. These schemes encompass centralized, decentralized, distributed, and hierarchical approaches to effectively utilize and control DERs within the DN, ensuring they can contribute to grid stability and reliability
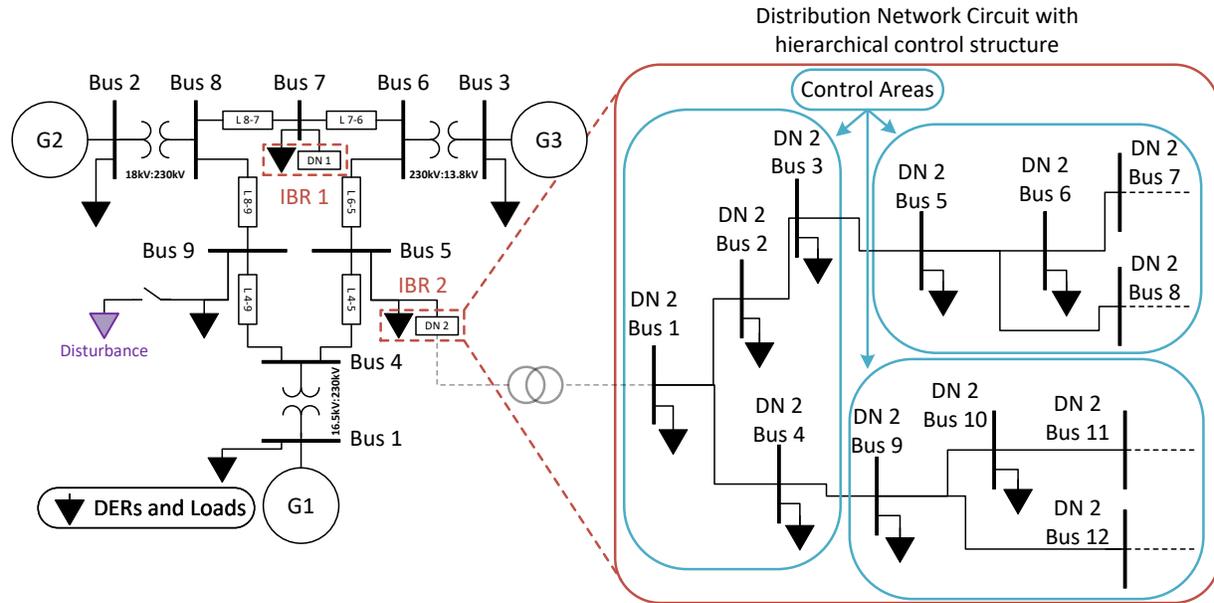
Figure 1.1: Illustration of a general power grid structure with DERs integrated at both TN and DN levels. A hierarchical control structure is applied at the distribution network level.

Figure 1.1 depicts a general power grid structure that integrates DERs at both the TN

and DN layers. This work focuses on utilizing DN-DERs to provide ancillary services to the bulk grid by responding quickly to TSO commands. The TSO would issue requests to the Distribution System Operator (DSO) to provide or consume power or to track pre-scheduled set-points, for example. In turn, the DSO would optimally control the available DERs to satisfy the request while maintaining grid constraints and meeting the reliability and stability requirements. In our scheme, we maintain the privacy of the DN — there is no sharing of internal structure, measurements, DER status, or other sensitive information with the TN — and hence, this structure of coordination falls under decentralized coordination.

In the following subsection, we describe the ancillary services, their types, and their critical role in maintaining system stability and reliability

1.2.1 Ancillary Services

Ancillary services ensure the operational reliability of the bulk power system. Although these services represent a relatively small fraction of overall electric power costs, their importance in maintaining system stability and preventing widespread outages is critical. Different Independent System Operators (ISOs) may have variations in the types and definitions of ancillary services they utilize. Ancillary services refer to a variety of functions that support the transmission of electric power from generators to consumers while maintaining the quality and reliability of the electricity supply.

As defined by the Federal Energy Regulatory Commission (FERC), *ancillary services are those services that are necessary to support the transmission of capacity and energy from resources to loads while maintaining reliable operation of the Transmission Service Provider's transmission system in accordance with good utility practice* [29, 30]. These services are integral to the stability and efficiency of the power grid. They include various types of reserves, frequency response services, voltage control, and black start capabilities, among others [30].

Types of Ancillary Services

(i) **Operating Reserves**:

- **Secondary Contingency Reserves**: These are reserves that can be activated to replace primary reserves and restore the system's frequency back to its normal state after an unexpected loss of generation [30].

- **Tertiary Contingency Reserves**: These reserves come into play after secondary reserves and are used to manage longer-duration imbalances [30].
- **Regulating Reserves**: These reserves help manage minute-to-minute variations in load and generation to maintain the balance between power supply and demand [30].
- **Flexibility Reserves**: These are reserves maintained to accommodate forecast errors and sudden changes in power demand [30].
- **Ramping Reserves**: These reserves address the need for additional power when there is a significant change in demand over a short period [30].

(ii) **Inertia Service**: Inertia service helps in the initial response to a frequency disturbance by slowing down the rate of change of frequency, buying time for other frequency control services to respond [30].

(iii) **Frequency Response**:

- **Primary Frequency Response**: This service involves the immediate and automatic adjustment of active power output to stabilize the frequency following a disturbance [30].
- **Fast Frequency Response**: A quicker response service than traditional frequency response, providing immediate support to maintain system frequency [30].

(iv) **Voltage Support and Reactive Power**: This service ensures that voltage levels within the transmission system remain within required limits, which is vital for the efficient operation of the power grid [30].

(v) **Black Start and Restoration Services**: These services enable the recovery of the power grid from a total or partial shutdown without relying on external power sources [30].

(vi) **Long-Term Planning Reserves**: These reserves ensure that sufficient generation capacity is available in the long term to meet peak demand and provide a buffer against unforeseen events [30].

In summary, ancillary services are vital for the reliable operation of the electric power system, supporting various functions necessary for maintaining grid stability and preventing disruptions. With this understanding in place, we now turn our attention to the criteria for designing control architectures that can effectively utilize DERs within the DN layer to participate in these essential services [31].

1.3 Candidate Control Architecture Criteria

Following the general power grid architecture considered, we end up with two control layers that are going to be integrated together to utilize DN-DERs for ancillary services. Due to the fact that multiple stakeholders are present, including various DSOs and independent DERs operators, the TSO often lacks detailed visibility and control over the DN and its resources. Additionally, operational constraints such as authority boundaries between different operators and practical challenges like large delays in communication for extensive networks, limited communication bandwidth, and restricted computing power make real-time monitoring and control spanning large distribution feeders infeasible. Therefore, we consider a decoupled design approach for each control layer, where each controller satisfies and maintains a different set of requirements. In Chapter 2, we discuss and elaborate on these requirements and evaluate recently proposed coordination methodologies against these criteria.

1.3.1 Distribution Level Controller Criteria

For the goal of providing fast ancillary services to the bulk grid, a robust control architecture for large-scale real-time coordination of DERs within distribution networks must adhere to several key criteria:

- **Rapid Coordination:** Optimize resource coordination within a time-scale of seconds or faster, as emphasized by recent studies on fast frequency and voltage regulation [32–34].

- **Model Independence:** Minimize reliance on detailed system and component models, preserving data and structural privacy for stakeholders [19], while mitigating the risk of instability due to model mismatch or unexpected grid events.

- **Localized Control:** Prioritize the use of local models, measurements, and communication channels, with flexibility in the amount of measurement feedback utilized. This adaptability is crucial given the ongoing development and potential cost constraints associated with distribution-level data acquisition and communication infrastructures.

- **Circuit Constraints:** Ensure that the utilization of DERs does not cause local imbalances within the distribution network.

These criteria, detailed in Section 2.2 and formulated as requirements, serve as fundamental benchmarks for assessing the efficacy of recently proposed coordination schemes.

1.3.2 Transmission and Distribution Coordination Criteria

The transmission and distribution coordination architecture must meet several essential criteria to ensure reliable and practical performance. These include:

- **Minimal Data Sharing:** Ensure the privacy of DNs and their DERs is maintained by avoiding the need for detailed models, measurements, and structures behind the meter[1].

- **Autonomous Coordination of DERs:** DN-DERs are managed by the DN control structure, independently from the TN controller[2].

These criteria will be further detailed and formulated as requirements in Section 2.3.

1.4 Research Objectives

The primary goal of this work is to design and validate a control framework that coordinates DN-DERs to participate in ancillary service provision by responding swiftly to TSO commands. Additionally, this work aims to integrate the framework with a recently proposed TN fast frequency control architecture. At first, a comprehensive list of requirements needs to be formulated for the DN control layer and its integration with the TN controller following the criteria above. Given that DN feeders potentially could host thousands of DERs spanning large distances, a decentralized control framework is essential. Each controller within the framework would have limited visibility over the network while managing DERs under its authority. This decentralized approach necessitates a hierarchical structure that ensures efficient control of DERs.

The decentralized approach requires that each controller within the framework relies on local measurements and circuit models to optimize DER utilization, ensuring the protection of data privacy across diverse control areas managed by different stakeholders. To ensure robustness, the utilization of feedback-based optimization is essential in this framework. This approach enables the system to respond to real-time data and dynamics, effectively mitigating uncertainties and disturbances. This structured approach promotes cooperation

---

[1]This is based on the privacy concerns and cyber-threats due to increased data communication within the grid [35, Sections 3.4 & 9.3]

[2]Without access to measurements within the DN, the TN controller could cause local imbalances within the DN.

among controllers to optimize DERs utilization while adhering to local circuit constraints. Below, we articulate the research objectives:

(i) **DN Hierarchical Control Structure**
The first objective is to design a fast, reliable, scalable, and flexible control structure that optimally coordinates DN-DERs in response to TSO requests. This work aims to establish a hierarchical multi-area control architecture capable of swiftly coordinating distribution-level DERs (and DER aggregates). A critical aspect of this architecture is *maintaining data privacy* while being highly scalable to manage large distribution feeders. The hierarchical setup requires cooperative efforts among controllers to meet TSO commands, optimize resource utilization, and uphold local circuit constraints (i.e., voltage and current). To ensure stakeholder privacy and enhance communication efficiency within feeder structures, controller visibility will be restricted primarily to their respective local authorities, referred to as Control Areas (CAs). Each CA represents a specific segment of the network over which the controller has oversight and control. Moreover, minimal information sharing between controllers will facilitate faster and more efficient communication among CAs.

(ii) **Integration of The DN Hierarchical Control Structure with fast frequency TN Controller**
The second objective builds directly upon objective (i), focusing on integrating the developed DN control architecture with a recently proposed TN fast frequency controller. Integrating DN dynamics into the TSO controller's decision-making process enhances robustness and stability, leading to a faster response and improved overall system performance. To achieve this, we will derive a linear model of the hierarchical DN control structure, which is then integrated within the TN controller design process. The simplified linear model of DN will be provided by the DSO, ensuring integration without exposing internal structures or private DERs data within the DN.

1.5   Contributions

Following the research objectives, we outline the main contributions of this work.

1.5.1 Multi-Area Architecture for Real-Time Feedback-Based Optimization of Distribution Grids

In Chapter 3, we develop a novel hierarchical multi-area control architecture for coordinating DN-DERs. The proposed architecture maintains data privacy for stakeholders while coordinating DERs on a time-scale of seconds or faster to fulfill TSO requests. The framework utilizes advancements in feedback-based optimization to enhance system robustness while minimizing the dependency on detailed system and component models. Operational boundaries and stakeholder privacy are enforced by relying on local measurements and through the introduction of the concept of Virtual DER (VDER), which acts as an interface between neighboring Control Areas (CAs). The proposed architecture enables optimal coordination of DERs while respecting local operational constraints and minimizing communication between controllers. The key contribution of this work is the rigorous closed-loop stability analysis, yielding intuitive and explicit analytical conditions for the stability of the proposed control structure. Additionally, we lay out a systematic and practical tuning procedure for the design. The proposed scheme is validated via case studies on several feeders, including IEEE-123 and IEEE-8500 feeders, and we describe several modifications that have been found to improve performance in implementation. The proposed framework has the following appealing characteristics:

(i) **Highly Scalable Multi-Area Control Architecture**: The proposed hierarchical multi-area control architecture provides scalability by dividing the DN into multiple control areas (CAs). Each CA is managed by a Local-Controller (LC) that uses sensitivity matrices to capture the impact of DERs set-points on measurements such as voltages, currents, active, and reactive powers. This partitioning allows the control system to effectively manage large distribution networks by scaling the control operations to handle the complexities of extensive networks while preserving local control and coordination. This approach ensures that each CA can be managed independently but still contributes to the overall system performance, allowing the system to handle large-scale networks without a significant increase in communication or computational load.

(ii) **Local-Controller (LC) manages local DERs**: Within each CA, the LC manages local DERs and measurements. This approach preserves operational boundaries and stakeholder privacy, as each LC only has visibility and control over resources within its designated area, minimizing the communication burden between controllers.

(iii) **Minimal Coordination Between Controllers**: The coordination between the controllers is minimized due to the hierarchical arrangement. This ensures that most

communication is local resulting in minimized delays and reduced complexity of the control system. Each LC communicates with its unique parent and children controllers (neighboring CAs).

(iv) **DERMS and DMS Integration**: The proposed architecture seamlessly aligns with the distinct functionalities of Distribution Management System (DMS) and Distributed Energy Resource Management System (DERMS), facilitating effective coordination between these modules for optimal DER management. DERMS manages DERs directly, utilizing comprehensive insights into their constraints and operational details, while DMS accesses critical circuit information and coordinates overall grid operations.

1.5.2 Development of MATDSS for Enhanced Distribution Network Simulation

MATDSS is a user-friendly MATLAB®-based GUI application developed to address specific challenges encountered during the implementation of complex control architectures in distribution networks. The integration with OpenDSS©facilitates efficient distribution network simulations, leveraging its power solver engine, while the time-series simulation is handled by MATLAB®. The application was conceived to streamline the management of highly complex system parameters and to enable real-time monitoring and control within the GUI. This capability became essential as traditional coding approaches struggled to handle the dynamic nature of simulations and real-time parameter adjustments. MATDSS offers extensive features including running complex simulations, generating and exporting data, and producing adaptive plots that dynamically update based on user selections. Additionally, it simplifies the simulation setup process by allowing users to save and recall initialization configurations, significantly reducing setup time for future simulations. This application facilitates the research and implementation of advanced control architectures with user-friendly intuitive navigation.

1.5.3 Enhanced Integration of DN Controller at the TN control layer

Integrating the DN architecture outlined in Chapter 3 at TN control layer represents a significant step towards leveraging DN-DERs for ancillary service provision. In Chapter 4, we introduce a method for deriving a simplified linear model of DN-DERs dynamics,

specifically tailored to capture their closed-loop response to TSO commands. This model integration is demonstrated within a recently developed TN control scheme that focuses on fast frequency regulation. The key characteristics of the integration with the TN controller design are:

(i) **Simplified Linear Model Extraction:** We propose a method to extract a simplified linear model that approximates the dynamic behavior of DN-DERs in response to TSO requests. This model captures the essential dynamics of DN-DERs while facilitating efficient integration with the TN control framework, enhancing system stability and responsiveness.

(ii) **Enhanced Stability**: Incorporating the DN model within the design process of the TN controller ensures that the TN controller is aware of the anticipated responses from the DN. Simulation results validate the efficacy of this integrated control approach in maintaining grid stability and reliability.

The integration of the two control layers (T & D) enhances grid resilience by leveraging DN-DERs while safeguarding stakeholder privacy. This integration ensures reliable grid operation with swift responses to TSO commands and optimizes DERs for efficient ancillary service provision. Compatible with existing infrastructure and adaptable to evolving grid dynamics, this approach minimizes operational costs and ensures long-term sustainability.

1.6   Notation

Throughout this thesis, the following notations and conventions are used:

- **Bolded symbols and letters** refer to matrices and column vectors.

- $(\cdot)^\top$ denotes the transpose of a matrix or vector.

- $(\cdot)^\mathsf{H}$ denotes the complex-conjugate transpose (Hermitian transpose).

- For a given vector $\mathbf{x} \in \mathbb{R}^N$, $|\mathbf{x}|$ denotes the entry-wise absolute value.

- For a given vector $\mathbf{c} \in \mathbb{C}^N$, $\mathbf{c}^*$ denotes the complex conjugate.

- For a function $f(\mathbf{x})$, we define the convex conjugate function $f^*(y)$ as [36]

$$f^*(y) = \sup_x y^\top x - f(x). \tag{1.1}$$

- The ℓ_2 norm is defined as $\|\mathbf{c}\|_2 := \sqrt{\mathbf{c}^\mathsf{H}\mathbf{c}}$.

- Given a matrix $\mathbf{X} \in \mathbb{R}^{M \times N}$, $\mathbf{X}_{m,n}$ denotes its (m, n)-th entry, and $\|\mathbf{X}\|_2$ denotes the ℓ_2-induced matrix norm.

- Grouping variables in brackets, such as $(\cdot, \cdot)$, indicates stacking them as a column vector. Additionally, col represents stacking variables as a column vector.

- $\mathsf{diag}(\mathbf{x})$ returns an $N \times N$ matrix with the elements of $\mathbf{x}$ on its diagonal.

- blkdiag indicates the block diagonal stacking of vectors or matrices.

- For a function $f : \mathbb{R}^N \to \mathbb{R}$, $\nabla_{\mathbf{x}} f(\mathbf{x})$ returns the gradient vector of $f(\mathbf{x})$ with respect to $\mathbf{x} \in \mathbb{R}^N$.

- The symbols $\mathbb{1}$ and $\mathbb{0}$ denote matrices and vectors (to be inferred from context) of ones and zeros with appropriate sizes, respectively.

- $\mathcal{P}_{\mathcal{X}}(\mathbf{x})$ denotes the Euclidean projection of $\mathbf{x}$ onto the set $\mathcal{X}$, defined as the closest point to $\mathbf{x}$ in $\mathcal{X}$:
$$\mathcal{P}_{\mathcal{X}}(\mathbf{x}) \in \arg\min_{\mathbf{y} \in \mathcal{X}} \|\mathbf{x} - \mathbf{y}\|_2. \tag{1.2}$$

- $\mathcal{P}_{\geq 0}(\mathbf{x})$ specifically denotes the Euclidean projection of $\mathbf{x}$ onto the nonnegative orthant.

- In our difference equations, $(\cdot)^+$ denotes the updated (next time step) value, with the time step-size inferred from the context.

1.7   Thesis Outline

The remainder of this thesis is organized as follows. Chapter 2 provides a comprehensive background information and literature review on control architectures for distribution and transmission networks, focusing on the integration of DN-DERs. In Chapter 3, we present a novel multi-area architecture designed for real-time feedback-based optimization of distribution grids to manage DN-DERs. Chapter 4 introduces a simplified linear model of DN dynamics that encapsulates the hierarchical control structure discussed in Chapter 3, integrated within the TN controller framework, particularly focusing on its application in fast frequency regulation. Finally, Chapter 5 summarizes the thesis findings and outlines future research directions.

Chapter 2

Background and Literature Review

In this chapter, we first describe the coordination scheme we aim to develop, and the mechanism of the interaction between different layers of the system. Then, we survey the literature on the coordination between transmission and distribution systems for effective utilization of DN-DERs. We explore various approaches to controlling DN-DERs and investigate integration and control techniques of these resources at the Transmission Network (TN) level to provide fast ancillary services to the bulk grid. These services include frequency and voltage regulation, following a scheduled loading profile (set-points), emergency load response and more. Researchers have proposed various control architectures at both the transmission and distribution layers of the network.

2.1 Transmission & Distribution Coordination Framework

Our coordination framework emphasizes maintaining separate control layers for enhanced manageability and improved coordination across multiple system operators. Under this scheme, the Transmission System Operator (TSO) oversees measurements and controls within the TN. For instance, during frequency disturbances, the TSO monitors network conditions, estimates required power adjustments, and communicates these needs to Distribution System Operators (DSOs) under its jurisdiction or interfaced with it.

DSOs receive power requests from the TSO and manage controllable resources (i.e., DERs), to meet these demands. To streamline TN-DN coordination, we develop a model of DN-DERs response to TSO requests. This model serves as a cornerstone for TSOs to design

Figure 2.1: Block diagram illustrating the TN-DN coordination with hierarchical DN control structure.

TN controllers that are aware of DN dynamics, thereby enhancing system responsiveness and stability.

Figure 2.1 illustrates the block diagram of the TN-DN coordination framework and controllers' interactions. The DN control structure is hierarchical, with Control Areas (CAs) nested within parent-child relationships. Each CA is governed by a Local-Controller (LC), which adjusts DERs contribution based on updated set-points received from its parent CA's LC.

The TSO's control scheme involves two main stages: disturbance estimator and power allocator. The disturbance estimator utilizes TN measurements and DNs dynamic models

provided by DSOs to estimate disturbances. Then, the TN controller issues set-points to DNs for ancillary services, such as frequency support, without requiring extensive data sharing of proprietary information such as measurements and detailed structures.

In subsequent sections, we survey the literature on various control and coordination schemes for utilizing DN-DERs in ancillary services. We establish evaluation criteria based on the requirements discussed in Section 1.3 and relying on the coordination scheme described above, to assess proposed architectures effectively.

2.2 Distribution Network Control Architectures

As more DERs are integrated into the DN, it becomes increasingly essential to design a fast DN control architecture that enables the full potential of collective responses from numerous small-scale DERs. These DERs are typically spread across large feeder networks and, when collectively participating, can provide ancillary services to the bulk grid [19, 31–34]. In Chapter 1, we outlined the criteria for effective DN control architecture. Here, we formulate these criteria into detailed requirements to ensure rapid response and effective large-scale real-time DER coordination within the DN.

2.2.1 Distribution Level Controller Requirements

(D.R1) **Optimal Coordination**: The framework must optimally coordinate resources on a time-scale of seconds or faster.

This requirement is motivated by recent studies [32–34] emphasizing the need for rapid frequency and voltage regulation using transmission-connected Inverter-Based Resources (IBRs). Effective DER coordination at this speed is essential for achieving comparable control performance to transmission-connected resources in TN-DN coordination schemes.

(D.R2) **Minimal Dependency on Detailed Models:** The design should not rely on detailed system and component models.

This is essential, particularly considering that DN circuit models are often approximate or aggregated. By minimizing the dependence on detailed models, the architecture enhances resilience against model inaccuracies and unforeseen events such as grid changes or disturbances. Moreover, it is critical for preserving data and structural privacy across different stakeholders [37, 38].

(a) Centralized   (b) Decentralized
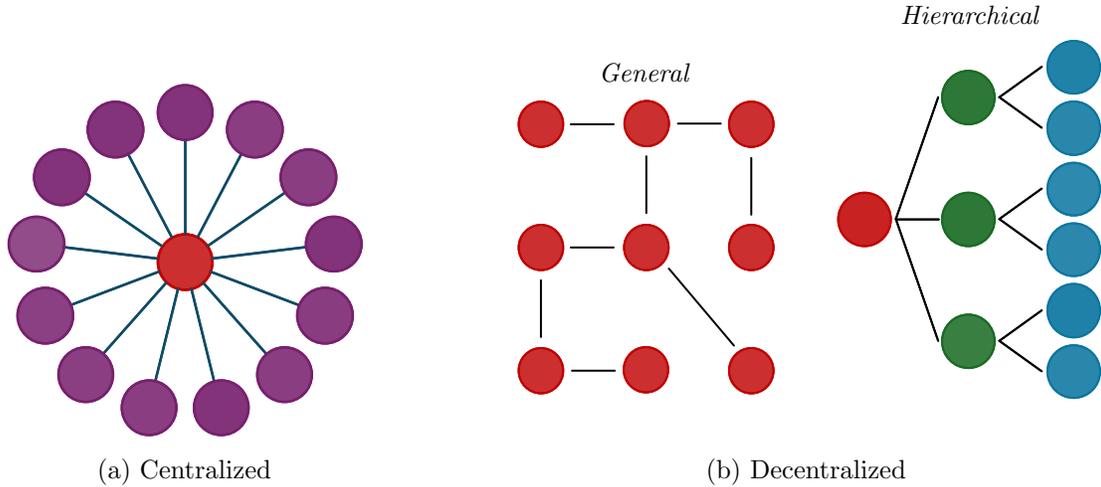
Figure 2.2: Centralized and decentralized control structures illustrations. Decentralized structure is exemplified by two variations: a general and a hierarchical strictures.

(D.R3) **Utilization of Local Models and Measurements:** The framework should primarily utilize local models, measurements, and communication, with flexibility on available measurement feedback.

Flexibility in measurement feedback is important given the ongoing development of data acquisition and communication infrastructure at the distribution level [19].

(D.R4) **Privacy and Operational Integrity:** operational boundaries (e.g. DERs, local models, measurements, etc.) behind the substation and stakeholder privacy must be maintained[1].

    This structured approach ensures that DN control architectures meet stringent performance and practicality requirements, enabling the effective utilization of flexibility within the distribution network to participate in ancillary services. By responding to TSO commands while preserving privacy, optimizing resource coordination, and ensuring rapid response, these criteria serve as foundational pillars for achieving seamless integration and operation of DN-DERs. In the literature, researchers propose different control structures such as centralized and decentralized.

---

[1]This is based on the privacy concerns and cyber-threats due to increased data communication within the grid [35, Sections 3.4 & 9.3]

In centralized control structures, the central controller directly manages the DERs by issuing commands in response to TSO requests, see Figure 2.2a where the purple circles represent the DER units. In some partially decentralized structures, the central controller can issue incentive signals, which individual DERs respond to accordingly.

In decentralized control structures, no central entity has authority over all DN-DERs. Instead, the network is partitioned into authority areas, with each area having its own controller to manage the resources within its jurisdiction. These controllers can communicate with each other to collectively manage the resources. The decentralized structure is leveraged when multiple operators are responsible for different parts of the network, requiring coordination while maintaining control over their respective resources.

In the following sections, we provide an overview of recently proposed coordination methodologies, evaluating them against the requirements (D.R1)-(D.R4), and classify them into the two categories: centralized and decentralized.

2.2.2 Centralized Control Architectures

In the pursuit of efficient DER coordination for providing fast ancillary services, centralized optimization techniques have been extensively studied. Centralized feeder control approaches leverage various optimization methods to achieve globally optimal coordination of heterogeneous DERs. Both [39] and [40] focus on solving the Distribution Optimal Power Flow (DOPF) problem through a centralized control scheme to maintain voltages by utilizing the available resources. In [39], two iterative algorithms — based on Linear Programming (LP) and Second-Order Cone Programming (SOCP) — are proposed to solve the DOPF problem in unbalanced DN. These algorithms significantly reduce computation time while optimizing power flow by minimizing losses, maintaining voltage levels, and integrating DERs efficiently. In [40], the voltage support is provided while minimizing DERs control costs and network losses using Linearized DOPF.

Relying on centralized Model Predictive Control (MPC), [41] proposes a control scheme that addresses the problem of coordinating EV charging stations to minimize costs while ensuring stable distribution grid operation. On the other hand, [37] proposes a feedback-based optimization technique where DERs' power set-points are adjusted in real-time based on available measurements. The centralized controller receives voltage, current and power measurements from the network and controls the available resources to track a reference signal from the TSO at the TN-DN interface bus (feeder head bus). Both [41] and [37] introduce a decentralized implementation of their algorithms, which we also discuss in the next section.

While these centralized techniques aim to achieve globally optimal coordination of heterogeneous DERs, they face challenges in meeting all desired criteria (D.R1)-(D.R4) outlined earlier. Real-time operation on a scale of seconds or less, particularly in large distribution feeders, may be hindered by limitations in communication infrastructure, thereby compromising requirement (D.R1). Some centralized techniques, such as in [37], successfully minimize dependency on detailed models of the network by employing feedback control and measurements, satisfying (D.R2). However, these approaches still require extensive data sharing with a central controller, raising concerns about data privacy and potentially violating requirements (D.R3)-(D.R4).

2.2.3   Decentralized Control Architectures

Several recent studies [41–49] have aimed to overcome the limitations of centralized DER coordination methods by leveraging decentralized optimization algorithms. While the specific DER coordination problems differ in these references, we focus on the proposed coordination architectures. Both [41] and [42] propose decentralized control structures based on centralized MPC, which are then decentralized using Alternating Direction Method of Multipliers (ADMM). In [42], a power set-point tracking problem is considered wherein a pre-scheduled set-point curve is planned through a stochastic optimization problem, and the central coordinator dispatches the DERs. This however occurs over a timescale of 30s, and does not consider real-time disturbance regulation. On the other hand, [41] addresses the problem of coordinating EV charging stations to minimize costs while ensuring stable distribution grid operation. Similarly, [43] proposes a decentralized voltage control structure for distribution systems with PV and EV DERs. This structure includes a dynamic network clustering based on network structure, voltage sensitivities and regulation capabilities. Additionally, each cluster is equipped with a MPC-based voltage controller. In [44] and [45], a DER coordination scheme is proposed through a distributed MPC framework. This scheme relies on a method for modeling and quantifying the aggregate power flexibility within the feeder. The primary goal is to maintain the privacy of DERs by only sharing information about their flexibility. The proposed control structures in [41–45] successfully limit data sharing with the DSO controller but still involve centralized coordination and do not use real-time feedback to maintain DN operating constraints.

Steps towards a true hierarchical framework were taken in [46] and [47], which propose two-level control architectures to coordinate low-voltage DERs. In [46], a primary-secondary (leader-follower) framework using decentralized Integral Model Predictive Control (IMPC) is introduced, with a focus on maintaining data privacy. This framework serves as an

18

interface layer connecting medium-voltage and low-voltage networks for coordinating low-voltage DERs. In contrast, [47] proposes a hierarchical distributed structure that centrally updates the set-points for low-voltage DERs. In both architectures, data-sharing between the layers/controllers is minimized, but both lack the flexibility to partition the feeder into multiple areas, which is essential for preserving stakeholder data privacy and operation when multiple operators are present in large low-voltage networks.

In [48], a decentralized feedback-based method is proposed for solving DN OPF problems with prosumers. This approach leverages local voltage measurements within a gradient descent method while minimizing communication with a central entity. In [49], a distributed control structure is introduced, utilizing a Lyapunov Optimization-Based Online Distributed (LOOD) algorithmic framework for Active Distribution Networks (ADNs). The framework effectively controls numerous DERs through the ADN operator, acting as a central coordinator. The ADN operator receives set-point reference signals from the TSO and tracks them by sending incentive signals to the DERs. Each DER relies on local information and measurements to update their power set-points. Similarly, an online feedback-based algorithm is proposed in [37] to coordinate DERs within DN while ensuring circuit constraints are maintained. The algorithm leverages online projected-gradient methods to track the solution of a time-varying optimization problem implemented by a centralized controller to track requested set-points from the TSO. In contrast, [50] proposes a centralized control scheme, where the controller estimates DERs' sensitives in real-time using network measurements. Additionally, the controller updates DERs set-points to control and track voltages and powers at network buses, ensuring they remain within limits. However, the centralized nature in [37, 48–50] architectures violates requirements (D.R3)-(D.R4).

Following the overview of various studies that explored centralized and decentralized structures, we propose a hierarchical and multi-area control architecture in Chapter 3, leveraging recent advances in control theory, specifically so-called *feedback-based optimization* [33,37,38,51–58], to optimally coordinate DERs. Our decentralized control structure, coupled with feedback-based optimization, promises to fulfill the design requirements (D.R1)-(D.R4) for distribution networks.

At a macro-level, our control scheme receives active and reactive power set-point commands from the TSO and optimally re-dispatches DERs within the DN to track the set-point, leveraging real-time grid feedback to ensure compliance with line current and bus voltage constraints. The scheme's use of measurement feedback enhances robustness against DN grid model inaccuracies. Compared to existing literature, our approach introduces a highly scalable multi-area control architecture. At a micro-level, the DN is hierarchically divided into local control areas, where controllers manage DERs and DN measurements to preserve operational boundaries and stakeholder privacy. Minimal and hierarchical coordination

19

between controllers minimizes long-distance communication, addressing multi-stakeholder challenges and reducing overall communication needs. Additionally, we provide a rigorous closed-loop stability analysis and a systematic tuning procedure. Case studies, including IEEE-123 and IEEE-8500 feeders, validate the scheme's performance, with identified modifications enhancing implementation efficiency. Simulation results demonstrate our scheme's ability to achieve fast and highly scalable DER coordination in large multi-stakeholder DNs.

2.3 Transmission and Distribution Coordination Architectures

The goal of the coordination framework is to develop a scheme that facilitates the integration between transmission and distribution networks. This framework aims to optimally utilize the flexibility of multiple DNs for fast ancillary services. To achieve this goal, the integration framework should meet the following performance and practicality requirements:

2.3.1 Transmission & Distribution Coordination Requirements

(T.R1) **Minimize data sharing:** The framework should minimize data exchange among different stakeholders, controllers, and control layers to protect privacy and streamline communication.

This simplifies the communication process and reduces the volume of data exchange, leading to faster decision making and lower communication overhead. In addition, this ensures that proprietary information including measurements and structures behind the meter remain confidential, safeguarding the privacy of DN operators.

(T.R2) **DN-DERs coordination managed independently from the TN controller:** This requirement ensures the separation of control design, preventing TN actions from disrupting DN networks (e.g. causing local imbalances), and vice versa.

Independent coordination is essential for maintaining stability and reliability within both the TN and DN. It allows local optimization within each DN and ensures that actions taken by the transmission level do not negatively impact the distribution level, preventing local imbalances and inefficiencies that could destabilize the network.

(T.R3) **Operate in real-time and coordinate within seconds:** The TN coordination framework with DN control structure should operate in real time and successfully coordinate to utilize the available flexibility within seconds.

Real-time operation is critical for responding to rapid changes in the grid and maintaining system stability, especially during disturbances.

Next, we focus on the TN control architectures in the literature designed to leverage DN-DERs for fast ancillary services. Similar to DN control architectures, the objectives of these proposed architectures vary. Here, our focus is on analyzing their architecture and assessing their alignment with the requirements outlined above.

In [59] and [60], direct control of DN-DERs by the TSO is proposed for level-3 frequency (or voltage) deviation, wherein the TSO overrides local controllers to ensure system stability. However, this method requires extensive monitoring and direct control of DERs within distribution networks, violating requirement (T.R1). Moreover, it may lead to local imbalances within the DN, violating requirement (T.R2).

A hierarchical control structure for fast frequency response is introduced in [61], employing a central supervisor to coordinate local controllers distributed across the network. The local controllers manage real-time control over the DERs, while the central controller collects live resource information and identifies optimal resources for Fast Frequency Control (FFC) purposes. Despite its potential, the optimization process is not conducted in real time due to extensive data collection requirements, violating requirement (T.R3). To achieve real-time optimization, [62,63] propose using multiple Dynamic Virtual Power Plants (DVPPs), each consisting of controllable DERs and uncontrollable devices (e.g. generators, uncontrollable loads...*etc.*). The control structure distributes the Multi-Input Multi-Output (MIMO) Adaptive Dynamic Participation Matrices (ADPMs) among local devices to achieve localized desired behavior, with each device featuring a local feedback controller that optimally match the behavior. However, potential circuit instability within the Virtual Power Plant (VPP) (i.e., DN feeder structure) is not addressed, violating requirement (T.R2).

Controllable packetized DERs are proposed in [64,65] to simplify DERs management and provide synthetic damping for primary control response. While privacy is preserved in the decentralized scheme, it requires some form of centralized coordination (potentially through the TSO), which may violate requirements (T.R1) and (T.R2). Active network management system, acting as a centralized controller, is proposed in [66] aiming to utilize DN-DERs in power system frequency restoration. However, the proposed system violates requirements (T.R1)-(T.R2), lacking decentralized coordination and potentially compromising data privacy.

21

Following the overview of various studies that explored different integration and control strategies of DN-DERs in TSO control scheme, we propose a novel approach that can leverage the proposed control structure in Chapter 3 [31]. We obtain a dynamic model of the distribution feeder that can be utilized in TSO control design, with minimal data sharing between different system operators.

Chapter 3

Multi-Area Architecture for Real-Time Feedback-Based Optimization of Distribution Grids

3.1   Introduction

The coordination of DN-DERs offers a promising approach to providing ancillary services to the bulk grid. The Transmission System Operator (TSO) provides power set-point requests (reference signals) to the Distribution Network (DN), which DN controllers are expected to track. We envision a multi-feeder distribution network interconnected with the Transmission Network (TN) at a shared interface bus, as illustrated in Figure 3.1. Here, a central coordinator receives power set-points requests $\mathbf{X}^\star = \mathsf{col}(\mathbf{P}^\star, \mathbf{Q}^\star) \in \mathbb{R}^2$ from the TSO and subsequently generates set-points $X_0^{f_i}$ for each feeder i to track

$$\mathbf{X}^\star = \sum_i X_0^{f_i}. \tag{3.1}$$

A simple example of such controller can be obtained by defining $X_0^{f_i}$ via a set of participation factors specific to each distribution feeder

$$X_0^{f_i} = \alpha_i \mathbf{X}^\star, \tag{3.2}$$

where $\sum_i \alpha_i = 1$ and $\alpha_i > 0$. These participation factors can either be predefined or computed through an optimization problem. One approach could be based on the available

23
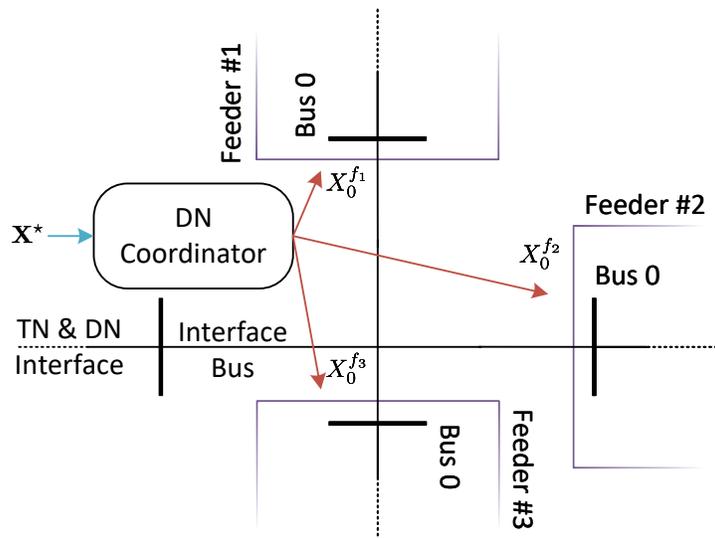
Figure 3.1: Multiple distribution network feeders coordination scheme.

DER powers (reserves) in each feeder. For this implementation, a power estimation problem can be considered following the approach in [44]. This approach estimates the available flexibility in a feeder, which runs continuously. The flexibility estimation updates periodically (e.g., every 15 minutes), enabling the coordinator to dynamically adjust participation factors for each feeder based on received information. This process may also integrate cost functions, assuming different operators and different costs. In subsequent sections, we delve into the scenario where a single feeder is situated at the interface bus, simplifying our analysis by omitting feeder indexing.

3.2 Overview of Proposed Hierarchical Control Structure

Our focus is on controlling a single-feeder DN that has been partitioned into a hierarchy of areas, as shown in Figure 3.2. The high-level control objective is to leverage controllable DERs within the DN to achieve the following goals: (i) track an overall power set-point $X_0^{\text{set}} = (p_0^{\text{set}}, q_0^{\text{set}}) \in \mathbb{R}^2$ at the transmission-distribution (TN-DN) interface bus, which is provided by the TSO, (ii) maintain operational constraints throughout the DN, and (iii) optimally utilize these controllable DERs. Additionally — and as the most distinguishing

feature of this work — the design is subject to the constraint that information and management boundaries between different areas of the DN must be respected. This leads to a hierarchical area-based control architecture, which will be described next.
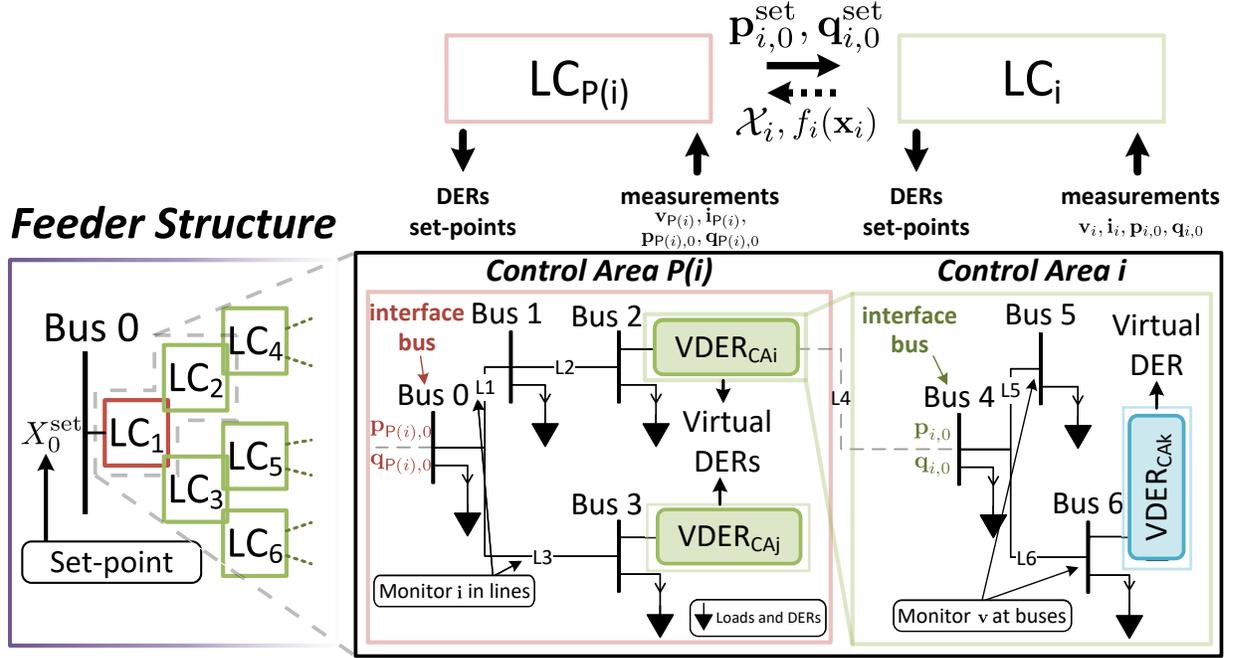
Figure 3.2: Single-feeder DN internal structure. Zoomed-in areas illustrate the interaction between parent and child areas within a feeder. Red and green boxes illustrate the visibility of each Local-Controller (LC) over the local infrastructure and resources, including local grid measurements $(\mathbf{v}, \mathbf{i}, \mathbf{p}, \mathbf{q})$ and local DERs.

3.2.1 Feeder Architecture and Local-Controllers (LCs)

We consider the feeder as already partitioned into N Control Areas (CAs), which are predefined segments of the feeder infrastructure. These CAs may represent contractual arrangements for managing DER resources through aggregators or operational divisions based on factors such as communication capabilities or having uniform division of control resources within each area [67, 68]. Each CA is managed by a Local-Controller (LC), which oversees the local electrical infrastructure and coordinates the operation of DERs. Notably, the controller will *not* have visibility of neighboring CAs, and hence the control structure will be decentralized.

25
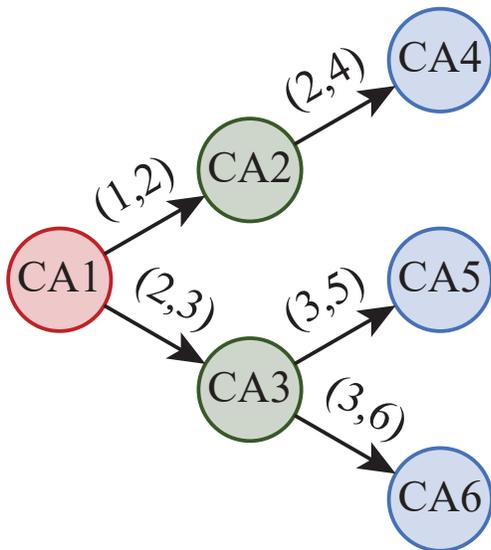
Figure 3.3: Example of a directed rooted tree graph with 6 control areas (nodes) and 5 edges.

The arrangement of CAs and the communication between the associated LCs is hierarchical, ensuring several key benefits: (i) any required communication is local, which minimizes communication delays, (ii) the control architecture is scalable to large numbers of control areas, and (iii) the majority of local measurements and area data are not shared to maintain the privacy of stakeholders within the area. We describe the hierarchical arrangement between the CAs with a directed rooted tree graph $\mathcal{G}_{\text{CA}} = (\mathcal{N}_{\text{CA}}, \mathcal{E}_{\text{CA}})$ with nodes $\mathcal{N}_{\text{CA}} = \{1, \ldots, N\}$ and edges $\mathcal{E}_{\text{CA}}$; the root of the tree is the first CA at the head of the feeder; see Figure 3.2. For any CA $i \in \mathcal{N}_{\text{CA}}$, we let $\mathsf{P}(i)$ denote the unique parent CA and $\mathsf{C}(i)$ denote the set of child CAs; by convention $\mathsf{P}(1) = \emptyset$ and $\mathsf{C}(N) = \emptyset$. We let $\mathcal{A} \in \{0, 1\}^{N \times N}$ denote the adjacency matrix of $\mathcal{G}_{\text{CA}}$, with elements $\mathcal{A}_{ij} = 1$ if $(i, j) \in \mathcal{E}_{\text{CA}}$ and 0 otherwise.

To illustrate this hierarchical structure, consider a tree graph with six CAs, as shown in Figure 3.3. The root node, CA1, is the head of the feeder and acts as the parent to CA2 and CA3, creating two edges directed from CA1 to these child nodes: (1,2) and (1,3). Further down the hierarchy, CA2 is the parent of CA4, forming the edge (2,4). Similarly, CA3 is the parent of CA5 and CA6, forming the edges (3,5) and (3,6). Within this structure, each CA is assigned a controller LC, where it manages only local devices and monitors only local measurements. This structure results in having the adjacency matrix $\mathcal{A}$ for this directed

tree graph given by

$$\mathcal{A} = \begin{bmatrix} 0 & 1 & 1 & 0 & 0 & 0 \\ 0 & 0 & 0 & 1 & 0 & 0 \\ 0 & 0 & 0 & 0 & 1 & 1 \\ 0 & 0 & 0 & 0 & 0 & 0 \\ 0 & 0 & 0 & 0 & 0 & 0 \\ 0 & 0 & 0 & 0 & 0 & 0 \end{bmatrix}. \tag{3.3}$$

This adjacency matrix represents the parent-child relationships between the control areas, indicating which ones communicate directly within the hierarchy.

Each control area $i \in \mathcal{N}_{\text{CA}}$ is connected to its parent area $\mathsf{P}(i)$ through a single bus which we call the *interface bus*; see Figure 3.2. From the perspective of the parent area $\mathsf{P}(i)$, the ith CA is represented as a Virtual DER (VDER) located at this interface bus. The VDER is a fictitious DER which will be "dispatched" by the parent area LC by providing a power set-point $X_{i,0}^{\text{set}} = (\mathsf{p}_{i,0}^{\text{set}}, \mathsf{q}_{i,0}^{\text{set}})$ to the LC of area i. Recall that the set-point for CA 1 at the head of the feeder is provided by the TSO. The control cost f_i and capacity limits $\mathcal{X}_i$ of this VDER (i.e., of the child area) are assumed known by the LC of the parent area[1], and may be updated by exception through communication from the child to the parent area; further discussion on capacity limits and cost functions is deferred to Section 3.3.1. Within the LC, the objective is then to track this provided set-point at the interface bus by re-dispatching local DERs, while maintaining local constraints on voltages and currents. This tracking control will be accomplished through a combination of local optimization and feedback, to be described in Section 3.3.1.

Remark 3.2.1 (Cost function f_i and Capacity limits $\mathcal{X}_i$ of the VDER)
The cost function and capacity limits of the VDER are updated by the child area to reflect any changes in its DERs and VDERs. An online aggregator algorithm as proposed in [44] can be employed to update the flexibility (i.e. capacity limits) of the VDER.

Remark 3.2.2 (Control Areas Vs. DER Aggregators, VPPs, Microgrids) *Within our framework, the CAs can represent various structures. For example, a small CA can represent DER aggregator (CA controlling DERs within a building for example). In addition, a CA can represent a Virtual Power Plant (VPP) with distributed generation, controllable loads and smart metering. A microgrid that is mainly managed locally can also be represented by a CA within our structure.*

For more information about DER aggregators, VPPs, and Microgrids, see [69, 70].

---

[1]For the ith CA and from the parent area $\mathsf{P}(i)$ perspective, the VDER cost function is $f_j(x_j) = f_i(\mathbf{x}_i)$ and the feasibility set is $\mathcal{X}_j = \mathcal{X}_i$, for $j \in \mathcal{D}_{\mathsf{P}(i)}$.

3.2.2 Model of a Single Control Area

We now describe the model for the distribution system and the DER components contained within a specific control area.

Controllable DERs

Let $\mathcal{D}_i$ denote the set of controllable DERs (including any VDERs) within the CA $i \in \mathcal{N}_{\mathrm{CA}}$. The DERs are assumed to have local controllers which allow them to quickly track set-points provided by the LC. For any DER $j \in \mathcal{D}_i$, we let $x_j = (p_j, q_j) \in \mathbb{R}^2$ denote its overall active and reactive power set-points, which are constrained to be within capacity limits specified by the closed, non-empty convex set $\mathcal{X}_j \subset \mathbb{R}^2$. We let $\mathbf{x}_i = \mathsf{col}(x_1, \ldots, x_{|\mathcal{D}_i|}) \in \mathbb{R}^{2|\mathcal{D}_i|}$ denote the stacked vector of all DER power set-points for the ith CA, and is subject to the overall limits $\mathbf{x}_i \in \boldsymbol{\mathcal{X}}_i \triangleq \mathcal{X}_1 \times \cdots \times \mathcal{X}_{|\mathcal{D}_i|}$.

In the literature, DERs are modeled with cost functions and constraint sets that reflect their operational capabilities. For example, in [37, 40], the cost functions for various DERs are defined as follows:

(i) **Photovoltaic (PV) Systems:** These systems typically have a maximum real power available, denoted by $p_{i,av}$. The active and reactive power set-points for a PV system, $x_j = (p_j, q_j)$, must lie within a constraint set that ensures the power output does not exceed the available capacity. The cost function for these DERs can be expressed as:

$$f_j(x_j) = \begin{cases} (p_{j,av} - p_j)^2 + (q_j)^2, & \text{for three-phase PV systems} \\ a_p(p_{j,av} - p_j)^2 + (q_j)^2, & \text{for single-phase PV systems} \end{cases} \tag{3.4}$$

where $a_p > 0$.

(ii) **Battery Energy Storage System (BESS):** The constraint set of BESS is defined following the charging and discharging limits. The cost function for a battery can be expressed as:

$$f_j(x_j) = (p_j)^2 + (q_j)^2 \tag{3.5}$$

.

(iii) **Electric Vehicles (EVs):** EVs have specific charging rates, and their power set-points are constrained by the maximum charging capacity, $p_{j,max}$. The cost function for an EV can be expressed as:

$$f_j(x_j) = a(p_j - p_{j,max})^2 \tag{3.6}$$

where $a > 0$.

For advanced DER modeling, see [71–78].

The DER feasibility set $\mathcal{X}_j$ models different constraints reflecting the type and operation of the DER. For BESS and EVs, a boxed (rectangular) constraint set represents the limits on the feasible set-points that are permitted. To account for the dependency between active and reactive powers (apparent power limits), a semi-circle constraint set can be considered. In this work, we focus on the hierarchical structure and the interaction between the controllers, where we consider general DER device models with general cost functions and boxed constraint sets, which we detail in subsequent sections.

Distribution Network Model

Let $\overline{\mathcal{N}}_i = \{0\} \cup \mathcal{N}_i$ with $\mathcal{N}_i := \{1, 2, \ldots, N_i\}$ denote the set of buses in the ith CA, where the interface bus of the CA is given the node "0"; each bus is potentially multi-phase, with up to three phases. Not necessarily all buses and lines within the CA will be monitored for control purposes; we let $\mathbf{M}_i^{\mathbf{v}} \subseteq \mathcal{N}_i$ denote the set of buses where phase-to-ground voltage magnitude measurements are available, with the understanding that all phases will be monitored if the bus is multi-phase, and let $\mathbf{v}_i$ be the vector of measured voltages. Similarly, we let $\mathbf{i}_i$ denote the vector of measured line current magnitudes for a subset of monitored distribution lines $\mathbf{M}_i^{\mathbf{i}} \subseteq \overline{\mathcal{N}}_i \times \overline{\mathcal{N}}_i$. Finally, we let $\mathbf{p}_{i,0}, \mathbf{q}_{i,0} \in \mathbb{R}^{m_i}$ denote the net active and reactive power injections at the interface bus, where m_i is the number of phases at the interface bus.

We adopt the distribution network model from [79, 80], which is capable of modeling both radial and meshed unbalanced networks, as well as wye and delta connections for loads and DERs. The model provides linearized equations relating the DERs' powers to the CA's voltages and currents measurements, and to the interface bus power injections. In the current work, we have adjusted these equations to combine both wye and delta-connected DERs, leading to the model

$$\mathbf{v}_i(\mathbf{x}_i) = \mathbf{A}_i\mathbf{x}_i + \mathbf{a}_i, \tag{3.7a}$$

$$\mathbf{i}_i(\mathbf{x}_i) = \mathbf{B}_i\mathbf{x}_i + \mathbf{b}_i, \tag{3.7b}$$

$$\mathbf{p}_{i,0}(\mathbf{x}_i) = \mathbf{M}_i\mathbf{x}_i + \mathbf{m}_i, \tag{3.7c}$$

$$\mathbf{q}_{i,0}(\mathbf{x}_i) = \mathbf{H}_i\mathbf{x}_i + \mathbf{h}_i, \tag{3.7d}$$

where $\mathbf{A}_i$, $\mathbf{B}_i$, $\mathbf{M}_i$ and $\mathbf{H}_i$ are constant matrices which can be computed from the operating point, the admittance matrix, and the specification of DER phase connections. The vectors

$\mathbf{a}_i$, $\mathbf{b}_i$, $\mathbf{m}_i$ and $\mathbf{h}_i$ are constants. For detailed insights into the linearization process, refer to Appendix A. Note that the matrices $\mathbf{A}_i$, $\mathbf{B}_i$, $\mathbf{M}_i$ and $\mathbf{H}_i$ can be interpreted as sensitivity matrices; for instance, $\mathbf{A}_i$ captures the sensitivity between DER set-points and voltage magnitudes at the measurement points.

Remark 3.2.3 (Vectors of measurements in the ith CA)

- *Voltage magnitudes at buses k (per phase ϕ):* $\mathbf{v}_i = \mathsf{col}(|V_{\mathrm{LN}_{i,k_\phi}}|)$

- *Branch current magnitudes between buses k and l (per phase ϕ):* $\mathbf{i}_i = \mathsf{col}(|I_{i,kl_\phi}|)$

- *Active power injection at the interface bus (per phase ϕ):* $\mathbf{p}_{i,0} = \mathsf{col}(\mathrm{p}_{i,0_\phi})$

- *Reactive power injection at the interface bus (per phase ϕ):* $\mathbf{q}_{i,0} = \mathsf{col}(\mathrm{q}_{i,0_\phi})$

Remark 3.2.4 (Nonlinear System Dynamics vs Linear System Model) *The use of an approximate linear model in this work is justified by its widespread acceptance in power systems literature and its computational efficiency, particularly for real-time control applications. While acknowledging that power systems are inherently nonlinear, the linearization around the operating point provides a practical balance between accuracy and simplicity. The model's accuracy under normal operating conditions ensures that stability can be rigorously analyzed, and the integration of feedback from real-time measurements helps mitigate the effects of any inaccuracies introduced by the linear approximation. This approach also facilitates the establishment of stability conditions for the control structure, with simulations further validating the robustness of the method under realistic conditions.*

3.3   Hierarchical Feedback-Based Optimization of Distribution Feeders

3.3.1   LC Optimization Problem

The control objectives of the LC for the ith CA will be formulated by specifying an optimization problem. The problem aims to re-dispatch DERs within their limits to track provided power set-points $X_{i,0}^{\mathrm{set}} = (\mathrm{p}_{i,0}^{\mathrm{set}}, \mathrm{q}_{i,0}^{\mathrm{set}})$ at the interface bus, while maintaining measured voltages $\mathbf{v}_i$ and currents $\mathbf{i}_i$ within constraints, and by efficiently using DER resources.

As described in Section 3.2.1, the set-points $\mathrm{p}_{i,0}^{\mathrm{set}}$ and $\mathrm{q}_{i,0}^{\mathrm{set}}$ to be tracked will be computed as VDER set-points by the parent area, which we express as

$$\mathrm{p}_{i,0}^{\mathrm{set}}(\mathbf{x}_{\mathsf{P}(i)}) = T_i^{\mathrm{p}}\mathbf{x}_{\mathsf{P}(i)}, \quad \mathrm{q}_{i,0}^{\mathrm{set}}(\mathbf{x}_{\mathsf{P}(i)}) = T_i^{\mathrm{q}}\mathbf{x}_{\mathsf{P}(i)}, \tag{3.8}$$

for appropriate matrices T_i^{p} and T_i^{q}. Mathematically, we can now express the optimization problem for the ith CA as

$$\operatorname*{minimize}_{\mathbf{x}_i \in \boldsymbol{\mathcal{X}}_i} \; f_i(\mathbf{x}_i) \triangleq \sum_{j \in \mathcal{D}_i} f_{ij}(x_j) \tag{3.9a}$$

subject to

$$s_i\left(|\mathbb{1}^{\mathsf{T}}\mathbf{p}_{i,0}(\mathbf{x}_i) - \mathrm{p}_{i,0}^{\mathrm{set}}(\mathbf{x}_{\mathsf{P}(i)})|\right) \le E_{i_{\mathrm{p}}} \tag{3.9b}$$

$$s_i\left(|\mathbb{1}^{\mathsf{T}}\mathbf{q}_{i,0}(\mathbf{x}_i) - \mathrm{q}_{i,0}^{\mathrm{set}}(\mathbf{x}_{\mathsf{P}(i)})|\right) \le E_{i_{\mathrm{q}}} \tag{3.9c}$$

$$\mathbf{v}_i(\mathbf{x}_i) \le \overline{\mathbf{v}}_i \tag{3.9d}$$

$$\underline{\mathbf{v}}_i \le \mathbf{v}_i(\mathbf{x}_i) \tag{3.9e}$$

$$\mathbf{i}_i(\mathbf{x}_i) \le \overline{\mathbf{i}}_i \tag{3.9f}$$

The linear inequalities (3.9b)–(3.9c) enforce total active and reactive power tracking at the interface bus of the provided set-points $\mathrm{p}_{i,0}^{\mathrm{set}}$ and $\mathrm{q}_{i,0}^{\mathrm{set}}$, within specified tolerances $E_{i_{\mathrm{p}}}, E_{i_{\mathrm{q}}} > 0$. We emphasize that from the perspective of the optimization (3.9) for the ith CA, the parent variable $\mathbf{x}_{\mathsf{P}(i)}$ is *fixed*. The fixed binary variable $s_i \in \{0,1\}$ can be used to enable or disable this tracking feature. The inequalities (3.9d), (3.9e) enforce upper and lower limits $\overline{\mathbf{v}}_i$ and $\underline{\mathbf{v}}_i$ on the voltage magnitudes at the measurement points, with (3.9f) limiting the current magnitude along monitored lines below $\overline{\mathbf{i}}_i$.

DER Costs and Constraints

The objective function (3.9a) is a separable cost over each DER and VDER which penalizes its use for control purposes. Our only assumption will be that f_i in (3.9) is continuously differentiable and strongly convex; we let $m_i > 0$ denote the strong convexity parameter, and by convention, the units of the cost will be W^2. For example, in our case studies we will use quadratic costs of the form

$$f_{ij}(x_j) = x_j^{\mathsf{T}} C_j'' x_j + x_j^{\mathsf{T}} C_j', \tag{3.10}$$

where $C_j'' \succ 0$ is a diagonal 2×2 matrix and $C_j' \in \mathbb{R}^2$. These coefficients can be set to reflect the preference of using different types of DERs; larger costs will lead to lower control usage

of a given DER. This can be crucial when different DERs with different characteristics (e.g., capacities or speed dynamics) are controlled together. The power capacity constraint set $\mathcal{X}_j$ for DER $j \in \mathcal{D}_i$ may simply be the box constraint $\mathcal{X}_j = [\underline{x}_j, \overline{x}_j]$ specifying independent active and reactive power limits, or may instead encode more complex apparent power constraints via intersections of half-planes and semi-circular regions.

VDER Costs and Constraints

As the VDERs of the ith CA provides an aggregated representation of all DERs and VDERs in the child areas $\mathsf{C}(i)$, assigning appropriate costs to VDERs is critical to ensure resources are appropriately leveraged throughout the DN. To ensure downstream DERs provide control action, a VDER should have lower cost compared to other DERs available within the same CA. If $j \in \mathcal{D}_i$ is the VDER corresponding to child area $k \in \mathsf{C}(i)$, then a choice that roughly mimics the allocation obtained from a global centralized optimization is

$$f_{ij}(x_j) = \left(\sum\nolimits_{\ell \in \mathcal{D}_k} f_{k\ell}^*\right)^* (x_j), \tag{3.11}$$

where * denotes convex conjugate. For instance, with quadratic costs (3.10), equation (3.11) evaluates to

$$f_{ij}(x_j) = (x_j + \zeta_k)^\top \left(\sum\nolimits_{l \in \mathcal{D}_k} (C_\ell'')^{-1}\right)^{-1} (x_j + \zeta_k),$$

where $\zeta_k = 2 \sum_{\ell \in \mathcal{D}_k} (C_l'')^{-1} C_\ell'$. The following example illustrates how (3.11) mimics the allocation obtained from global centralized optimization.

Example 3.3.1 (Illustrative Example of VDER Cost function) *Let the ith CA have N_i DERs and only one VDER. Let the kth CA be the corresponding area of the VDER in area i, with N_k DERs. Each DER has a cost function as in (3.10), where $C_j' = 0$. We show below that the decentralized optimization mimics the centralized global optimization for active power allocation under certain assumptions. Since the allocation of active and reactive powers is decoupled, a similar result can be obtained for reactive power.*

Let $\hat{\mathcal{D}}_i \subset \mathcal{D}_i$ indicate the subset of actual DERs (excluding the VDER) within area i. Assuming that all DERs have equal sensitivities, the only factor affecting their contribution now is their cost functions. Thus, for the ℓth DER in area i, the centralized power allocation

can be expressed as (considering that all DERs belong one CA)

$$p_\ell = \frac{1/C_\ell''}{\displaystyle\sum_{j \in \hat{\mathcal{D}}_i \cup \mathcal{D}_k} 1/C_j''} \; p_{0,i}^{\text{set}} \; . \tag{3.12}$$

$$= \frac{1/C_\ell''}{\displaystyle\sum_{j \in \hat{\mathcal{D}}_i} 1/C_j'' + \sum_{j \in \mathcal{D}_k} 1/C_j''} \; p_{0,i}^{\text{set}}$$

From (3.11), we have

$$C_{\text{VDER}}'' = \frac{1}{\displaystyle\sum_{j \in \mathcal{D}_k} 1/C_j''} \; . \tag{3.13}$$

Substituting (3.13) in (3.12) yields

$$p_\ell = \frac{1/C_\ell''}{\displaystyle\sum_{j \in \hat{\mathcal{D}}_i} 1/C_j'' + 1/C_{\text{VDER}}''} \; p_{0,i}^{\text{set}} \tag{3.14}$$

$$= \frac{1/C_\ell''}{\displaystyle\sum_{j \in \mathcal{D}_i} 1/C_j''} \; p_{0,i}^{\text{set}} \; .$$

Hence, the VDER cost (3.13) represent all DERs within area k when solving the decentralized optimization problem in area i, mimicking the centralized allocation.

One can interpret this formula as akin to an equivalent impedance from a parallel combination of impedances, as all downstream DERs would be used in parallel in a centralized dispatch. While the proposed VDER cost in (3.11) is developed to emulate centralized controller implementation, it is worth noting that VDER costs can be configured in various ways. In the context of a competitive market, where multiple service providers engage in competition, setting VDER costs can be structured to adhere to a cost-effective plan, allowing different stakeholders to compete while delivering services to the grid.

3.3.2 Offline vs. Online Optimization

The optimization problem (3.9) is convex and could in principle be directly solved. However, the constants $\mathbf{a}_i, \mathbf{b}_i, \mathbf{m}_i, \mathbf{h}_i$ in the distribution system model (3.7) depend on unknown real-time loading conditions and disturbances throughout the system. Even if the best available

estimates are used for these quantities in (3.9), implementation of the resulting set-points in the system will likely lead to constraint violation, and the system will not actively respond as disturbances change. Instead, following [37] and inspired also by recent advances in feedback-based optimization, we pursue an iterative approach which uses real-time measurement feedback from the system in place of this model information.

3.3.3 LC Control Algorithm

To introduce the LC controller, we first re-write the constraints (3.9b)-(3.9c) as linear constraints to obtain

$$\underset{\mathbf{x}_i \in \mathcal{X}_i}{\text{minimize}} \ f_i(\mathbf{x}_i) \triangleq \sum_{j \in \mathcal{D}_i} f_{ij}(x_j) \tag{3.15a}$$

subject to

$$s_i \left(\mathbb{1}^{\mathsf{T}} \mathbf{p}_{i,0}(\mathbf{x}_i) - \mathbf{p}_{i,0}^{\text{set}}(\mathbf{x}_{\mathsf{P}(i)})\right) \leq E_{i_\mathrm{p}} \tag{3.15b}$$

$$s_i \left(\mathbf{p}_{i,0}^{\text{set}}(\mathbf{x}_{\mathsf{P}(i)}) - \mathbb{1}^{\mathsf{T}} \mathbf{p}_{i,0}(\mathbf{x}_i)\right) \leq E_{i_\mathrm{p}} \tag{3.15c}$$

$$s_i \left(\mathbb{1}^{\mathsf{T}} \mathbf{q}_{i,0}(\mathbf{x}_i) - \mathbf{q}_{i,0}^{\text{set}}(\mathbf{x}_{\mathsf{P}(i)})\right) \leq E_{i_\mathrm{q}} \tag{3.15d}$$

$$s_i \left(\mathbf{q}_{i,0}^{\text{set}}(\mathbf{x}_{\mathsf{P}(i)}) - \mathbb{1}^{\mathsf{T}} \mathbf{q}_{i,0}(\mathbf{x}_i)\right) \leq E_{i_\mathrm{q}} \tag{3.15e}$$

$$\mathbf{v}_i(\mathbf{x}_i) \leq \overline{\mathbf{v}}_i \tag{3.15f}$$

$$\underline{\mathbf{v}}_i \leq \mathbf{v}_i(\mathbf{x}_i) \tag{3.15g}$$

$$\mathbf{i}_i(\mathbf{x}_i) \leq \overline{\mathbf{i}}_i. \tag{3.15h}$$

The *regularized Lagrangian* function L_i^{r} of the problem (3.15) is given by

$$
\begin{aligned}
L_i^{\mathrm{r}}(\mathbf{x}_i, \mathbf{d}_i; \mathbf{x}_{\mathsf{P}(i)}) := \ & f_i(\mathbf{x}_i) \\
& + \lambda_i \left(s_i \left(\mathbb{1}^{\mathsf{T}} \mathbf{p}_{i,0}(\mathbf{x}_i) - \mathbf{p}_{i,0}^{\text{set}}(\mathbf{x}_{\mathsf{P}(i)})\right) - E_{i_\mathrm{p}}\right) \\
& + \mu_i \left(s_i \left(\mathbf{p}_{i,0}^{\text{set}}(\mathbf{x}_{\mathsf{P}(i)}) - \mathbb{1}^{\mathsf{T}} \mathbf{p}_{i,0}(\mathbf{x}_i)\right) - E_{i_\mathrm{p}}\right) \\
& + \eta_i \left(s_i \left(\mathbb{1}^{\mathsf{T}} \mathbf{q}_{i,0}(\mathbf{x}_i) - \mathbf{q}_{i,0}^{\text{set}}(\mathbf{x}_{\mathsf{P}(i)})\right) - E_{i_\mathrm{q}}\right) \\
& + \psi_i \left(s_i \left(\mathbf{q}_{i,0}^{\text{set}}(\mathbf{x}_{\mathsf{P}(i)}) - \mathbb{1}^{\mathsf{T}} \mathbf{q}_0(\mathbf{x}_i)\right) - E_{i_\mathrm{q}}\right) \\
& + \boldsymbol{\gamma}_i^{\mathsf{T}} \left(\mathbf{v}_i(\mathbf{x}_i) - \overline{\mathbf{v}}_i\right) + \boldsymbol{\nu}_i^{\mathsf{T}} \left(\underline{\mathbf{v}}_i - \mathbf{v}_i(\mathbf{x}_i)\right) \\
& + \boldsymbol{\zeta}_i^{\mathsf{T}} \left(\mathbf{i}_i(\mathbf{x}_i) - \overline{\mathbf{i}}\right) \\
& + \tfrac{r_i^{\mathrm{p}}}{2} \|\mathbf{x}_i\|_2^2 - \tfrac{1}{2} \mathbf{d}_i^{\mathsf{T}} \mathbf{R}_i^{\mathrm{d}} \mathbf{d}_i
\end{aligned}
\tag{3.16}
$$

where $\mathbf{d}_i = \mathsf{col}(\lambda_i, \mu_i, \eta_i, \psi_i, \boldsymbol{\gamma}_i, \boldsymbol{\nu}_i, \boldsymbol{\zeta}_i)$ is the vector of *dual variables*, $r_i^{\mathrm{p}} \geq 0$ is the primal regularization parameter, and

$$\mathbf{R}_i^{\mathrm{d}} = \mathrm{blkdiag}(r_{\lambda_i}, r_{\mu_i}, r_{\eta_i}, r_{\psi_i}, r_{\gamma_i} I, r_{\nu_i} I, r_{\zeta_i} I) \succeq 0 \tag{3.17}$$

are the dual regularization parameters, with some elements being diagonal matrices of appropriate dimensions. We refer to [37, 81] for extensive discussion on the theoretical and practical benefits of including regularization; for our purposes, these will be tuning parameters of the approach, and a systematic procedure for setting these parameters will be described in Section 3.4.3. Our proposed CA controller will operate online with a sampling period of $T_{\mathrm{s}} > 0$, and is outlined in Algorithm 1, where $\mathcal{P}_{\geq 0}$ denotes Euclidean projection of the argument onto the nonnegative orthant.

Algorithm 1 consists of several computationally straightforward steps and involves hierarchical interaction between the CAs. The dual variables $\mathbf{d}_i = \mathsf{col}(\lambda_i, \mu_i, \eta_i, \psi_i, \boldsymbol{\gamma}_i, \boldsymbol{\nu}_i, \boldsymbol{\zeta}_i)$ are internal states of the ith LC, and the dual update rules in Step 3 directly use the measurements $(\mathbf{v}_i, \mathbf{i}_i, \mathbf{p}_{i,0}, \mathbf{q}_{i,0})$ and the provided set-points $\mathrm{p}_{i,0}^{\mathrm{set}}$ and $\mathrm{q}_{i,0}^{\mathrm{set}}$ in what can be interpreted as a measurement-based gradient ascent step to maximize the Lagrangian (3.16). The update rules in Step 3 are parameterized by the controller gains

$$\boldsymbol{\alpha}_i \triangleq \mathrm{blkdiag}(\alpha_{\lambda_i}, \alpha_{\mu_i}, \alpha_{\eta_i}, \alpha_{\psi_i}, \alpha_{\gamma_i} I, \alpha_{\nu_i} I, \alpha_{\zeta_i} I), \tag{3.20}$$

which are tuning parameters; our theoretical results to follow will address the constraints on these gains, and a systematic tuning procedure will be provided in Section 3.4.3 for both the regularization parameters and the gains. Next, the new DER set-points $\mathbf{x}_i^+$ are computed by the LC by solving the local optimization problem in Step 4. Note that this local optimization can be equivalently written as

$$\begin{aligned} \mathbf{x}_i^+ = \underset{\mathbf{x}_i \in \boldsymbol{\mathcal{X}}_i}{\arg\min} \; f_i(\mathbf{x}_i) &+ \tfrac{r_i^{\mathrm{p}}}{2} \|\mathbf{x}_i\|_2^2 + (\lambda_i^+ - \mu_i^+) s_i \mathbb{1}^{\mathsf{T}} \mathbf{M}_i \mathbf{x}_i \\ &+ (\eta_i^+ - \psi_i^+) s_i \mathbb{1}^{\mathsf{T}} \mathbf{H}_i \mathbf{x}_i + (\boldsymbol{\gamma}_i^+ - \boldsymbol{\nu}_i^+)^{\mathsf{T}} \mathbf{A}_i \mathbf{x}_i + (\boldsymbol{\zeta}_i^+)^{\mathsf{T}} \mathbf{B}_i \mathbf{x}_i \end{aligned} \tag{3.21}$$

and thus requires knowledge of the sensitivity matrices $(\mathbf{A}_i, \mathbf{B}_i, \mathbf{M}_i, \mathbf{H}_i)$ from (3.7), but *does not* require the unknown load-dependent constants $(\mathbf{a}_i, \mathbf{b}_i, \mathbf{m}_i, \mathbf{h}_i)$. Finally, the updated set-points are transmitted to the child areas in Step 5.

Remark 3.3.2 (Unbalanced Per-Phase Implementation) *While the current algorithm (optimization problem) considers overall power tracking constraints, one can modify them to per-phase set-point tracking. The linear model in (3.7) models unbalanced distribution networks. Extending the algorithm to multi-phase tracking requires simple modification by expanding active and reactive power tracking in (3.9) to three constraints each (for three-phase set-points for example).*

Algorithm 1: LC Controller for ith CA

At each sampling time

[**Step 1**]: Receive set-points from LC of parent area $\mathsf{P}(i)$

$$\mathrm{p}_{i,0}^{\mathrm{set}}(\mathbf{x}_{\mathsf{P}(i)}) = T_i^{\mathrm{p}}\mathbf{x}_{\mathsf{P}(i)}, \quad \mathrm{q}_{i,0}^{\mathrm{set}}(\mathbf{x}_{\mathsf{P}(i)}) = T_i^{\mathrm{q}}\mathbf{x}_{\mathsf{P}(i)}.$$

[**Step 2**]: Collect local measurements $\mathbf{p}_{i,0}, \mathbf{q}_{i,0}, \mathbf{v}_i, \mathbf{i}_i, \boldsymbol{\mathcal{X}}_i$.

[**Step 3**]: LC performs the updates

$$\begin{aligned}
\lambda_i^+ &= \mathcal{P}_{\geq 0}\left(\lambda_i + \alpha_{\lambda_i}\left(\mathbb{1}^{\mathsf{T}}\mathbf{p}_{i,0} - \mathrm{p}_{i,0}^{\mathrm{set}} - E_{i_{\mathrm{p}}} - r_{\lambda_i}\lambda_i\right)\right), \\
\mu_i^+ &= \mathcal{P}_{\geq 0}\left(\mu_i + \alpha_{\mu_i}\left(\mathrm{p}_{i,0}^{\mathrm{set}} - \mathbb{1}^{\mathsf{T}}\mathbf{p}_{i,0} - E_{i_{\mathrm{p}}} - r_{\mu_i}\mu_i\right)\right), \\
\eta_i^+ &= \mathcal{P}_{\geq 0}\left(\eta_i + \alpha_{\eta_i}\left(\mathbb{1}^{\mathsf{T}}\mathbf{q}_{i,0} - \mathrm{q}_{i,0}^{\mathrm{set}} - E_{i_{\mathrm{q}}} - r_{\eta_i}\eta_i\right)\right), \\
\psi_i^+ &= \mathcal{P}_{\geq 0}\left(\psi_i + \alpha_{\psi_i}\left(\mathrm{q}_{i,0}^{\mathrm{set}} - \mathbb{1}^{\mathsf{T}}\mathbf{q}_{i,0} - E_{i_{\mathrm{q}}} - r_{\psi_i}\psi_i\right)\right), \\
\boldsymbol{\gamma}_i^+ &= \mathcal{P}_{\geq 0}\left(\boldsymbol{\gamma}_i + \alpha_{\gamma_i}\left(\mathbf{v}_i - \overline{\mathbf{v}}_i - r_{\gamma_i}\boldsymbol{\gamma}_i\right)\right), \\
\boldsymbol{\nu}_i^+ &= \mathcal{P}_{\geq 0}\left(\boldsymbol{\nu}_i + \alpha_{\nu_i}\left(\underline{\mathbf{v}}_i - \mathbf{v}_i - r_{\nu_i}\boldsymbol{\nu}_i\right)\right), \\
\boldsymbol{\zeta}_i^+ &= \mathcal{P}_{\geq 0}\left(\boldsymbol{\zeta}_i + \alpha_{\zeta_i}\left(\mathbf{i}_i - \overline{\mathbf{i}}_i - r_{\zeta_i}\boldsymbol{\zeta}_i\right)\right).
\end{aligned}$$

[**Step 4**]: LC updates (V)DER set-points

$$\mathbf{x}_i^+ = \underset{\mathbf{x}_i \in \boldsymbol{\mathcal{X}}_i}{\arg\min}\, L_i^{\mathrm{r}}(\mathbf{x}_i, \mathbf{d}_i^+; \mathbf{x}_{\mathsf{P}(i)})\,.$$

[**Step 5**]: Transmit set-points to LCs of each child area

$$\mathrm{p}_{j,0}^{\mathrm{set}}(\mathbf{x}_i^+) = T_j^{\mathrm{p}}\mathbf{x}_i^+, \quad \mathrm{q}_{j,0}^{\mathrm{set}}(\mathbf{x}_i^+) = T_j^{\mathrm{q}}\mathbf{x}_i^+, \qquad j \in \mathsf{C}(i).$$

3.3.4 Evaluation of Proposed Controller Against Distribution Level Controller Requirements

In this section, we summarize the key aspects of the proposed controller and evaluate it against the Distribution Level Controller requirements (D.R1)-(D.R4) identified earlier.

Key Features and Benefits of the Controller Architecture

The proposed controller architecture embodies several critical features designed to enhance the integration of DERs into the distribution network control:

(i) **Feedback-Based Optimization:** The LC controller directly uses real-time local measurements from the CA. This use of feedback allows the LC to react to unmeasured disturbances, and confers significant robustness against imperfections in knowledge of the sensitivity matrices $(\mathbf{A}_i, \mathbf{B}_i, \mathbf{M}_i, \mathbf{H}_i)$. Tuning selections which guarantee stability will be established in Section 3.4.2.

(ii) **Localized Control:** The design and online implementation of the controllers uses only local network information. Measurements of current, voltage, and power, local grid sensitivity matrices, and DER costs/limits are used locally within each CA by the LC; this information is not shared.

(iii) **Scalability:** All coordination between CAs occurs through the passing of set-points down through the feeder, from parent areas to child areas, as described in Section 3.2.1. This minimal coordination allows the architecture to be scalable to extremely large distribution systems. While in principle this scalability should result in a decrease in speed of the overall system compared to a centralized solution, our case studies in Section 3.6 indicates that this effect is indeed minor and can be overcome.

(iv) **Computational Burden:** The computation involved in Algorithm 1 is dominated by the set-point update in Step 4, which requires the solution of a local convex optimization problem. This is a centralized optimization problem for the LC to solve, which scales with the number of DERs to be controlled, and standard methods can be applied. For instance, if f_i is quadratic and the constraint set $\mathcal{X}_i$ is polytopic, then Step 4 is a quadratic program.

(v) **DMS and DERMS Coordination within Our Hierarchical Control Framework:** In the evolving landscape of power distribution systems, the proposed hierarchical structure aligns seamlessly with the distinct functionalities of Distribution Management System (DMS) and Distributed Energy Resource Management System (DERMS). The coordination between these modules is vital for effective management of DERs. The DERMS assumes a critical role in overseeing and managing DERs under its jurisdiction, responding to power requests from the DMS. Meanwhile, the DMS module associated with each CA accesses essential information such as

37

circuit model, measurements, and DER locations. However, detailed internal structures, operating limits, and specific models of DERs are intentionally withheld from the DMS. On the other hand, DERMS serves as the communication hub directly interfacing with DERs, equipped with comprehensive insights into their constraints, internal models, and communication requirements.

This collaborative framework enables the DMS to provide DERMSs with critical data, including DERs sensitivities and updated dual variables related to power tracking and circuit constraints. Subsequently, DERMS, armed with updated duals and DERs sensitivities received from DMS (without sharing circuit model or measurements), issues set-points to DERs in response. Within the proposed structure, each CA may be managed by a distinct stakeholder, equipped with their own DMS and DERMSs. additionally, DER service providers independent from stakeholders may have their own DERMS modules integrated with the CA's DMS. For further details on DERMS and DMS functionalities and their intricate coordination, refer to [82–84].

Evaluation Against Requirements

Now, we evaluate the proposed controller against the Distribution Level Controller Requirements described in Section 2.2:

- **Optimal Coordination (D.R1):** The proposed controller optimally coordinates DERs on a rapid time-scale, leveraging real-time data processing and localized decision-making to achieve comparable performance to transmission-connected resources (see Sections 3.4, 3.6 and 4.5).

- **Minimal Dependency on Detailed Models (D.R2):** By prioritizing local models and measurements, the controller reduces reliance on detailed system models, enhancing stability and resilience against model inaccuracies or changes within the distribution network. Additionally, leveraging feedback-based optimization allows the controller to dynamically adjust for real-time conditions, thereby increasing its robustness to model inaccuracies and its ability to effectively respond to unforeseen disturbances.

- **Utilization of Local Models and Measurements (D.R3):** The framework primarily utilizes local models, measurements, and communication. Each CA operates independently using local data such as current, voltage, power, grid sensitivity matrices, and DER costs and limits. This localized approach ensures cost-effective deployment and adaptability to varying operational needs and infrastructure capabilities.

- **Privacy and Operational Integrity (D.R4):** The design minimizes data sharing among stakeholders, maintaining privacy and operational integrity. The architecture does not require sharing detailed information across different control areas, thus preserving data and structural privacy while reducing dependencies on shared models and data.

The proposed control scheme meets and exceeds the stringent performance and practicality requirements considered for Distribution Level Controllers (D.R1)-(D.R4), providing an effective and scalable solution for the integration of DERs into the distribution network control framework.

3.4 Stability Analysis and Tuning of Proposed Algorithm

In this section, we perform a stability analysis of the proposed design from a control perspective, employing a state-space method. Specifically, we analyze the behavior of the closed-loop system by modeling the local controllers and their interactions within the distribution network using the linearized models.

To begin, let

$$\mathbf{y}_i = \mathsf{col}(\mathbf{p}_{0,i}, \mathbf{q}_{0,i}, \mathbf{v}_i, \mathbf{i}_i) \tag{3.22}$$

denote the vector of grid measurements taken by the ith LC, which are used within Algorithm 1. Recall that the linearized distribution system model (3.7) captures the *local* model of the grid within the ith CA, and the sensitivity matrices

$$\mathbf{K}_i \triangleq \mathsf{col}(\mathbf{M}_i, \mathbf{H}_i, \mathbf{A}_i, \mathbf{B}_i) \tag{3.23}$$

defined in (3.7) are used within Algorithm 1. This local model ignores the impacts of DER actions in *other* CAs. In contrast, the measurements (3.22), as they are generated by the real grid, will include these interactions. To capture this, we introduce a full linearized model of the feeder which relates all DER set-points $\mathbf{x} = \mathsf{col}(\mathbf{x}_1, \ldots, \mathbf{x}_N)$ to all area measurements $\mathbf{y} = \mathsf{col}(\mathbf{y}_1, \ldots, \mathbf{y}_N)$, as $\mathbf{y} = \mathbf{K}\mathbf{x} + \mathbf{k}$, or

$$\begin{bmatrix} \mathbf{y}_1 \\ \vdots \\ \mathbf{y}_N \end{bmatrix} = \begin{bmatrix} \mathbf{K}_{11} & \cdots & \mathbf{K}_{1N} \\ \vdots & \ddots & \vdots \\ \mathbf{K}_{N1} & \cdots & \mathbf{K}_{NN} \end{bmatrix} \begin{bmatrix} \mathbf{x}_1 \\ \vdots \\ \mathbf{x}_N \end{bmatrix} + \begin{bmatrix} \mathbf{k}_1 \\ \vdots \\ \mathbf{k}_N \end{bmatrix} \tag{3.24}$$

for appropriate matrices $\mathbf{K}_{ij}$ and vectors $\mathbf{k}_j$. Note that if the local sensitivity model (3.23) is accurate, then we expect that $\mathbf{K}_i \approx \mathbf{K}_{ii}$. The closed-loop control system now consists of Algorithm 1 for each CA $i \in \{1, \dots, N\}$ with the distribution system model (3.24).

For readers interested in a broader discussion of power system stability, including voltage and frequency stability, we recommend referring to the following resources: [85–88].

3.4.1 Equilibrium Analysis

As the controller of Algorithm 1 was developed beginning from the optimization problem (3.9), one should expect some relationship between the equilibrium points of the closed-loop system and the optimal points of the problems (3.9). We will show that the closed-loop equilibrium can be understood as the *Generalized Nash Equilibrium (GNE)* of a related set of game-theoretic optimization problems, one for each CA.[2]

When taking into account the full distribution system model (3.24), the optimization problems (3.9a) should be expressed together as the set of N decentralized decision problems

$$\mathbb{P}_i(\mathbf{x}_{-i}): \qquad \begin{aligned} &\inf_{\mathbf{x}_i \in \mathcal{X}_i} && f_i(\mathbf{x}_i) \\ &\text{subject to} && \mathbf{C}_i \mathbf{y}_i + \mathbf{b}_i + \mathbf{D}_i \mathbf{x}_{\mathsf{P}(i)} \leq 0 \end{aligned} \tag{3.25}$$

for $i \in \{1, \dots, N\}$, where $\mathbf{y}_i$ is determined by (3.24) and

$$\begin{aligned} \mathbf{b}_i &= -\mathsf{col}(E_{i_\mathrm{p}}, E_{i_\mathrm{p}}, E_{i_\mathrm{q}}, E_{i_\mathrm{q}}, \overline{\mathbf{v}}_i, -\underline{\mathbf{v}}_i, \overline{\mathbf{i}}_i), \\ \mathbf{C}_i &= \mathsf{blkdiag}\left(\begin{bmatrix} s_i \mathbb{1}^\mathsf{T} \\ -s_i \mathbb{1}^\mathsf{T} \end{bmatrix}, \begin{bmatrix} s_i \mathbb{1}^\mathsf{T} \\ -s_i \mathbb{1}^\mathsf{T} \end{bmatrix}, \begin{bmatrix} I \\ -I \end{bmatrix}, I\right), \\ \mathbf{D}_i &= \mathsf{col}(-s_i T_i^\mathrm{p}, s_i T_i^\mathrm{p}, -s_i T_i^\mathrm{q}, s_i T_i^\mathrm{q}, 0, 0, 0). \end{aligned} \tag{3.26}$$

In (3.25), the decisions of the other LCs $\mathbf{x}_{-i} = (\mathbf{x}_j)_{j \neq i}$ are interpreted as fixed. A *Generalized Nash Equilibrium (GNE)* is a collection of set-point decisions $(\mathbf{x}_1^\star, \dots, \mathbf{x}_N^\star)$ such that $\mathbf{x}_i^\star \in \arg\min_{\mathbf{x}_i} \mathbb{P}_i(\mathbf{x}_{-i}^\star)$ for all $i \in \{1, \dots, N\}$. Consider now the modified set of problems $\mathbb{P}_i'(\mathbf{x}_{-i})$ given by

$$\mathbb{P}_i'(\mathbf{x}_{-i}): \qquad \inf_{\mathbf{x}_i \in \mathcal{X}_i} \; f_i(\mathbf{x}_i) + \tfrac{r_i^\mathrm{p}}{2}\|\mathbf{x}_i\|_2^2 + \mathcal{M}_i(\mathbf{C}_i \mathbf{y}_i + \mathbf{b}_i + \mathbf{D}_i \mathbf{x}_{\mathsf{P}(i)}) \tag{3.27}$$

---

[2]While the equilibrium is best understood in game-theoretic terms, this *does not* imply that the CAs are in competition with one another, and indeed CAs cooperate within our scheme by accepting set-points from parents and sending set-points to children. The Nash equilibrium concept is the natural one due purely to the area-wise decentralized nature of the control system.

where again $\mathbf{y}_i$ is given by (3.24). Compared to the problems $\mathbb{P}_i(\mathbf{x}_{-i})$, in $\mathbb{P}'_i(\mathbf{x}_{-i})$ we have (i) introduced additional convexity into the objective function with the term $\frac{r_i^{\mathrm{p}}}{2}\|\mathbf{x}_i\|_2^2$, and (ii) *softened* the inequality constraints by replacing them with a differentiable quadratic penalty function $\mathcal{M}_i$, with penalty weights given by the inverse elements of $\mathbf{R}_i^{\mathrm{d}}$. For instance, the first component of $\mathcal{M}_i$ is

$$
\mathcal{M}_{i,1}(\xi_{i,1}) = \begin{cases} 0, & \xi_{i,1} \leq 0 \\ \frac{1}{2r_{\lambda_i}}|\xi_{i,1}|^2, & \xi_{i,1} > 0. \end{cases}
$$

When both r_i^{p} and $\mathbf{R}_i^{\mathrm{d}}$ are small, the problem (3.27) closely approximates the problem (3.25). While the details are beyond our scope here, if $\mathbf{K}_i = \mathbf{K}_{ii}$, then Algorithm 1 is precisely a measurement-based and decentralized dual gradient algorithm for computing a GNE of (3.27); see [89–91] for related game-theoretic online optimization concepts. In summary, and in rough terms, this means that each LC will make the best set-point decision that it can, given the limited information it has due to the decentralized control architecture.

Remark 3.4.1 (Nash Equilibria Vs. Generalized Nash Equilibria) *The distinction between Nash Equilibria (NE) and Generalized Nash Equilibria (GNE) lies in the dependency of each agent's strategy on the strategies of others. In a standard NE, each agent optimizes its own objective assuming the strategies of others are fixed. In contrast, a GNE accounts for the fact that each agent's feasible set may also depend on the strategies of others, making the GNE concept more suitable for problems where agents' decisions are coupled through shared constraints, as is the case in decentralized control systems [92, 93].*

3.4.2   Closed-Loop Stability Analysis

Section 3.4.1 interprets closed-loop equilibrium points as generalized Nash equilibria, but does not assert that an equilibrium point exists, nor whether it is stable; our main stability result addresses both of these items.

As notation, let $\boldsymbol{\alpha} = \mathrm{blkdiag}(\boldsymbol{\alpha}_1, \ldots, \boldsymbol{\alpha}_N)$ and similarly for block diagonal $\mathbf{C}, \mathbf{D}, \mathbf{R}^{\mathrm{d}}$, and let $\mathbf{K}_{\mathrm{d}} = \mathrm{blkdiag}(\mathbf{K}_1, \ldots, \mathbf{K}_N)$. Recall the adjacency matrix $\mathcal{A}$ of Section 3.2.1, and let $\boldsymbol{\mathcal{A}}$ denote an expanded version of this matrix, where each 1 or 0 becomes an identity matrix or zero matrix of appropriate dimension. Based on these, and on the previously

defined control parameters, define the constant $\mathsf{L} > 0$ and the matrix $\mathsf{M} \in \mathbb{R}^{N \times N}$ by

$$\mathsf{L} = \frac{\|\mathbf{R}^{\mathrm{d}}\|_2 + \|\mathbf{CK} + \mathbf{D}\boldsymbol{\mathcal{A}}^{\mathsf{T}}\|_2 \|\mathbf{K}_{\mathrm{d}}\|_2 \|\mathbf{C}\|_2}{\min_{i \in \{1,\dots,N\}}(m_i + r_i^{\mathrm{p}})},$$

$$\mathsf{M}_{ij} = \begin{cases} \|\mathbf{R}_i^{\mathrm{d}}\|_2 - \frac{\|\mathbf{K}_{ii} - \mathbf{K}_i\|_2}{m_i + r_i^{\mathrm{p}}}(\|\mathbf{D}_i\|_2 \|\mathbf{C}_i\|_2^2 \|\mathbf{K}_i\|_2), & i = j \\ -\frac{\|\mathbf{K}_{ij}\|_2}{m_j + r_j^{\mathrm{p}}}(\|\mathbf{C}_i\|_2 \|\mathbf{C}_j\|_2 \|\mathbf{K}_j\|_2) - N_{ij}, & i \neq j, \end{cases}$$

where $N_{ij} = \mathcal{A}_{ij} \|\mathbf{D}_i\|_2 \|\mathbf{C}_j\|_2 / (m_j + r_j^{\mathrm{p}})$. We can now succinctly state the main result.

Theorem 3.4.2 (Closed-Loop Stability) *Consider the closed-loop system consisting of Algorithm 1 for each CA $i \in \{1, \dots, N\}$ with the distribution system model (3.24). If $\mathsf{M} + \mathsf{M}^{\mathsf{T}} \succ 0$, then the closed-loop system possesses a unique equilibrium point $(\mathbf{x}_i^\star, \mathbf{d}_i^\star)_{i \in \{1,\dots,N\}}$, and the equilibrium is globally exponentially stable for all gain selections $\boldsymbol{\alpha} = \mathrm{blkdiag}(\boldsymbol{\alpha}_1, \dots, \boldsymbol{\alpha}_N)$ satisfying $\lambda_{\max}(\boldsymbol{\alpha})^2 / \lambda_{\min}(\boldsymbol{\alpha}) < \lambda_{\min}(\mathsf{M} + \mathsf{M}^{\mathsf{T}}) / \mathsf{L}^2$.*

Proof of Theorem 3.4.2: After eliminating the power set-points using (3.8), the dual update laws in Step 3 of Algorithm 1 for the ith CA can be compactly expressed as

$$\mathbf{d}_i^+ = \mathcal{P}_{\geq 0}\left(\mathbf{d}_i + \boldsymbol{\alpha}_i\left(\mathbf{C}_i\mathbf{y}_i + \mathbf{b}_i + \mathbf{D}_i\mathbf{x}_{\mathsf{P}(i)} - \mathbf{R}_i^{\mathrm{d}}\mathbf{d}_i\right)\right), \tag{3.28}$$

where $\mathbf{C}_i, \mathbf{D}_i, \mathbf{b}_i$ are as in (3.26) and $\boldsymbol{\alpha}_i, \mathbf{R}_i^{\mathrm{d}}$ are as in Section 3.3.3. With $\mathbf{d} = (\mathbf{d}_1, \dots, \mathbf{d}_N)$ the stacked vector of all dual variables for all CAs, we can express all updates together in vector form as

$$\mathbf{d}^+ = \mathcal{P}_{\geq 0}\left(\mathbf{d} + \boldsymbol{\alpha}(\mathbf{Cy} + \mathbf{D}\boldsymbol{\mathcal{A}}^{\mathsf{T}}\mathbf{x} - \mathbf{R}^{\mathrm{d}}\mathbf{d} + \beta\mathbf{X}_0^{\mathrm{set}}),\right) \tag{3.29}$$

Where $\beta = \mathrm{col}(I_2, \mathbb{0})$ (mapping feeder set-point to the first control area). Proceeding similarly, and using (3.23), the DER set-point update (3.21) can be compactly written as

$$\mathbf{x}_i^+ = \arg\min_{\mathbf{x}_i \in \boldsymbol{\mathcal{X}}_i} f_i(\mathbf{x}_i) + \frac{r_i^{\mathrm{p}}}{2}\|\mathbf{x}_i\|_2^2 + (\mathbf{d}_i^+)^{\mathsf{T}}\mathbf{C}_i\mathbf{K}_i\mathbf{x}_i. \tag{3.30}$$

The update (3.30) can be equivalently expressed as [94]

$$\mathbf{x}_i^+ = \nabla\mathbf{F}_i^*(-\mathbf{K}_i^{\mathsf{T}}\mathbf{C}_i^{\mathsf{T}}\mathbf{d}_i^+), \tag{3.31}$$

where $\mathbf{F}_i(\xi_i) = f_i(\xi) + \frac{r_i^{\mathrm{p}}}{2}\|\xi_i\|_2^2 + \mathbb{I}_{\boldsymbol{\mathcal{X}}_i}(\xi_i)$, with $\mathbb{I}_{\boldsymbol{\mathcal{X}}_i}(\xi_i)$ being the indicator function of the constraint set $\boldsymbol{\mathcal{X}}_i$ and $*$ denoting convex conjugation. By assumptions in Sections 3.2.2, 3.3.1 & 3.4, $\mathbf{F}_i$ is $(m_i + r_i^{\mathrm{p}})$-strongly convex, and hence $\mathbf{F}_i^*$ is continuously differentiable

42

and $\frac{1}{m_i+r_i^{\mathrm{p}}}$-strongly smooth [94]. With $\mathbf{K}_{\mathrm{d}} = \mathrm{blkdiag}(\mathbf{K}_1,\ldots,\mathbf{K}_N)$, the stacked vector of all set-point updates for all areas can then be written as

$$\mathbf{x}^+ = \nabla \mathbf{F}^*(-\mathbf{K}_{\mathrm{d}}^{\mathsf{T}}\mathbf{C}^{\mathsf{T}}\mathbf{d}^+), \tag{3.32}$$

where $\mathbf{F}(\boldsymbol{\xi}) = \sum_{i=1}^N \mathbf{F}_i(\xi_i)$. The closed-loop system is now described by the controller (3.29),(3.32) with the grid model (3.24). Eliminating $\mathbf{y}$ and $\mathbf{x}$, we obtain the simplified representation

$$\mathbf{d}^+ = \mathcal{P}_{\geq 0}\left(\mathbf{d} - \boldsymbol{\alpha}\boldsymbol{G}(\mathbf{d}) + \boldsymbol{\alpha}(\mathbf{C}\mathbf{k} + \beta\mathbf{X}_0^{\mathrm{set}})\right), \tag{3.33a}$$
$$\mathbf{G}(\mathbf{d}) \triangleq \mathbf{R}^{\mathrm{d}}\mathbf{d} - (\mathbf{C}\mathbf{K} + \mathbf{D}\boldsymbol{\mathcal{A}}^{\mathsf{T}})\nabla\mathbf{F}^*(-\mathbf{K}_{\mathrm{d}}^{\mathsf{T}}\mathbf{C}^{\mathsf{T}}\mathbf{d}). \tag{3.33b}$$

Let $\mathbf{E}_{ii} = \mathbf{K}_{ii} - \mathbf{K}_i$. Then we may write

$$\mathbf{K} = \mathbf{K}_{\mathrm{d}} + \begin{bmatrix} \mathbf{E}_{11} & \cdots & \mathbf{K}_{1N} \\ \vdots & \ddots & \vdots \\ \mathbf{K}_{N1} & \cdots & \mathbf{E}_{NN} \end{bmatrix} \triangleq \mathbf{K}_{\mathrm{d}} + \boldsymbol{\Delta}.$$

Now we write $\mathbf{G}(\mathbf{d}) = \sum_{k=1}^4 \mathbf{G}_k(\mathbf{d})$, where $\mathbf{G}_1(\mathbf{d}) = \mathbf{R}^{\mathrm{d}}\mathbf{d}$ and

$$\mathbf{G}_2(\mathbf{d}) = -\mathbf{C}\mathbf{K}_{\mathrm{d}}\nabla\mathbf{F}^*(-\mathbf{K}_{\mathrm{d}}^{\mathsf{T}}\mathbf{C}^{\mathsf{T}}\mathbf{d}),$$
$$\mathbf{G}_3(\mathbf{d}) = -\mathbf{C}\boldsymbol{\Delta}\nabla\mathbf{F}^*(-\mathbf{K}_{\mathrm{d}}^{\mathsf{T}}\mathbf{C}^{\mathsf{T}}\mathbf{d}),$$
$$\mathbf{G}_4(\mathbf{d}) = -\mathbf{D}\boldsymbol{\mathcal{A}}^{\mathsf{T}}\nabla\mathbf{F}^*(-\mathbf{K}_{\mathrm{d}}^{\mathsf{T}}\mathbf{C}^{\mathsf{T}}\mathbf{d}).$$

Let $\mathbf{d}, \mathbf{d}'$ be two dual vectors, and let $\delta_i(\mathbf{d},\mathbf{d}') = (\mathbf{d}-\mathbf{d}')^{\mathsf{T}}(\mathbf{G}_i(\mathbf{d}) - \mathbf{G}_i(\mathbf{d}'))$. Since $\mathbf{R}^{\mathrm{d}} \succ 0$ and $\nabla\mathbf{F}^*$ is monotone [94], we immediately have the bounds

$$\delta_1(\mathbf{d},\mathbf{d}') \geq \sum_{i=1}^N \|\mathbf{R}_i^{\mathrm{d}}\|_2\|\mathbf{d}_i - \mathbf{d}_i'\|_2^2, \quad \delta_2(\mathbf{d},\mathbf{d}') \geq 0.$$

For $\mathbf{G}_3$ and $\mathbf{G}_4$, using strong smoothness of $\mathbf{F}_i$ one quickly obtains the bounds

$$|\delta_3(\mathbf{d},\mathbf{d}')| \leq \sum_{i,j=1}^N \mathbf{Q}_{ij}\|\mathbf{d}_i - \mathbf{d}_i'\|_2\|\mathbf{d}_j - \mathbf{d}_j'\|_2,$$
$$|\delta_4(\mathbf{d},\mathbf{d}')| \leq \sum_{i,j=1}^N \tilde{\mathbf{Q}}_{ij}\|\mathbf{d}_i - \mathbf{d}_i'\|_2\|\mathbf{d}_j - \mathbf{d}_j'\|_2,$$

where $\mathbf{Q}, \tilde{\mathbf{Q}} \in \mathbb{R}_{\geq 0}^{N \times N}$ are defined element-wise as

$$\tilde{\mathbf{Q}}_{ij} = \begin{cases} \frac{\|\mathbf{C}_j\|_2 \|\mathbf{D}_i\|_2 \|\mathbf{K}_j\|_2}{m_j + r_j^{\mathrm{p}}}, & (i,j) \in \mathcal{E}_{\mathrm{CA}} \\ 0 & (i,j) \notin \mathcal{E}_{\mathrm{CA}} \end{cases}$$

$$\mathbf{Q}_{ij} = \begin{cases} \frac{\|\mathbf{C}_i\|_2^2 \|\mathbf{K}_{ii} - \mathbf{K}_i\|_2 \|\mathbf{K}_i\|_2}{m_i + r_i^{\mathrm{p}}}, & i = j \\ \frac{\|\mathbf{C}_i\|_2 \|\mathbf{C}_j\|_2 \|\mathbf{K}_{ij}\|_2 \|\mathbf{K}_j\|_2}{m_j + r_j^{\mathrm{p}}}, & i \neq j. \end{cases}$$

Putting things together, we obtain the lower bound

$$\delta(\mathbf{d}, \mathbf{d}') \geq \sum\nolimits_{i,j=1}^{N} \mathsf{M}_{ij} \|\mathbf{d}_i - \mathbf{d}_i'\|_2 \|\mathbf{d}_j - \mathbf{d}_j'\|_2,$$

where M is as defined in the theorem statement. Since $\mathsf{M} + \mathsf{M}^{\mathsf{T}} \succ 0$, it therefore holds that

$$\delta(\mathbf{d}, \mathbf{d}') \geq \tfrac{1}{2} \lambda_{\min}(\mathsf{M} + \mathsf{M}^{\mathsf{T}}) \|\mathbf{d} - \mathbf{d}'\|_2^2,$$

so we conclude that $\mathbf{G}$ is strongly monotone. One quickly observes that $\mathbf{G}$ is also Lipschitz continuous, with Lipschitz constant bounded by L as given in the theorem statement. By Theorem 12.1.2 in [95], it now follows that (3.33) possess a unique equilibrium point $\mathbf{d}^\star \geq 0$ and the equilibrium is globally exponentially stable if $\lambda_{\max}(\boldsymbol{\alpha})^2 / \lambda_{\min}(\boldsymbol{\alpha}) < \lambda_{\min}(\mathsf{M} + \mathsf{M}^{\mathsf{T}})/\mathsf{L}^2$, which completes the proof. $\square$

The diagonal elements of the matrix M can be interpreted as capturing the margin of "local" closed-loop stability for each CA, while the off-diagonal elements capture any potentially negative effects of interaction between the CAs. The stability condition $\mathsf{M} + \mathsf{M}^{\mathsf{T}} \succ 0$ then has the elegant interpretation that local stability should outweigh inter-area coupling. It is clear that this condition can *always* be satisfied by selecting sufficiently large values for the dual and primal regularization parameters $\mathbf{R}_i^{\mathrm{d}}$ and r_i^{p}, and that smaller values for these parameters are permissible if the local sensitivity mismatch $\|\mathbf{K}_{ii} - \mathbf{K}_i\|_2$ and the cross-area coupling $\|\mathbf{K}_{ij}\|_2$ are small. The gain restriction $\lambda_{\max}(\boldsymbol{\alpha})^2 / \lambda_{\min}(\boldsymbol{\alpha}) < \lambda_{\min}(\mathsf{M} + \mathsf{M}^{\mathsf{T}})/L^2$ states that one can obtain a stable tuning by starting $\boldsymbol{\alpha}$ small and slowly increasing. Further details on tuning will be presented next.

Remark 3.4.3 (Nonlinear System Dynamics & Stability) *Theorem 3.4.2 is based on the linearized system model* (3.24), *which may lose accuracy in heavily loaded feeders due to power flow and load non-linearity. For such cases, low controller gains are recommended to mitigate the impact of these non-linearities. A nonlinear stability analysis using robust control tools from [96] appears feasible and is considered for future work.* $\square$

3.4.3 Practical Tuning Guidelines

Before moving to our case studies, we provide practical guidelines for tuning the parameters in Algorithm 1. Each LC must set the following parameters, which can be systematically tuned, as follows:

Sampling period T_s

The sampling period is mainly constrained by the quality and speed of the communication infrastructure; see [97, 98] for discussion on communication technologies and standards. As is the case in all digital control systems, lower sampling periods are preferred.

Cost functions $f_{ij}(x_j)$

The DERs and VDERs cost functions will determine the relative steady-state allocation of control actions to DERs by the LC. The LC manager can set these costs to preferentially use or discourage certain DERs based on any desired operational criteria, e.g., speed of response, or to introduce different marginal costs for high vs. low utilization of a DER. As mentioned previously, for VDERs the selection (3.11) will mimic the case of a single grid-wide centralized dispatch.

Tracking Tolerances E_{i_p} and E_{i_q}

These tolerances should be set based on desired set-point tracking accuracy at the feeder head. Due to the constraint-softening effects of regularization (Section 3.4.1), tightening of these tolerances may be beneficial.

Regularization parameters r_i^p and $\mathbf{R}_i^\mathrm{d}$

From the result of Theorem 3.4.2, larger values of regularization parameters help ensure closed-loop stability. Conversely though, from the discussion in Section 3.4.1, larger regularization parameters lead to softer enforcement of voltage, current, and tracking constraints. Thus, there is a trade-off; these parameters should be large enough to ensure stability, but small enough to ensure minimal or no constraint violation. From (3.17), setting $\mathbf{R}_i^\mathrm{d}$ means setting 7 parameters for each CA. To simplify this, we express these 7 parameters as multiples of a single constant $\tilde{r}_i^\mathrm{d} > 0$, as shown in the third column of Table 3.1; the constants

$(c_{\lambda,i}, c_{\mu,i}, \ldots)$ are unit conversions and are shown in the third column of Table 3.2. For each LC, the only regularization parameters to set are now $\tilde{r}_i^{\mathrm{d}}$ and r_i^{p}; these values can always be initialized for stability based on Theorem 3.4.2 and then decreased if voltage/current constraint violation is observed.

Dual Step Sizes α

The step sizes $\boldsymbol{\alpha}$ control how aggressively each LC reacts to constraint violations, and can be thought of as integral control gains. From (3.20), each LC has 7 such gains to set, and it is again helpful to express all gains as multiples of a single dimensionless constant $\alpha_i > 0$, as shown in the second column of Table 3.1; the constants $(a_{\lambda,i}, a_{\mu,i}, \ldots)$ are shown in the second column of Table 3.2. This reduces the gain tuning to a single parameter α_i; following Theorem 3.4.2, we recommend that one slowly increases α_i to ensure stability. The constants $(a_{\lambda,i}, a_{\mu,i}, \ldots)$ are fixed based on unit conversions, but are further adjusted to reflect the relative dynamic importance of voltage/current limits, and power tracking constraints in implementation (see Sections 3.6.1-3.6.3). In particular

(i) the constants $(a_{\boldsymbol{\gamma},i},\ a_{\boldsymbol{\nu},i})$ associated with voltage constraints have been made larger compared to constant $(a_{\boldsymbol{\zeta},i})$ associated with current constraints; this ensures voltage constraints are quickly maintained, as transient violation of currents above their steady-state limits is acceptable over time-frames of $\sim 10 - 20$s.

(ii) the constants $(a_{\lambda,i},\ a_{\mu,i})$ associated with active power tracking have been made larger compared to the constants $(a_{\eta,i},\ a_{\psi,i})$ associated with reactive power tracking. This prioritizes fast active power tracking, and minimizes transient voltage fluctuations, particularly in CAs deeper within the network.

3.5   MATDSS

MATDSS Application is a MATLAB$^{\circledR}$-based tool that seamlessly integrates with OpenDSS$^{\circledcopy}$ [99], a specialized standalone application for distribution network simulations[3]. OpenDSS$^{\circledcopy}$

---

[3]OpenDSS$^{\circledcopy}$is an established electric power distribution system simulation tool. It supports multi-phase unbalanced simulations, uses a nonlinear power flow solver, and includes nonlinear load models, making it particularly suitable for realistic distribution network simulation [99].

Table 3.1: Dual variables step-sizes and regularization parameters; units of the scaling coefficients can be inferred from Algorithm 1.

Controller State (unit)	Gain	Regularization
λ_i (W)	$\alpha_{\lambda,i} = a_{\lambda,i}\alpha_i$	$r_{\lambda,i} = c_{\lambda,i}\tilde{r}_i^{\mathrm{d}}$
μ_i (W)	$\alpha_{\mu,i} = a_{\mu,i}\alpha_i$	$r_{\mu,i} = c_{\mu,i}\tilde{r}_i^{\mathrm{d}}$
η_i (Var)	$\alpha_{\eta,i} = a_{\eta,i}\alpha_i$	$r_{\eta,i} = c_{\eta,i}\tilde{r}_i^{\mathrm{d}}$
ψ_i (Var)	$\alpha_{\psi,i} = a_{\psi,i}\alpha_i$	$r_{\psi,i} = c_{\psi,i}\tilde{r}_i^{\mathrm{d}}$
$\boldsymbol{\gamma}_i$ $\left(\frac{\mathrm{W}^2}{\mathrm{V}}\right)$	$\alpha_{\boldsymbol{\gamma},i} = a_{\boldsymbol{\gamma},i}\alpha_i$	$r_{\boldsymbol{\gamma},i} = c_{\boldsymbol{\gamma},i}\tilde{r}_i^{\mathrm{d}}$
$\boldsymbol{\nu}_i$ $\left(\frac{\mathrm{W}^2}{\mathrm{V}}\right)$	$\alpha_{\boldsymbol{\nu},i} = a_{\boldsymbol{\nu},i}\alpha_i$	$r_{\boldsymbol{\nu},i} = c_{\boldsymbol{\nu},i}\tilde{r}_i^{\mathrm{d}}$
$\boldsymbol{\zeta}_i$ $\left(\frac{\mathrm{W}^2}{\mathrm{A}}\right)$	$\alpha_{\boldsymbol{\zeta},i} = a_{\boldsymbol{\zeta},i}\alpha_i$	$r_{\boldsymbol{\zeta},i} = c_{\boldsymbol{\zeta},i}\tilde{r}_i^{\mathrm{d}}$

Table 3.2: Default configurations for LC controllers.

Parameter	Value	Parameter	Value	Parameter	Value
α_i	0.002	$a_{\lambda,i}$	10^3	$c_{\lambda,i}$	10^{-3}
r_i^{p}	10^{-4}	$a_{\mu,i}$	10^3	$c_{\mu,i}$	10^{-3}
$\tilde{r}_i^{\mathrm{d}}$	10^{-3}	$a_{\eta,i}$	10^3	$c_{\eta,i}$	10^{-3}
$E_{i_{\mathrm{p}}}$	100W	$a_{\psi,i}$	10^3	$c_{\psi,i}$	10^{-3}
$E_{i_{\mathrm{q}}}$	100Var	$a_{\boldsymbol{\gamma},i}$	$10^{12}\frac{\mathrm{W}^2}{\mathrm{V}^2}$	$c_{\boldsymbol{\gamma},i}$	$10^{-12}\frac{\mathrm{V}^2}{\mathrm{W}^2}$
$\overline{\mathbf{v}}_i$	1.05p.u.	$a_{\boldsymbol{\nu},i}$	$10^{12}\frac{\mathrm{W}^2}{\mathrm{V}^2}$	$c_{\boldsymbol{\nu},i}$	$10^{-12}\frac{\mathrm{V}^2}{\mathrm{W}^2}$
$\underline{\mathbf{v}}_i$	0.95p.u.	$a_{\boldsymbol{\zeta},i}$	$10^7\frac{\mathrm{W}^2}{\mathrm{A}^2}$	$c_{\boldsymbol{\zeta},i}$	$10^{-7}\frac{\mathrm{A}^2}{\mathrm{W}^2}$

provides an engine that interfaces with MATLAB®via a COM interface [99], enabling efficient communication between the two platforms.

The development of MATDSS was driven by two main challenges. Firstly, the control framework developed for this research resulted in a highly complex system with numerous parameters to manage. Handling these parameters within the code proved difficult, and monitoring the system's performance during simulations was nearly impossible. MATDSS addresses this by providing a graphical user interface (GUI) that allows for live monitoring, parameters management, and the ability to enable different components (such as low-pass filters, PD control and disturbances). In addition, MATDSS allows for modifying control parameters, and plotting outputs for control areas and DERs directly within the application. A standout feature of MATDSS is its ability to partition a feeder without

altering the simulation files of OpenDSS$^{\copyright}$, thereby managing control actions and time-series simulations from within the same application.

Secondly, while OpenDSS$^{\copyright}$is recognized as a standard solver for distribution systems, it lacks built-in time-series simulations for controlled structures like the ones proposed in this research. Integrating OpenDSS$^{\copyright}$with MATLAB$^{\circledR}$was essential to conduct these simulations and verify the presented work. This integration allows the framework to be easily adapted for different circuits and scales to control multiple areas within a feeder, as demonstrated with the IEEE-8500 simulation involving 49 control areas (see Section 3.6).

MATDSS serves as a core platform available for researchers to link MATLAB$^{\circledR}$and Simulink with OpenDSS$^{\copyright}$, providing a foundation for further development and integration of advanced control structures with distribution networks. The Application primarily focuses on modeling distribution network feeders within MATLAB$^{\circledR}$using OpenDSS$^{\copyright}$solver engine. It manages the dynamics and time-series simulations, transmitting updates to OpenDSS$^{\copyright}$for circuit components as they occur. The simulations presented in this thesis utilize MATDSS Application V0.92 and V0.94 with OpenDSS$^{\copyright}$V9.6.1.3.

MATDSS facilitates the import of existing OpenDSS$^{\copyright}$distribution feeders or the creation of new feeders through OpenDSS$^{\copyright}$scripts. The software is available at [100]. In the following subsections, we outline the key functionalities of MATDSS Application and provide a succinct overview of its user interface.

3.5.1 MATDSS Key Features

MATDSS Application was developed to ease the integration of MATLAB$^{\circledR}$with OpenDSS$^{\copyright}$, especially for implementing complex control architectures such as the one described in previous sections. The development process focused on the following key features:

- **Modular Functions**: Allows extensive modification and overriding of default characteristics, enhancing adaptability for advanced control schemes.

- **Feeder Structure and Control Areas**: Supports partitioning feeders into multiple control areas and saving customized structures for easy access and modification.

- **DER and LC Configurations**: Provides comprehensive control over DER and LC configurations, including advanced control features like PID and low-pass filtering.

- **Simulation Setup Data**: Pre-defines simulation variables and parameters for quick recall, significantly reducing simulation setup time.

- **Additional features**: Provides precise control over time configuration, real-time monitoring, customizable plotting, and export functions for comprehensive simulation analysis.

Modular Functions

MATDSS allows for extensive modification and overriding of default characteristic, enhancing adaptability. For instance, users can easily modify or include multiple models of DERs dynamic behavior by updating `MATDSS_DERUpdate.m`. This modular approach empowers researchers and engineers to implement advanced control schemes and simulations efficiently.

Feeder Structure and Control Areas

Using OpenDSS engine, MATDSS is compatible with all pre-defined feeders in the OpenDSS$^{©}$ library. Moreover, the application allows partitioning the feeder structure into multiple control areas, facilitating easy manipulation of the structures. These customized structures are saved in `xlsx` spreadsheets for convenient access from outside the application. MATDSS can read modified spreadsheets and update the setup accordingly, ensuring seamless integration and efficient workflow management.

DERs and LCs Configurations

MATDSS provides comprehensive control over DERs and LCs configurations, aligning with the setup discussed in Sections 3.3-3.4. It offers default values for newly defined DERs and LCs according to Tables 3.2 and 3.3. Additionally, the application allows for selecting branch currents and voltage phases that are monitored and controlled, automatically allocating them to their respective local controllers. Advanced control features such as PID and low-pass filtering (to be described in Section 3.6.1) are also included.

Simulation Setup Data

The pre-definition of *Simulation Setup Data* allows the application to generate all necessary simulation variables and parameters including sensitivity matrices, states and parameters of local controllers, configurations of DERs, simulation time settings, and disturbances. Users can swiftly recall this information before initiating a new simulation, significantly reducing the setup time. This feature proves particularly advantageous for large distribution feeders

with multiple control areas, where for IEEE-8500 feeder, the initialization of simulation setup for the 49 CAs structure typically takes 7 to 10 minutes. With MATDSS, the recall process merely takes 1 minute, leading to significantly faster experience.

Experiment Setup, Time Configuration, Real-time monitoring and Simulation Output Visualization and Export

MATDSS GUI features an intuitive design, providing the users with the flexibility to swiftly switch between different OpenDSS circuits. It allows for precise control over time-configuration for the simulation and control. Users can adjust controller time-steps and simulation times-steps to accommodate dynamic DERs response, if necessary.

Moreover, MATDSS enables real-time monitoring of DERs response, in addition to control areas' powers, voltages and currents along with their associated dual variables. The program offers a customizable plotting functionality that enhances the visualization experience. Users can select specific variables to be plotted, and the plotting environment dynamically updates accordingly. Additionally, the plots include legends describing the curves being displayed, which enhances clarity and interpretation.

Furthermore, MATDSS includes an export function that saves comprehensive information about the simulation run. This includes all parameters and configurations considered during the simulation, as well as any generated plots within the application. This feature facilitates accessible analysis of the output results, enabling users to review and interpret simulation data with ease.

3.5.2 MATDSS Application GUI

In this section, we provide a brief description of the GUI of MATDSS Application V0.92. In Figure 3.4, the main MATDSS Application window is shown. The main window contains a list of available OpenDSS files in the default directory. The main center block is occupied by a tab group that contains the simulation plots, configurations and OpenDSS file editor. The plot settings are controllable once the simulation is complete, and by selecting multiple entries, the plot is updated accordingly. The Application has a console that updates the user with the current status and what the program is calculating during the simulation process. In addition, a status bar is located at the bottom that shows the current functionality that program is performing. A progress meter is located at the bottom right to inform the user of the current progress percentage during the simulation. During simulation run time, the

focus is set automatically to the DER status tab, which displays live updates about the performance of the DERs while the simulation is running.
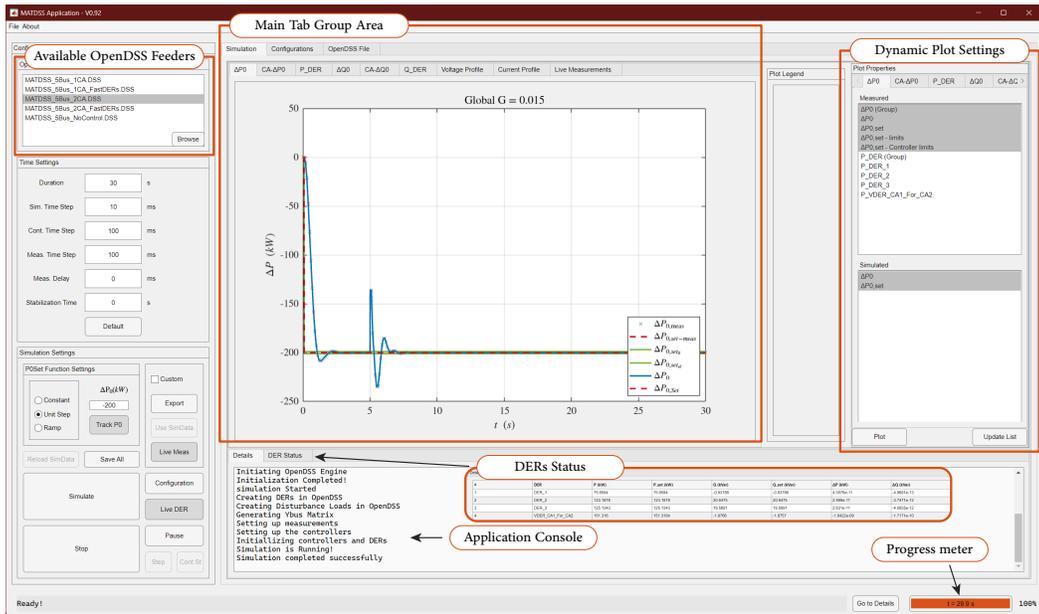
Figure 3.4: MATDSS Application Main Window.

Moving to the configuration tab, a sub tab-group is shown where the feeder configuration is set. The first tab within this group is the DERs configurations. Here, the table shows the parameters set for the DERs and their types (where one can predefine the models and the characteristics of the DERs beforehand), see Figure 3.5. The GUI allows for adding new or deleting DERs by selecting them and clicking on the button accordingly. Once the DERs are set and defined, the user can click on `Save` button to save the current table (or update the saved one) in Excel Configuration files. Clicking `Save All` would save all updated configurations from all tabs to the corresponding Excel files. The function would update existing tables in Excel or create new spreadsheets if the configurations are for a new feeder. The `Load Configs.` button loads saved configurations of the selected OpenDSS file, if available. The Console updates the user about the loading progress, and if successful, the tables in all configuration tabs are updated[4]. At the bottom, the global controller gain can be set, along with a table of custom disturbances that can be defined and set to be connected for a window of time.

---

[4]The 'Advanced Control' tab is not included yet in the save and load feature.

51
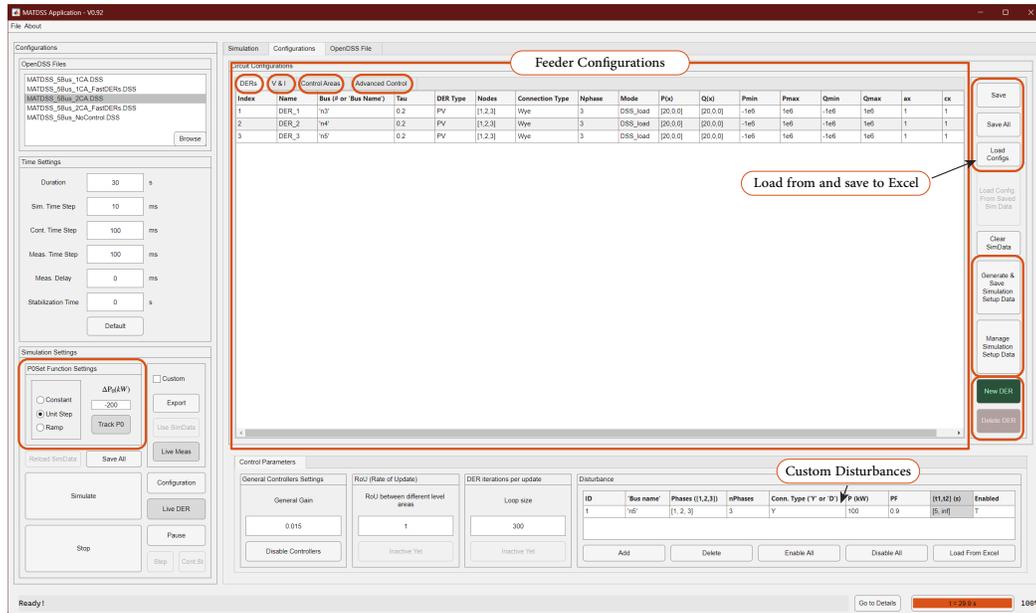
Figure 3.5: MATDSS Application Configuration Tab group and DERs configuration table.

Lastly, on the right side, there are two buttons `Generate and Save Simulation Setup Data` and `Manage Simulation Setup Data` that are concerned with generating a variable called `SimData` that contains all required variables for the simulations and parameters, including sensitivity matrices, control areas, and controllers states and related variables. The latter, when clicked, opens a `SimData` viewer that shows the available `mat` files and displays a summary of the configurations saved, see Figure 3.6. Loading saved simulation setup can speed up the initialization process, as the setup of the control structure is fixed for a system when tuning is in progress, or for different simulation cases.

The `V & I` tab lists available phases and branches for control. Selecting (by highlighting) a phase or branch instructs the corresponding local controller to monitor and control the corresponding voltage/current. Figure 3.7 shows the V & I configuration tab where some branches and phases are selected.

Control Areas tab is the one concerned with control areas definition, local controllers' configurations and VDERs setup, see Figure 3.8. The parameters shown are based on the setup discussed before in Sections 3.3-3.4.

52
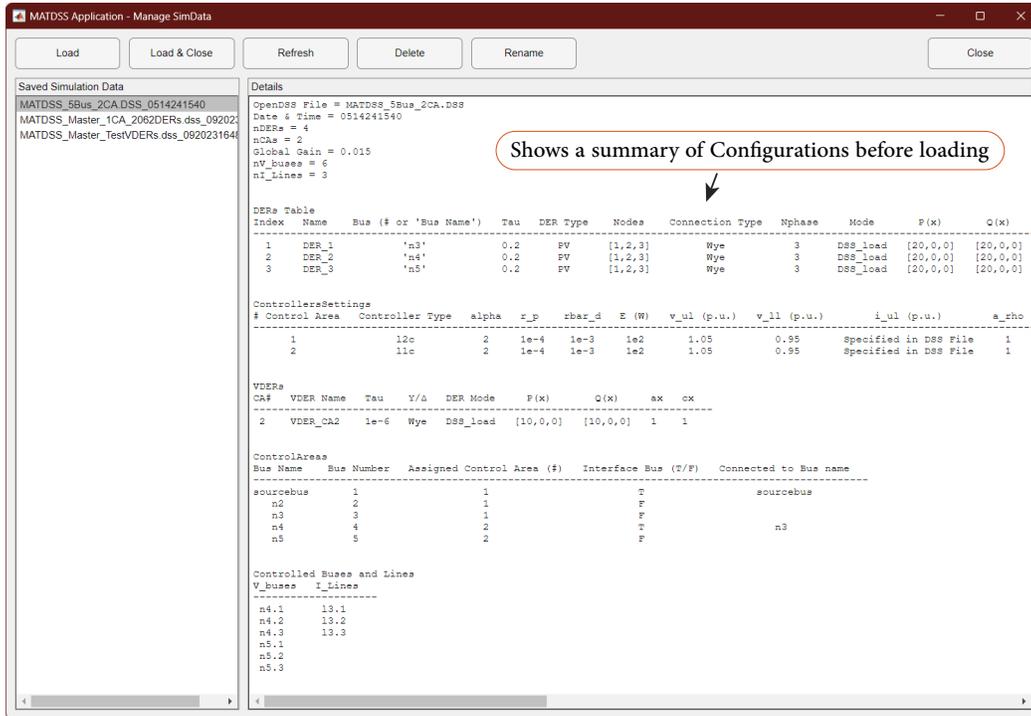
Figure 3.6: MATDSS Application - `SimData` management window.
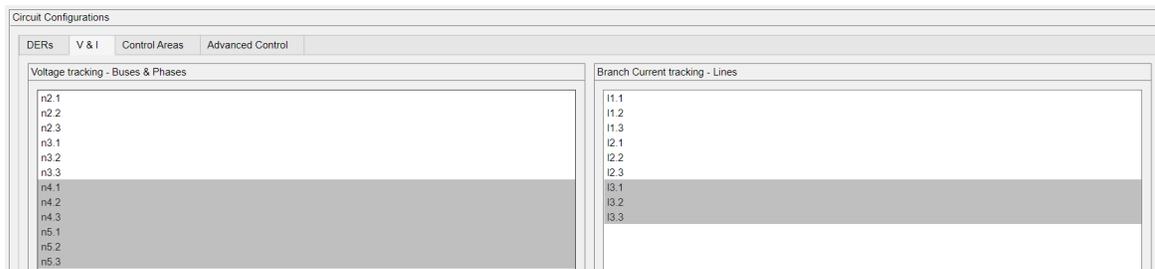
Figure 3.7: MATDSS Application V & I configuration tab.

Figure 3.8: MATDSS Application Control Areas Configuration Tab.

Lastly, Figure 3.9 shows the advanced control tab, which contains the optional setup and configurations for the low-pass filter (LPF), and the additional PD controllers.
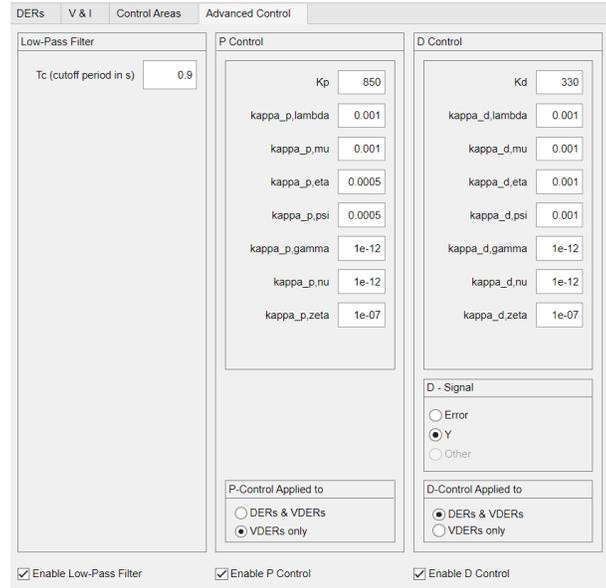
Figure 3.9: MATDSS Application optional configurations for low-pas filter and PD controllers
.

OpenDSS File tab is the last tab in the main tab group of the main window and displays the main OpenDSS script, see Figure 3.10. The text editor allows for direct changes to be made to the OpenDSS script and saving the edits. The file needs to be saved to reflect the changes when calling OpenDSS solver as it reads the file separately.

3.6 Case Studies

We present three case studies of increasing complexity to illustrate and validate the proposed design: (1) a simple 5 bus feeder, (2) the IEEE-123 bus feeder, and (3) the IEEE-8500 bus feeder. The simple 5-bus feeder will be used to demonstrate the basic functionality of the controller, including how CAs and LCs interact with one another; the latter two test systems will demonstrate scalability of the approach.

The tests were run using the customized application, MATDSS V0.92. The feeders are defined using OpenDSS Scripting Language, with the IEEE-123 and IEEE-8500 feeders
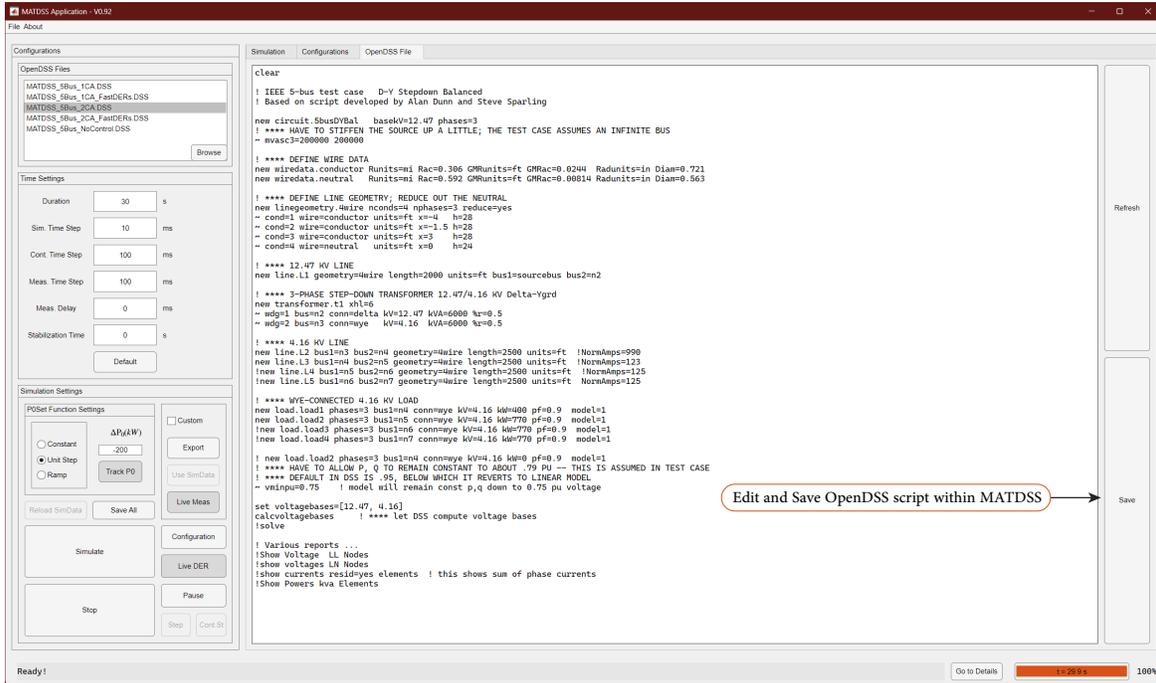
Figure 3.10: MATDSS Application OpenDSS script editor.

receiving minor modifications from their original versions in OpenDSS$^{©}$; see Appendix B for details on these modifications. We set all LCs control parameters to the nominal values in Table 3.2, unless specified otherwise; current limits vary by line. For current control examples, we report the limits considered. Controllable DERs are integrated throughout the test systems. As our only requirement is that these DERs are responsive to dispatch commands, the internal dynamics and specific nature of the DERs are of secondary importance; each DER is modelled as having a first-order response to power commands with time constant τ; more detailed DER models with internal controls can be easily integrated within MATDSS, see [100, 101]. All DER power limits are box constraints $\mathcal{X}_j = [\underline{x}_j, \overline{x}_j]$; see Table 3.3.

Table 3.3: DER's Default parameters.

Parameter	Value	Parameter	Value
τ_j	0.2s	C_j'', C_j'	$\mathsf{diag}(20, 20)$, $(0, 0)$
$\underline{x}_j$	$(-10^6\mathrm{W}, -10^6\mathrm{Var})$	$\overline{x}_j$	$(10^6\mathrm{W}, 10^6\mathrm{Var})$

56

Each test system is divided into CAs. Our design will be compared and contrasted with a baseline centralized controller, labelled 1CA, which is a 1-area implementation of our hierarchical controller, acting with global information to control *all* DERs within the feeder; this serves as a "best case" against which to compare our hierarchical design. For all feeders, we consider the case where the TSO request is of the form $X_0^{\text{set}} = (\text{p}_0^{\text{set}}, 0)$, i.e., active power tracking at the DN-TN interface. The sampling time of the controller is set as $T_s = 100\text{ms}$. Throughout the tests and for all controllers, we set $r_i^{\text{p}} = 10^{-4}$, $\tilde{r}_i^{\text{d}} = 10^{-3}$, and $\alpha_i = 0.002$, and we set the corresponding gains as in Table 3.2. With these regularization parameters, for tracking within $\pm 1\text{kW}$ for $\text{p}_{i,0}^{\text{set}}$, we tighten the power tracking constraints and set $E_{i_{\text{p}}} = 100\text{W}$ and $E_{i_{\text{q}}} = 100\text{Var}$. Appendix B lists all MATDSS related configurations used for the simulation runs shown here.

Remark 3.6.1 (Synchronous CAs) *We consider synchronous controllers where all LCs use the same sampling time; however, the framework does not require the nested controllers to wait for updated set-points from their parent LCs. Each controller considers the last set-point when updated set-point is not provided, and utilize feedback measurements to control the DERs within the CA.* $\qquad\square$

3.6.1 5-Bus Feeder

Consider the three-phase 5-bus feeder of Figure 3.11, which has been partitioned into two CAs. Within the feeder, three DERs are placed at buses n3, n4 and n5, with a VDER added to CA1, representing the LC in CA2. There are two loads of 400kW and 770kW with power factor of 0.9 at buses n4 and n5, respectively. The purpose of our test here is to illustrate the basic behaviour and response of the controller.
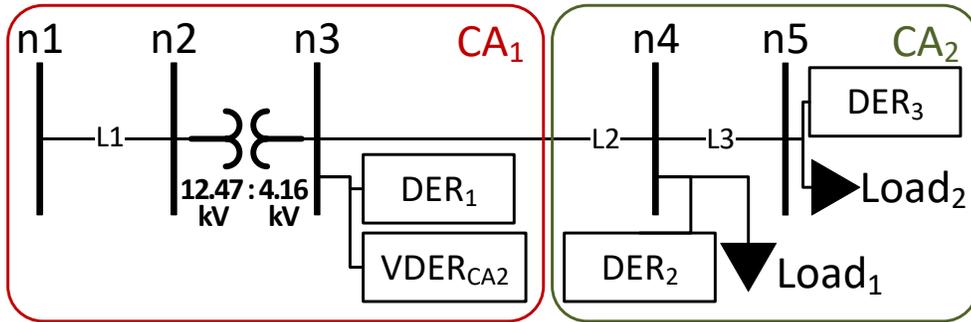

Figure 3.11: Three phase 5-Bus feeder circuit.

A reference change of 200kW is requested at the feeder head at $t = 0$, and a load change (disturbance) of 100kW (0.9pf) at $t = 5$s located at bus n5. The change in power at the feeder head serves as a metric to gauge the tracking performance of the controllers. Simultaneously, the response to disturbances provides insights into how both centralized and decentralized controllers effectively manage local constraints and disturbances. The power response at the feeder head is shown in Figure 3.12a, which as discussed plots both a hierarchical two-CAs and a centralized one-CA implementation. The figure shows the change in power flow at the *interface bus* of the feeder head across all phases, i.e., $\Delta p_0 = \Delta \mathbb{1}^\mathsf{T} \mathbf{p}_{1,0}$.

The multi-area implementation (2CAs) shows a more sluggish response compared to the centralized implementation (1CA). While not covered by our theory, we have found this sluggishness can be overcome by (i) incorporating proportional and derivative (PD) control action into the LC controller, and (ii) passing the control signal for VDERs through a Low-pass Filter (LPF). To explain the first modification, consider the λ_i update in Algorithm 1. This can be viewed as integral-type controller $\lambda_i^+ = \mathcal{P}_{\geq 0}(\lambda_i + \alpha_{\lambda_i} e_{\lambda_i})$ acting on the error $e_{\lambda_i} := \mathbb{1}^\mathsf{T} \mathbf{p}_{i,0} - \mathrm{p}_{i,0}^{\mathrm{set}} - E_{i_\mathrm{p}} - r_{\lambda_i} \lambda_i$. Let $\mathbf{e}_i$ denote the stacked vector of all these errors. Incorporating PD action alongside this integral controller can accelerate the overall response time. This is done by modifying Step 4 in Algorithm 1, wherein the argument $\mathbf{d}_i^+$ is replaced by $\tilde{\mathbf{d}}_i^+$, where

$$\tilde{\mathbf{d}}_i^+ = \mathbf{d}_i^+ + \kappa_\mathrm{p} \mathbf{e}_i + \kappa_\mathrm{d}(\mathbf{y}_i - \mathbf{y}_i^-),$$

where $\mathbf{y}_i = \mathsf{col}(\mathbb{1}^\mathsf{T} \mathbf{p}_{i,0}, -\mathbb{1}^\mathsf{T} \mathbf{p}_{i,0}, \mathbb{1}^\mathsf{T} \mathbf{q}_{i,0}, -\mathbb{1}^\mathsf{T} \mathbf{q}_{i,0}, \mathbf{v}_i, -\mathbf{v}_i, \mathbf{i}_i)$ is the stacked vector of raw measurements, and κ_p and κ_d are diagonal matrices of proportional and derivative gains. We have found that derivative action need only be used for VDERs. The second modification, a low-pass filter, is used to eliminate the passing of aggressive control actions down through VDERs, which allows higher level controllers to use larger integral gains. After Step 4 of Algorithm 1, the VDER set-points are passed through a low-pass filter before being sent to the child areas. See Appendix B for details on tuning of the proportional-derivative gains and low-pass filter time constants.

Returning now to Figure 3.12, the $\mathrm{2CA_{LPF-PID}}$ curve shows the response of the 2CAs structure with PID controllers and LPF filtering. With this implementation, one can achieve tracking results similar to single-area system (1CA) in terms of power set-points while preserving data privacy and maintaining a hierarchical control structure. The settling time after the step change was 1.07s for 1CA, 1.78s for 2CA, and 1.02s for 2CA with PID controllers and LPF filter. Note that the disturbance at $t = 5$s, which occurs in the child area, is quickly rejected by both the 1CA and 2CAs implementations.

Figure 3.12b plots the active power responses of the three DERs during the test. Notably, both 1CA and 2CAs (LPF $-$ PID) implementations exhibited similar settling times and

DER participation when responding to the initial step-change. Importantly however, when compensating for the disturbance at $t = 5$s located at bus n5, the 1CA and 2CA implementations behave differently. In the 2CAs implementation, the disturbance was regarded as local perturbation within CA2, and consequently, only DER_2 and DER_3 were responsible for providing compensation. In contrast, the 1CA implementation re-dispatched all DERs to mitigate the disturbance. In subsequent plots and tests, all multi-CA implementations will include PID action and low-pass filters, and we drop the 'LPF $-$ PID' annotation.

The dashed lines in Figure 3.13 show the voltage at bus n4 and the current on line L3 during the test; with voltage limits set to their nominal values and current limit of 135A. To illustrate how effectively the controllers maintain local circuit constraints, we tighten the voltage and current constraints to $\overline{\mathbf{v}} = 0.974$p.u. and $\overline{\mathbf{i}} = 123$A, and repeat the test, with results plotted in solid lines. Both configurations, 1CA and 2CA, showed similar response and enforced the operational constraints in equilibrium. For details on the controller gain settings, please refer to Appendix B.
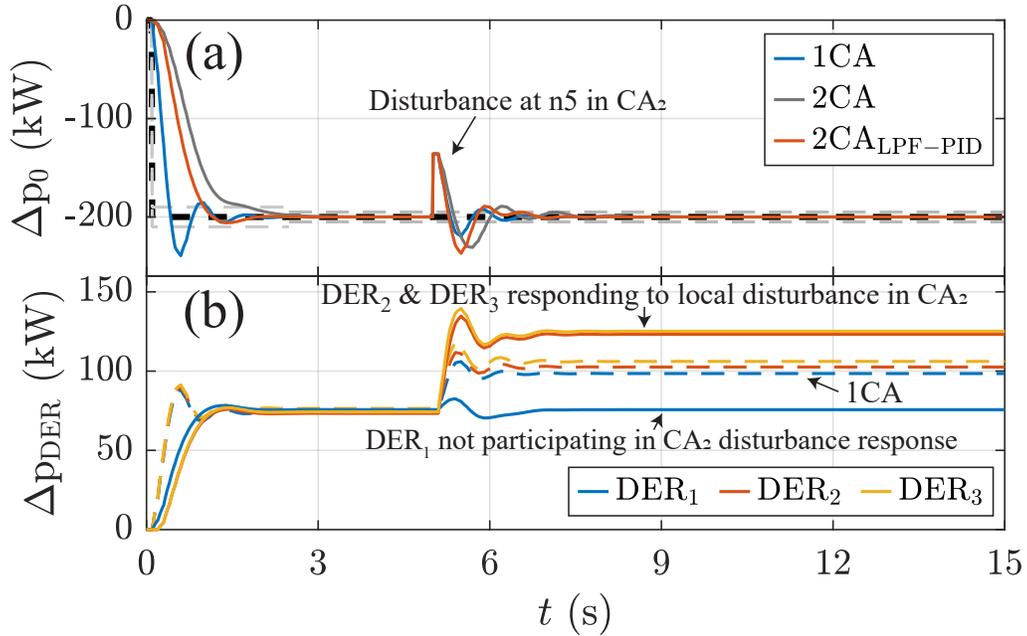
Figure 3.12: 5-Bus feeder step-tracking with disturbance response. (a) Tracking of Δp_0 with 1CA (blue) and 2CA (orange) configurations. (b) DERs active power responses. Dashed lines corresponds to single-area (1CA) while solid lines corresponds to multi-area ($2CA_{LPF-PID}$). (1CA: $a_{\lambda,1}, a_{\mu,1} = 5 \times 10^3$, 2CAs: $a_{\lambda,2}, a_{\mu,2} = 5 \times 10^3$, $2CA_{LPF-PID}$: $\alpha_1, \alpha_2 = 0.003$, $a_{\lambda,2}, a_{\mu,2} = 5 \times 10^3$)
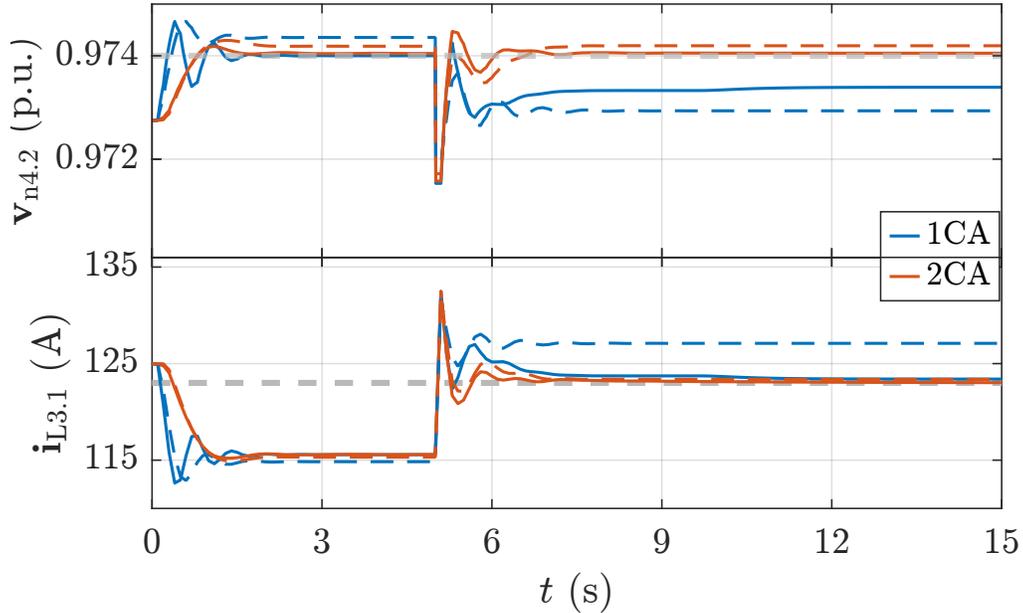
Figure 3.13: 5-Bus feeder step-tracking with disturbance voltage and current control with 1CA (blue) and 2CA (orange) configurations. Dashed lines corresponds to regular constraints on voltage ($\overline{\mathbf{v}} = 1.05$ p.u.) and 135A current limit.

Remark 3.6.2 (Low-Pass Filter Design & Stability) *Adding a low-pass filter to the interface between control areas introduces a pole into the system. The low-pass filter needs to be carefully designed to ensure that it does not cause instability. In this work, we designed the low-pass filter by observing the oscillation dynamics prior to adding the LPF to the VDER set-points.*

3.6.2 IEEE-123 Feeder

Following the proposed control structure described in Section 3.2, the IEEE-123 feeder is partitioned into 6 control areas as shown in Figure 3.14[5]. The feeder head area (CA1) is the parent area for both CA2 and CA3, with CA4 a further child of CA2, and CA5 and CA6 further children of CA3. This permits an investigation of the impact of multiple parent-child layers on the control performance.

---

[5]We partitioned the feeder into 6 CAs of approximately equal sizes with 3 levels of nested hierarchical structure. This is considered to analyze the impact of lower level CAs on higher level CAs when responding to set-point change requests and local disturbances.

As shown in Figure 3.14, there are 4 DERs per CA, with cost parameters $C_j'' = \text{diag}(40, 40)$ for all DERs, and remaining parameters as in Table 3.3. All VDER costs are set according to (3.11).

We next demonstrate the response of both configurations (1CA and 6CAs) to two test scenarios: 1) step-tracking with disturbances, and 2) stepped-ramp-tracking with disturbances.
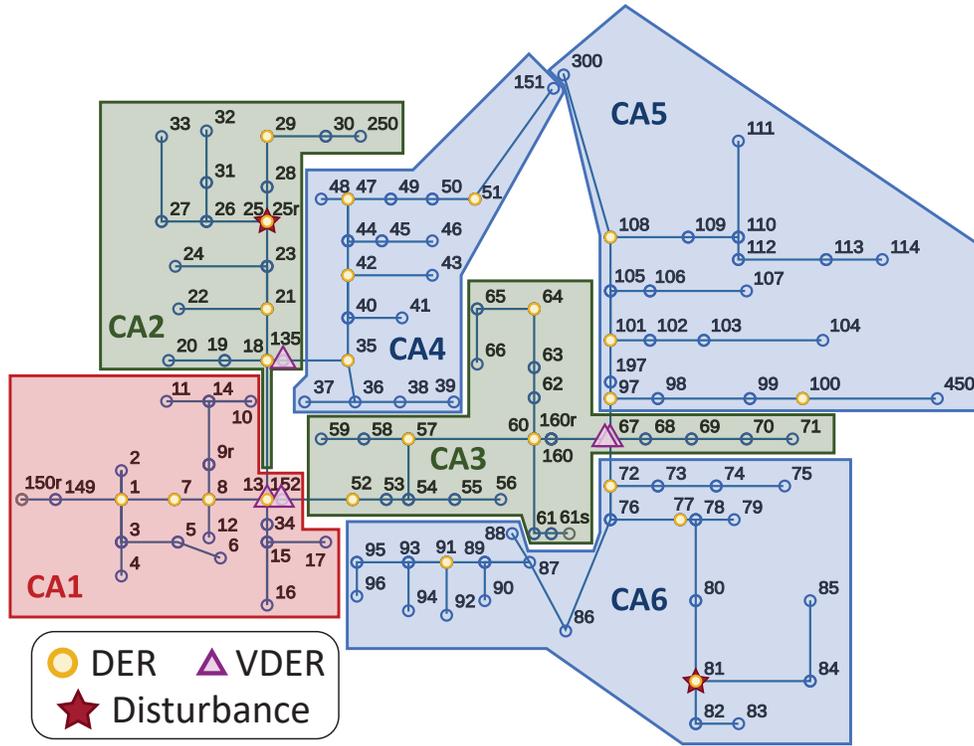
Figure 3.14: IEEE-123 bus feeder with six control areas.

Step-tracking with disturbances

A step change of 200kW is requested at the feeder head at $t = 0$s, followed by two disturbances: a 100kW (0.9pf) load change at bus 25 in CA2 at $t = 5$s, and a 100kW (0.9pf) load change at bus 81 in CA6 at $t = 10$s. The responses of the centralized controller and the multi-CAs implementation are shown in Figure 3.15. Note that the 6CA implementation incurs only a minor hit in performance, despite its decentralized hierarchical nature.

61
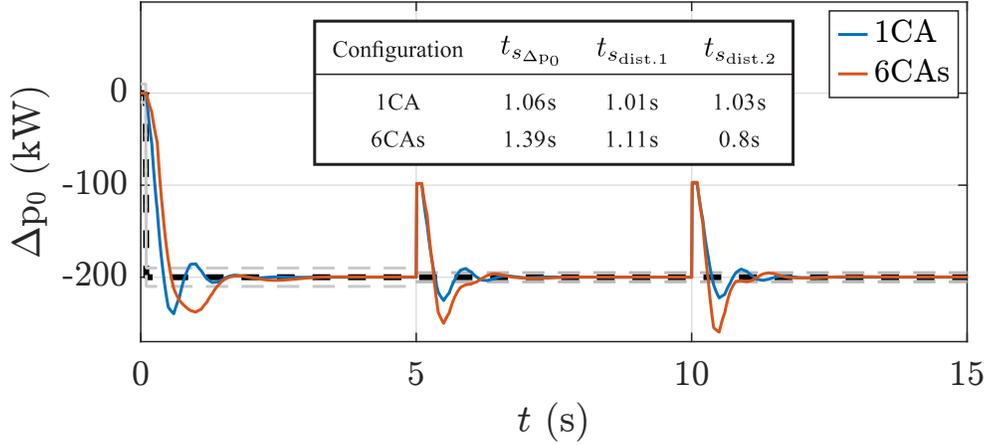
Figure 3.15: IEEE-123 feeder step-tracking with two disturbances. (1CA: $\alpha_1 = 0.001$, $a_{\lambda,1}, a_{\mu,1} = 2 \times 10^3$, 6CAs: $\alpha_1 = 0.0096$, $\alpha_{2,3,4,5,6} = 0.00432$, $a_{\lambda,1}, a_{\mu,1} = 5 \times 10^3$)

Stepped-ramp-tracking with disturbances

To demonstrate the tracking capabilities of the multi-CA design, we consider ramp-like reference signal at the feeder head, where a change of 20kW occurs every 1s. We consider the same two disturbances as in step-tracking test, where the disturbances are triggered at different times: *dist.* 1 (disturbance at bus 25 in CA2) is connected from $t = 10$s until $t = 50$s, while *dist.* 2 (disturbance at bus 81 in CA6) is connected from $t = 20$s until $t = 40$s. The power tracking response is shown in Figure 3.16, with insets showing details of the transient response. The multi-CAs implementation produces results similar to the centralized 1CA implementation.

Figure 3.17 shows the active power responses of the DERs in the feeder, where DERs have been grouped based on the CA they belong to, to focus on the collective response of different CAs. For the centralized controller (black curves), all DERs throughout the system show similar behavior when responding to set-point changes or disturbances, as they all have the same cost function, where all DERs respond promptly.

The DERs in the 6CA implementation behave differently. Focusing on the first 10 seconds, after each step-change in set-point at the feeder head, DERs within CA1 (dark blue) respond the fastest, followed by lower-level areas gradually increasing their participation. The DERs in child areas of CA1 (i.e., CA2 and CA3) accelerate their response faster than those in grandchild areas. Importantly, the "oscillations" here are *not* a form of instability, but are the result of CA1 responding aggressively to meet the set-point, then ramping down as other CAs begin to contribute. Focusing now on the disturbance at
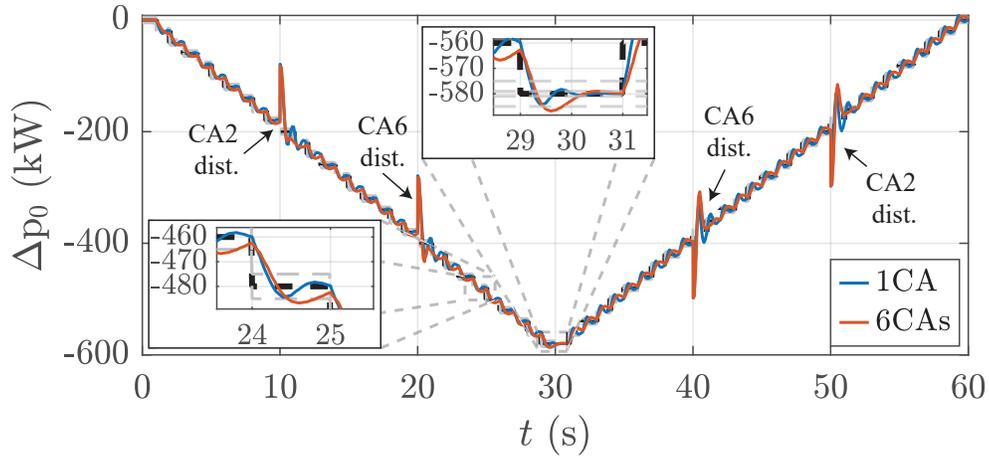
Figure 3.16: IEEE-123 feeder ramp-tracking with two disturbances.
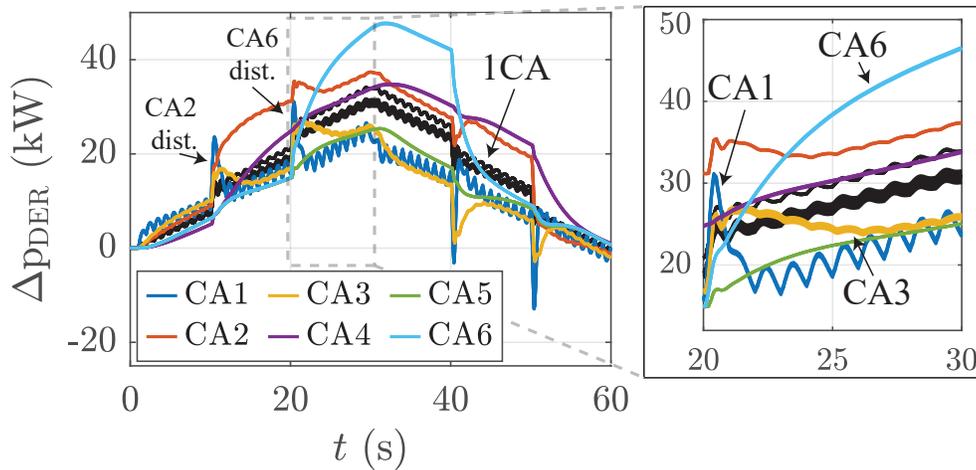
Figure 3.17: IEEE-123 feeder ramp-tracking DERs response. Black curves are DERs responses for centralized 1CA implementation.

bus 81 within CA6 at $t = 20$s, similar observations hold (Figure 3.17, inset). The parent areas CA3 and CA1 (parent of CA3) initially respond to maintain tracking at the feeder head, while concurrently, the contingent area (CA6) ramps up its DERs to counteract the disturbance locally; CA2 and CA4 display minimal response. Thus, in the multi-area setup, local disturbances are compensated by local DERs, while parent areas ensure set-point tracking during the transient adjustment.

Figure 3.18 plots selected voltages in the circuit during the previous test, with origi-

nal voltage limits (blue) and a tightened lower voltage limit $\underline{\mathbf{v}} = 0.99$p.u. (orange). The controllers effectively maintain voltage levels within these new limits while responding to step-changes and disturbances.
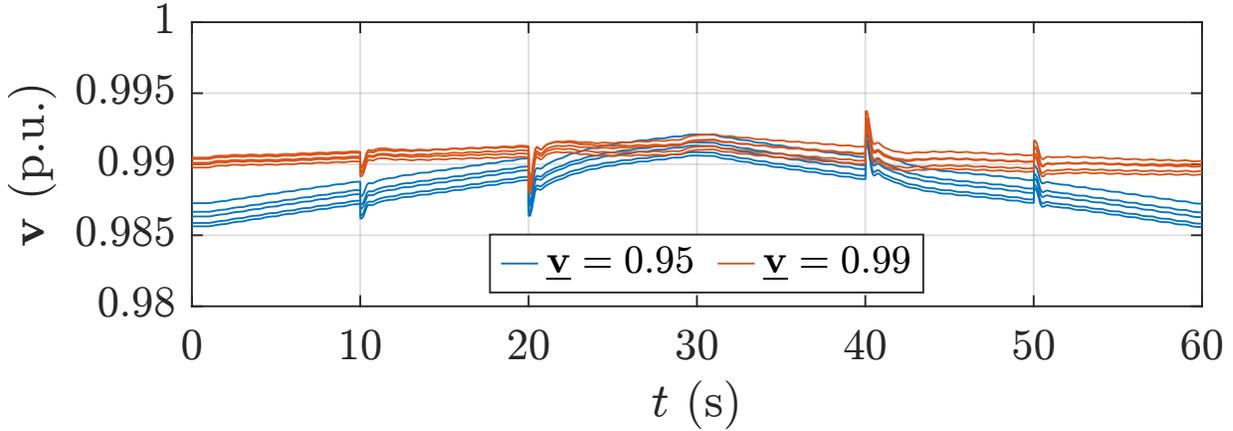
Figure 3.18: Voltage magnitudes for a representative set of buses using multi-CAs configuration. Blue: $\underline{\mathbf{v}} = 0.95$p.u. and Orange: $\underline{\mathbf{v}} = 0.99$p.u.

3.6.3 IEEE-8500 Feeder

Our case study of the IEEE-123 bus feeder in Section 3.6.2 highlighted interactions between parent CAs and their children in response to set-point changes and disturbances. In systems of this size, centralized control may still be feasible. For very large systems however, a centralized control approach becomes cumbersome, and suffers from increased computational, communication, and information privacy issues. Our final case study on the large IEEE 8500 bus feeder is aimed at demonstrating the scalability of the proposed multi-area controller, wherein the use of primarily local measurements and model information helps in overcoming the practical limitations of centralized optimization-based control.

The 8500 bus feeder is partitioned here into 49 CAs of varying sizes and composition, spread across a 13 layer hierarchy; the control area graph $\mathcal{G}_{\mathrm{CA}}$ is shown in Figure 3.19. The areas range from 10 to 322 buses, with some areas deeper within the feeder hierarchy containing entirely single-phase circuits. This variation in area sizes demonstrates the capability of the proposed structure to effectively coordinate multiple CAs with disparate sizes and structures. DERs are placed throughout the network across all areas, with the number of DERs ranging from 4 to 127 per area, resulting in a total of 2,062 DERs, including

1-, 2-, and 3-phase DERs. A color coded bus map of the feeder is shown in Figure 3.20. For more detailed information regarding the control areas and controllers configurations, please refer to Appendix B.

Figure 3.21 plots the tracking response of both configurations, 1CA and 49CAs, to a ramp change in power set-point at the feeder head, in increments of 120kW each second. Despite its
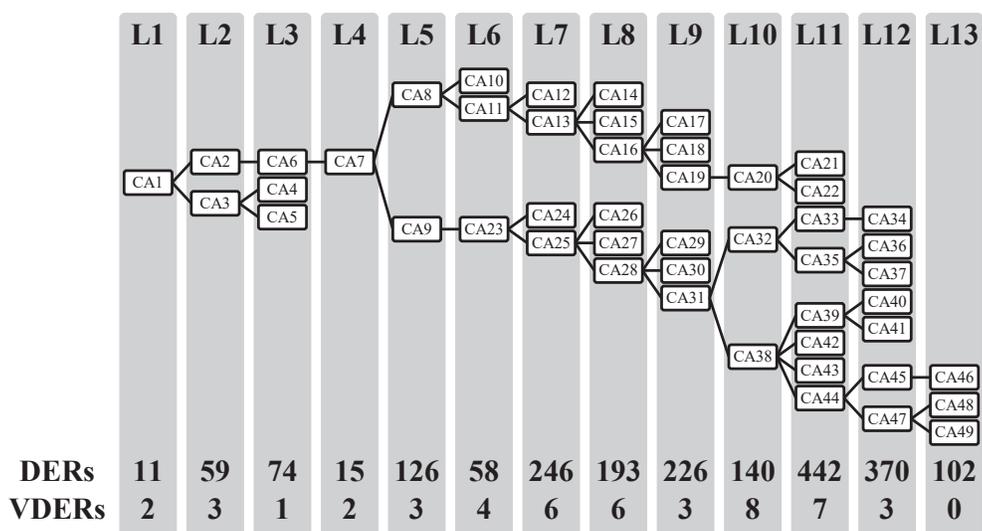
Figure 3.19: IEEE-8500 feeder control areas' tree with 13 nested levels of control areas.
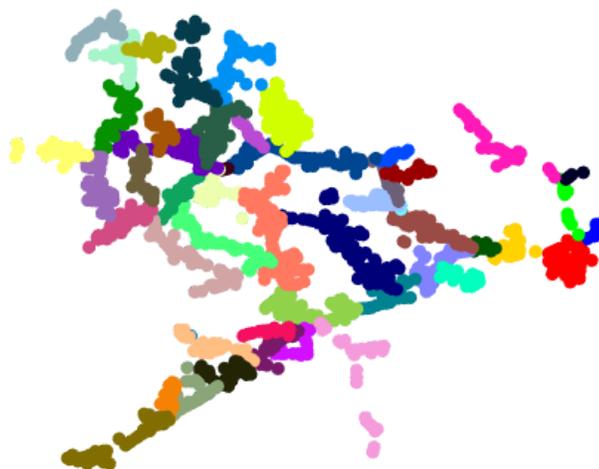
Figure 3.20: IEEE-8500 bus feeder with 49 control areas.
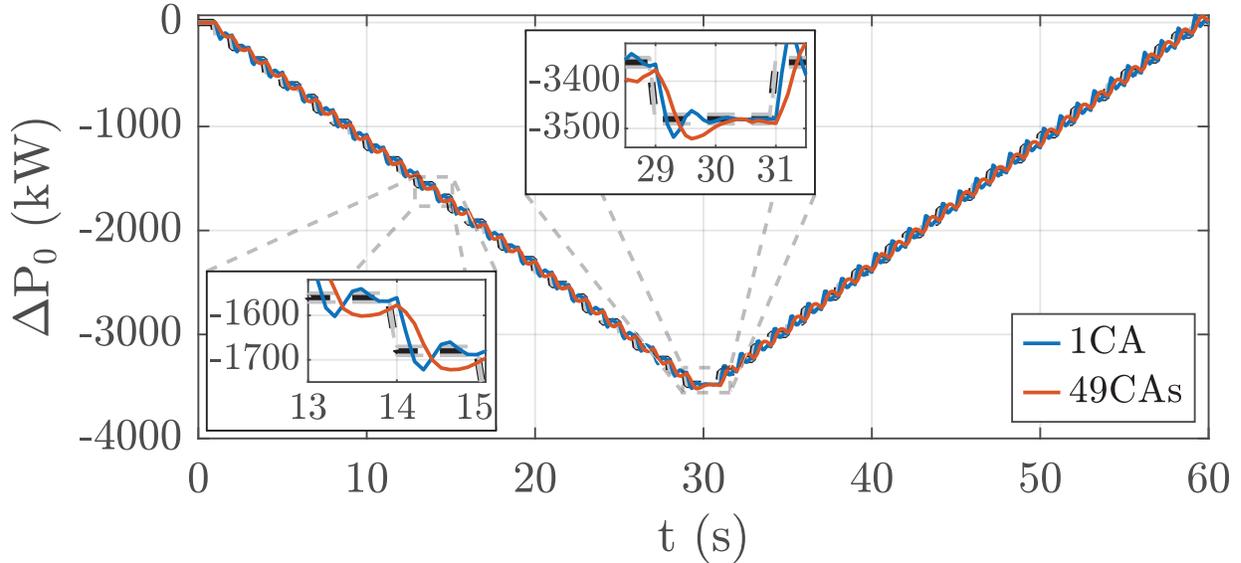
Figure 3.21: IEEE-8500 feeder ramp-tracking. (1CA: $\alpha_1 = 0.0015$, $a_{\lambda,\mu,\eta,\psi} = 20$, 49CAs: $\alpha_1 = 0.0004$, $\alpha_{\rm rest} = 0.0002$, $a_{\lambda,1}, a_{\mu,1} = 5 \times 10^3$)

highly decentralized and hierarchical architecture, our multi-area control scheme produces a response similar to an ideal centralized implementation. The multi-area architecture enables privacy preservation and operational boundaries while optimizing of thousands of DERs responses in real-time for fast TN-DN coordination.

3.7   Summary

We have developed, theoretically analyzed, and tested a multi-area feedback-based hierarchical control framework to coordinate distribution level DERs and DER aggregators in response to TSO power requests. The proposed framework addresses the pressing need for an effective and practical DER coordination framework that meets four critical requirements: speed, model independence, primarily local measurement and data reliance, and privacy/operational boundary preservation. The theoretical foundation of our framework is rooted in feedback-based hierarchical control theory, where the distribution network is partitioned into multiple Control Areas (CAs). Each CA operates with its own local controller, which communicates with neighboring CAs through limited information exchange. This hierarchical structure enables a scalable approach to managing DERs, allowing for both centralized oversight and decentralized decision-making at different levels of the network

hierarchy.

Additionally, our framework's practical application is exemplified through MATDSS. MATDSS Application is a MATLAB®-based tool designed to integrate seamlessly with OpenDSS©, a specialized application for simulating distribution networks. Using a `COM` interface, it efficiently communicates with MATLAB®to model distribution network feeders within an OpenDSS©solver engine. The software operates through a user-friendly GUI, enabling import of existing feeders or creation of new ones via OpenDSS©scripts. Key features include modular functions for customizable DER and local controller behavior, partitioning of feeders into control areas, and extensive simulation setup management. It offers real-time monitoring, customizable plotting, and export functionalities for simulation data analysis. MATDSS facilitates efficient workflow management and quick simulation initialization, enhancing usability for researchers and engineers working on complex control architectures and simulations.

Furthermore, the incorporation of PID and LPF controllers into the control actions was crucial for enhancing the dynamic response of DERs within our framework. The LPF-PID implementation aims to smooth control signals and mitigate high-frequency oscillations, thereby improving system stability and performance. This enhancement was driven by insights gained from the interactions within the hierarchical CAs, where oscillations were observed, as well as from established tuning guidelines. The identified need for robust control mechanisms capable of managing varying DER dynamics and network conditions necessitated this implementation.

Our methodology involved developing and analyzing the hierarchical control structure through detailed simulations on various test cases. Initially, we examined a simplified 5-bus feeder to validate the framework's ability to enforce voltage and current constraints under different operating conditions. This foundational study laid the groundwork for scaling our approach to larger and more complex networks. Moving to the IEEE-123 bus feeder, partitioned into six control areas, we explored the interaction between parent and child CAs within the hierarchical framework. This analysis demonstrated how hierarchical layers facilitate coordinated responses to dynamic disturbances and set-point changes while preserving local operational autonomy. The results highlighted that our approach maintains system stability and efficiency comparable to centralized methods, with enhanced resilience to local perturbations.

For the IEEE-8500 bus feeder, comprising 49 control areas across multiple nested levels, our framework showcased its scalability and robustness. This large-scale case study illustrated how the hierarchical structure optimally coordinates thousands of DERs distributed throughout a complex network. By leveraging primarily local measurements and

limited inter-area communication, our framework ensures rapid response times and effective coordination of DERs to meet fluctuating power demands. The case studies illustrate how the proposed architecture addresses the information, communication, computational, and scalability issues of a centralized feedback-optimization controller, with no significant degradation in dynamic performance compared to an idealized centralized implementation.

Chapter 4

Enhanced Integration of DN Controllers at the TN Control Layer for Fast Frequency Regulation

4.1 Introduction

In this chapter, we focus on developing an integration scheme to combine the Distribution Network (DN) hierarchical control structure, as developed in Chapter 3, with a recently proposed fast frequency regulation Transmission Network (TN) architecture [32]. This integration aims to harness DN-DERs to participate in frequency control at the TN layer.

We begin by constructing a linear model that captures the dynamic response of DN-DERs to commands from the TSO. This model is rooted in a simplified optimization problem for the DN control structure developed in Chapter 3. The model is then integrated into the TN controller design, thereby enhancing overall system performance compared to the approach presented in [32].

Key features of the integration method include:

- **Simplified Linear Model Extraction:** We propose a linear model representing the DN-DERs dynamics relying on a simplified optimization problem of the DN controllers. This model is then incorporated into the TN controller design process.

- **Enhanced Responsiveness:** Incorporating the DN model within the TN controller design process enhances system responsiveness and grid stability. Simulations of various DN configurations demonstrate the effectiveness of the proposed approach.

The integration scheme with the TN control architecture proposed in [32] is evaluated through simulations using MATDSS, Simulink and OpenDSS$^{©}$. In the following sections, we present a comprehensive approach to designing the TN controller, specifically following the referenced scheme for fast frequency regulation.

4.2 Overview of Proposed TN-DN Integration for Fast Frequency Regulation

The high-level objective of the TN-DN integration is to leverage the available flexibility within the DNs to provide ancillary services such as frequency and voltage support, by requesting active and reactive powers from the DN-DERs. The TSO would request a power set-point $X_{i,0}^{\text{set}} = (p_{i,0}^{\text{set}}, q_{i,0}^{\text{set}}) \in \mathbb{R}^2$ that is to be tracked by the ith DN hierarchical control structure at the interface bus between the two networks. In our scheme, the TN controller would not require detailed insights about the operation within the DN feeders; instead, it uses an approximate model of the anticipated response to design and tune the frequency controller at the TN layer.

The TN control scheme in [32] is designed to manage TN-IBRs to provide rapid and localized responses to frequency events in power grids. The scheme considers a power system with multiple control areas called Local Control Areas (LCAs). Within each LCA, a high-bandwidth low-latency measurements are available for local decision-making. A local controller within each LCA, comprising a disturbance estimator and a power allocator, re-dispatches the area's IBRs by estimating and rejecting local disturbances using frequency and area tie power flow measurements. The disturbance estimator uses a local dynamic model of the LCA and measurements to detect frequency events. It then generates real-time estimate of the net unmeasured active power imbalance within the LCA and the power allocator optimally re-dispatches local IBRs to correct the imbalance.

Control actions carried out within the framework in [32] assume a fast response from IBRs and do not consider their dynamic behavior. The IBRs are assumed to have immediate droop response directly proportional to the frequency deviation. The design of the local controllers is based on a simple aggregated area model. In the TN-DN integration, the DN hierarchical control structure replaces the TN-IBRs within the fast frequency regulation control framework.

In the following section, we introduce the TN frequency controller proposed in [32], focusing on a single LCA, as the TN-DN integration occurs within a single area. We then extend the proposed controller design to incorporate a linear DN dynamic model.

70

4.2.1 Transmission Network Fast Frequency Control

We focus on a TN consisting of a single control area with a local controller that will re-dispatch the TN-IBRs to reject disturbances and regulate frequency swiftly. The IBRs are assumed to be fast-acting resources available for the TN local controller to utilize. Consider the IEEE 9-bus system depicted in Figure 4.1. The overall system consists of 9 buses, 3 synchronous generators, 6 transmission lines and 2 TN-IBRs (the TN-IBRs will eventually be replaced with our distribution network control structures). The TN controller acts on power and frequency measurements, re-dispatches the IBRs to regulate the frequency and corrects local net-load imbalances.

The control scheme comprises two main phases: a disturbance estimator and a power allocator. The disturbance estimator processes system measurements to produce an estimate $\Delta \hat{P}_u$ of the unmeasured net active power imbalance within the TN, relative to the current dispatch point. This imbalance is then allocated to the IBRs within the system to reject the disturbance. We describe the design process of the estimator and allocator next for a
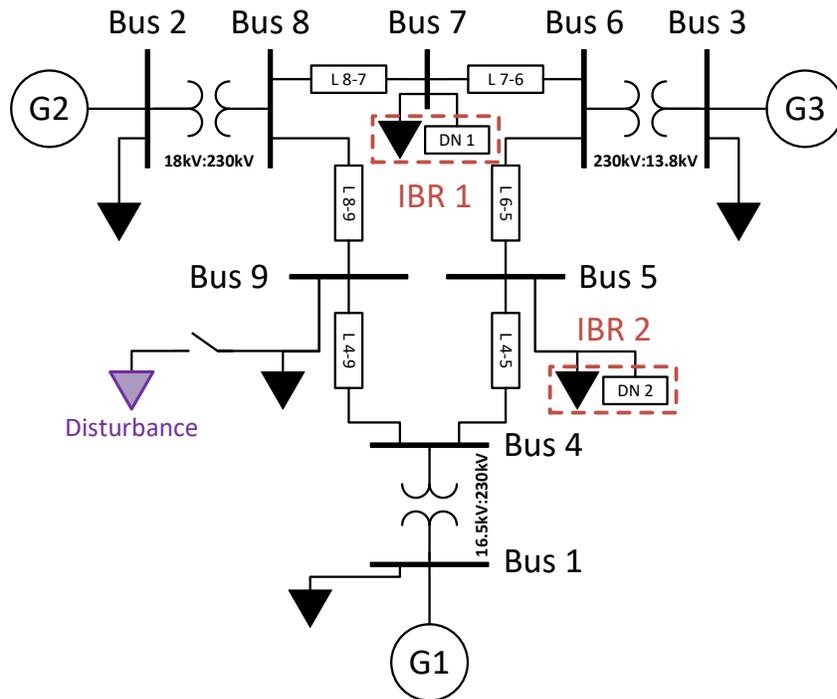
Figure 4.1: IEEE 9-bus power system with 2 distribution feeders integrated in place of TN-IBRs and a disturbance load.

single LCA network following the approach in [32].

Disturbance Estimator

The estimator design begins with a nominal (small-signal) dynamic model of the LCA dynamics at the current dispatch point. A two-state *System Frequency Response (SFR)* model that describes the machine mechanical and turbine-governor response [32,102,103] is considered. In this model, the frequency deviation represents the averaged system frequency response of all generators and frequency-responsive loads. The two-state model for the considered TN system in Figure 4.1 can be written as

$$2H\Delta\dot{\omega} = -(D + \tfrac{1}{R_{\text{ibr}}})\Delta\omega + \Delta P_m - \Delta P_u + \Delta P_{\text{ibr,tot}}, \tag{4.1a}$$

$$T_R\Delta\dot{P}_m = -\Delta P_m - R_g^{-1}(\Delta\omega + T_R F_H \Delta\dot{\omega}), \tag{4.1b}$$

where $\Delta\omega$ (p.u.) is the frequency deviation, ΔP_m (p.u.) is the mechanical power change, H (s) is the inertia constant, T_R (s) is the reheat time constant, D (p.u.) is the load damping, F_H is the fraction of total power generated by high pressure turbine and R_g, R_{ibr} (p.u.) are the generator and IBRs' primary droop constants, respectively. Note that in this setup, the IBRs dynamics are ignored. In (4.1), all power injections are represented at a single electrical point. This simple model leads to the following state-space representation

$$\dot{\mathbf{x}}_t = \tilde{A}_t\mathbf{x}_t + \tilde{B}_1\Delta P_{\text{ibr,tot}} + \tilde{B}_t\Delta P_u, \tag{4.2}$$

where $\tilde{A}_t$ is a Hurwitz stable matrix, $x_t = \mathsf{col}(\Delta\omega, \Delta P_m)$, $\Delta P_{\text{ibr,tot}}$ is the sum of all IBRs contributions (changes in their output powers) and ΔP_u is the net unmeasured active power imbalance in the LCA. The continuous model is discretized using the zero-order-hold method with a chosen sampling period T_s, resulting in

$$\mathbf{x}_t^+ = A_t\mathbf{x}_t + B_1\Delta P_{\text{ibr,tot}} + B_t\Delta P_u, \tag{4.3}$$

where A_t is Schur stable. The unknown net active power imbalance is modeled via a difference equation with an unknown initial condition (constant disturbance model)

$$\Delta P_u^+ = \Delta P_u. \tag{4.4}$$

We then combine the unmeasured disturbance into the model with the frequency deviation being measured as $y = \Delta\omega = C_t\mathbf{x}_t$ to get the augmented system

$$\xi_t^+ = \overline{A}_t\xi_t + \overline{B}_t\Delta P_{\text{ibr,tot}}, \tag{4.5}$$

$$y_t = \overline{C}_t\xi_t,$$

where $\xi_t = \mathrm{col}(\mathbf{x}_t, \Delta P_u)$ and

$$\overline{A}_t = \begin{bmatrix} A_t & B_t \\ \mathbb{0}^\top & 1 \end{bmatrix}, \quad \overline{B}_t = \begin{bmatrix} B_1 \\ 0 \end{bmatrix}, \quad \overline{C}_t = \begin{bmatrix} C_t & 0 \end{bmatrix}.$$

In (4.5), measurement and communication delays can be incorporated by appending extra states to account for the delays within the system model. Proposition 3.2.1 in [32] proves that the system in (4.5) is detectable, as long as the frequency deviation is one of the measurements. The proposition states that if matrix A_t is Schur stable and the augmented matrix $\begin{bmatrix} A_t - I & B_t \\ C_t & 0 \end{bmatrix}$ has full column rank, then $(\overline{C}_t, \overline{A}_t)$ is detectable. The rank condition ensures that the transfer matrix from ΔP_u to y has no transmission zeros at $z = 1$. Then, one can design a dynamic state estimator for the system [32, 104]

$$\hat{\xi}_t^+ = \overline{A}_t \hat{\xi}_t + \overline{B}_t \Delta P_{\mathrm{ibr,tot}} + L(\overline{C}_t \hat{\xi}_t - y_t), \tag{4.6}$$
$$\Delta \hat{P}_u = \begin{bmatrix} \mathbb{0}^\top & 1 \end{bmatrix} \hat{\xi}_t,$$

where L is the estimator gain matrix, which can be designed using, for example, linear-quadratic optimal methods. The estimator provides the required ongoing estimate $\Delta \hat{P}_u$ of the unmeasured disturbance that the allocator then assign to the IBRs, which we describe next.

Power Allocator

The power allocation mechanism for the IBRs uses the net power imbalance estimate $\Delta \hat{P}_u$ from the disturbance estimator to compute the active power reference for the IBRs. This re-dispatch is formulated as a simple optimization problem that is solved locally at each time step by the TN controller. Here, we describe the power allocator using DN notation as our proposed control structure integrates Distribution Network (DN) in-place of TN-IBRs. Let $\mathcal{N}_{\mathrm{DN}} = \{1, \ldots, N_{\mathrm{DN}}\}$ index the distribution networks that are integrated with the TN controller. Let $\mathcal{P}_i = [\Delta \underline{P}_{d,i}^{\mathrm{set}}, \Delta \overline{P}_{d,i}^{\mathrm{set}}]$ denote the power set-point limits for the ith DN. Then the optimal power set-points $\{\Delta P_{d,i}^{\mathrm{set}*}\}_{i \in \mathcal{N}_{\mathrm{DN}}}$ for the DNs are computed by minimizing the following cost function:

$$\underset{\Delta P_{d,i}^{\mathrm{set}} \in \mathcal{P}_i}{\arg\min} \quad f(\Delta P_{d,1}^{\mathrm{set}}, \ldots, \Delta P_{d,N_{\mathrm{DN}}}^{\mathrm{set}}) = \sum_{i=1}^{N_{\mathrm{DN}}} \frac{1}{2} \left(\frac{\Delta P_{d,i}^{\mathrm{set}}}{\Delta \overline{P}_{d,i}^{\mathrm{set}}} \right)^2 \tag{4.7a}$$

73

subject to

$$\sum_{i=1}^{N_{\text{DN}}} \Delta P_{d,i}^{\text{set}} = \Delta \hat{P}_u, \tag{4.7b}$$

where the reference (initial) set-points are assumed to be zero for simplicity[1]. The considered objective function reflects the available headroom for each DN, and determines the optimum allocation that results in balanced loading. Different objective functions can be considered to reflect operational convenience or to minimize the economic costs associated with the power allocation.

4.2.2 Evaluation of TN-Controller Design for TN-DN Integration

The TN controller design in [32] coordinates TN-IBRs to provide fast frequency support, successfully estimating the disturbance and regulating the frequency. This design approach aligns with the Internal Model Control (IMC) paradigm for internally stable systems, which enhances control performance by incorporating a model of the process within the controller. The use of feedback offers several advantages where it enhances robustness against model uncertainties.

For the goal of integrating DN-DERs within TN network for fast frequency support, and based on the performance analysis in Chapter 3 of DN controllers, we note the following:

(i) **Transient Response**: The assumption of fast IBRs with instant droop response within the estimator in [32] ignores the transient response of the DN. Ignoring the transient response can lead to inaccuracies in disturbance estimation, potentially causing slower and more oscillatory system response, as demonstrated in simulations.

(ii) **Stability**: In scenarios where DN control structures exhibit slow response, either due to less aggressive tuning of DN controllers or inherently slow dynamics of DERs, stability could be compromised.

While detuning the TN controller, by integrating a low-pass filter with the controller, can help mitigate the challenges described above, it results in slowed-down control actions. To

---

[1]If the reference points are not at zero, then one can shift the limits of the DN and set the reference to zero accordingly.

address these challenges, we propose extending the TN controller design to include DN-DERs dynamics. The observer design in Section 4.2.1 [32] is based on a linear system model. However, the closed-loop DN system developed in Chapter 3 is inherently nonlinear.

To integrate DN-DER dynamics into the framework of [32], we require a linear model of the closed-loop DN system. Given the nonlinear nature of the DN hierarchical structure, we develop a linear model by simplifying the DN controller optimization problem. This linear model can then be integrated within (4.5), aiding in better disturbance estimation and achieving a faster, less oscillatory response.

The following section develops the linear model of the DN structure. We then extend the TN controller to incorporate these dynamics.

4.3   Simplified Distribution Network Model

In this section, we develop a linear model of the hierarchical control structure of the DN that is developed in Chapter 3. We modify the LC optimization problem to obtain a linear model of the system. As observed in the simulations (Section 3.6), the p and q tracking are minimally affected when circuit constraints (current and voltage) are active. Therefore, we consider a DN consisting of a single feeder structure as described in Section 3.2.1 and consider the following modifications:

- **DER limits**: We assume that all DERs have enough capacity to respond to TSO commands and therefore DER limits are ignored (i.e., in (3.9), $\boldsymbol{\mathcal{X}} = \mathbb{R}^{2|\mathcal{D}|}$).

- **Perfect tracking**: We consider perfect tracking of $p_{i,0}^{\text{set}}$ and $q_{i,0}^{\text{set}}$, leading to equality constraints in (3.9b)-(3.9c) with $E_p = E_q = 0$. Consequently, the projection on the corresponding dual variables is removed, resulting in linear update laws of the dual variables.

- **Inactive circuit constraints**: We assume that current and voltage constraints remain inactive when DERs are responding and therefore constraints (3.9d)-(3.9f) are ignored.

- **Single Control Area**: For simplicity, we consider a single controller (single control area) acting on the whole distribution network.

- **DERs Dynamics**: We consider a 1st order DER model to model their dynamics. More complex models can be considered should they be available. The DERs' model will be integrated into the dual update laws.

These modifications addresses the sources of non-linearity in the DN closed-loop model. Ignoring DER limits is justified by assuming adequate capacity for ancillary services and operating within limits. Perfect tracking is ensured by small error tolerances in p and q set-points. Ignoring circuit constraints is valid due to the dominance of p and q tracking constraints (controlled by step-size $\boldsymbol{\alpha}$). Following these changes, the corresponding optimization problem of the DN becomes

$$\text{minimize } f(\mathbf{x}) \triangleq \sum_{j \in \mathcal{D}} f_j(x_j) \tag{4.8a}$$

subject to

$$\mathbb{1}^\mathsf{T} \mathbf{p}_d(\mathbf{x}) = \mathrm{p}_d^{\text{set}}, \tag{4.8b}$$

$$\mathbb{1}^\mathsf{T} \mathbf{q}_d(\mathbf{x}) = \mathrm{q}_d^{\text{set}}, \tag{4.8c}$$

where $\mathbf{x} = \mathsf{col}(x_1, x_2, \dots)$ and the set-points given to the controller at the interface bus are provided by the TSO. We drop the indexing of DN within TN layer for clarity. The problem in (4.8) is the simplified optimization of the centralized DN controller. Following the methodology from Section 3.3.3, we derive the regularized Lagrangian function $\hat{L}^\mathrm{r}$ for the problem (4.8) and define $X_d^{\text{set}} = \mathsf{col}(\mathrm{p}_d^{\text{set}}, \mathrm{p}_d^{\text{set}})$

$$
\begin{aligned}
\hat{L}^\mathrm{r}(\mathbf{x}, \hat{\mathbf{d}}; X_d^{\text{set}}) :=\ & f(\mathbf{x}) \\
& + \hat{\lambda} \left(\mathbb{1}^\mathsf{T} \mathbf{p}_0(\mathbf{x}) - \mathrm{p}_d^{\text{set}} \right) \\
& + \hat{\eta} \left(\mathbb{1}^\mathsf{T} \mathbf{q}_0(\mathbf{x}) - \mathrm{q}_d^{\text{set}} \right) \\
& + \tfrac{R^\mathrm{p}}{2} \|\mathbf{x}\|_2^2 - \tfrac{1}{2} \hat{\mathbf{d}}^\mathsf{T} \hat{\mathbf{R}}^\mathrm{d} \hat{\mathbf{d}}
\end{aligned}
\tag{4.9}
$$

Considering the same sampling period in Algorithm 1, the regularized Lagrangian (4.9) leads to Algorithm 2 for the centralized controller. The dual variables of the simplified optimization problem are collected as $\hat{\mathbf{d}} = \mathsf{col}(\hat{\lambda}, \hat{\eta})$, and the regularization of the dual variables as $\hat{\mathbf{R}}^\mathrm{d} = \mathrm{diag}(r_{\hat{\lambda}}, r_{\hat{\eta}}) \succeq 0$.

Remark 4.3.1 (Convergence of Algorithm 2) *Algorithm 2 introduces a simplified version of the dynamics of the dual variables (states) compared to the centralized algorithm (Algorithm in [37]). Given that the original algorithm (or the multi-area architecture Algorithm 1) has been proven to converge, the simplifications in Algorithm 2 should lead to even more straightforward dynamics, enhancing convergence properties.*

Algorithm 2: Simplified Algorithm for the Centralized Controller of the ith DN

At each sampling time

[**Step 1**]: Receive set-points from the TN controller $X_d^{\text{set}} = (\text{p}_d^{\text{set}}, \text{q}_d^{\text{set}})$

[**Step 2**]: Collect local measurements $\mathbf{p}_d, \mathbf{q}_d$

[**Step 3**]: Centralized controller performs the updates

$$\hat{\lambda}^+ = \hat{\lambda} + \alpha_\lambda \left(\mathbb{1}^{\mathsf{T}} \mathbf{p}_d - \text{p}_d^{\text{set}} - r_\lambda \hat{\lambda} \right)$$

$$\hat{\eta}^+ = \hat{\eta} + \alpha_\eta \left(\mathbb{1}^{\mathsf{T}} \mathbf{q}_d - \text{q}_d^{\text{set}} - r_\lambda \hat{\lambda} \right)$$

[**Step 4**]: Centralized controller updates DER set-points

$$\mathbf{x}^+ = \arg\min_{\mathbf{x} \in \mathcal{X}} \hat{L}^{\text{r}}(\mathbf{x}, \hat{\mathbf{d}}^+; X_d^{\text{set}})$$

Consider the DER cost functions of the form

$$f_j(\mathbf{x}_j) = x_j^\top C_j'' x_j, \tag{4.12}$$

where C_j' is set to $\mathbb{0}$. Then, the objective function in (4.8) can be expressed as

$$\begin{aligned} f(\mathbf{x}) &= \sum_{j \in \mathcal{D}} f_j(x_j) \\ &= \tfrac{1}{2} \mathbf{x}^\top Q \mathbf{x}, \end{aligned} \tag{4.13}$$

where $\mathcal{D}$ is the set of all DERs within the DN and

$$Q = \begin{bmatrix} 2C_1 & \mathbb{0} & \mathbb{0} \\ \mathbb{0} & \ddots & \mathbb{0} \\ \mathbb{0} & \mathbb{0} & 2C_{|\mathcal{D}|} \end{bmatrix}. \tag{4.14}$$

The corresponding regularized cost function for the DN is

$$\mathbf{F}(\mathbf{x}) = f(\mathbf{x}) + \tfrac{r^{\text{p}}}{2} \|\mathbf{x}\|_2^2. \tag{4.15}$$

Let $R^{\text{p}} = r^{\text{p}} I$. Substituting (4.13) into (4.15), we obtain the cost function

$$\mathbf{F}(\mathbf{x}) = \tfrac{1}{2} \mathbf{x}^\top Q \mathbf{x} + \tfrac{1}{2} \mathbf{x}^\top R^{\text{p}} \mathbf{x}. \tag{4.16}$$

Let $\mathbf{x}_{\mathrm{DER}}$ represent the vector of DERs output powers throughout the DN and consider the first order DER response as

$$\mathbf{x}_{\mathrm{DER}}^+ = A_{\mathrm{DER}}\mathbf{x}_{\mathrm{DER}} + B_{\mathrm{DER}}\mathbf{x}, \tag{4.17}$$

where

$$A_{\mathrm{DER}} = \mathsf{diag}(e^{-\frac{T_s}{\tau_1}}, e^{-\frac{T_s}{\tau_2}}, \dots),$$
$$B_{\mathrm{DER}} = I - A_{\mathrm{DER}},$$

τ_j is the time constant of the jth DER and T_s is the sampling time. As in Section 3.4, the dual updates can be combined as

$$\mathbf{G}(\hat{\mathbf{d}}) \triangleq \hat{\mathbf{R}}^d\hat{\mathbf{d}} - (\hat{\mathbf{C}}\hat{\mathbf{K}})\nabla\mathbf{F}^*(-\hat{\mathbf{K}}^\top\hat{\mathbf{C}}^\top\hat{\mathbf{d}}), \tag{4.18}$$

where $\hat{\boldsymbol{\alpha}} = \mathsf{diag}(\alpha_\lambda, \alpha_\eta)$, $\hat{\mathbf{K}}$ captures the sensitivities of all DER set-points to the active and reactive powers at the interface bus (i.e., $\hat{\mathbf{K}} \equiv \mathsf{col}(\mathbf{M}, \mathbf{H})$) and $\hat{\mathbf{C}} = \mathsf{blkdiag}(\mathbb{1}_3^\top, \mathbb{1}_3^\top)$ for three phase interface bus. We drop $\hat{\mathbf{C}}\hat{\mathbf{k}}$ and consider the input set-point request relative to the operating point (i.e., change in power request $\Delta X_d^{\mathrm{set}}$), as $\hat{\mathbf{C}}\hat{\mathbf{k}}$ represents the non-DER contribution at the operating point. Note that DERs set-points $\mathbf{x}$ can be evaluated as

$$\begin{aligned} \mathbf{x} &= \nabla\mathbf{F}^*(-\hat{\mathbf{K}}^\top\hat{\mathbf{C}}^\top\hat{\mathbf{d}}) \\ &= -(Q + R^{\mathrm{p}})^{-1}\hat{\mathbf{K}}^\top\hat{\mathbf{C}}^\top\hat{\mathbf{d}}. \end{aligned} \tag{4.19}$$

In the frequency control framework, the DSO receives active power set-points (i.e., $\Delta X_d^{\mathrm{set}} = \mathsf{col}(\Delta P_d^{\mathrm{set}}, 0)$). Considering only active power tracking in the model (4.16)-(4.19) and defining the states $\mathbf{x}_d = \mathsf{col}(\hat{\mathbf{d}}, \mathbf{x}_{\mathrm{DER}}^-)$ yield the following linear DN model

$$\mathbf{x}_d^+ = A_d\,\mathbf{x}_d + B_d\Delta P_d^{\mathrm{set}} \tag{4.20a}$$
$$\Delta P_d = C_d\mathbf{x}_d \tag{4.20b}$$

where

$$A_d = \begin{bmatrix} I - \hat{\boldsymbol{\alpha}}(\hat{\mathbf{R}}^d + \hat{\mathbf{C}}\hat{\mathbf{K}}B_{\mathrm{DER}}(Q + R^{\mathrm{p}})^{-1}\hat{\mathbf{K}}^\top\hat{\mathbf{C}}^\top) & \hat{\boldsymbol{\alpha}}\hat{\mathbf{C}}\hat{\mathbf{K}}A_{\mathrm{DER}} \\ -B_{\mathrm{DER}}(Q + R^{\mathrm{p}})^{-1}\mathbf{K}_{\mathrm{d},i}^\top\mathbf{C}_i^\top & A_{\mathrm{DER}} \end{bmatrix}$$
$$B_d = \begin{bmatrix} \hat{\boldsymbol{\alpha}} \\ \mathbb{0} \end{bmatrix}$$
$$C_d = \begin{bmatrix} -\hat{\mathbf{C}}\hat{\mathbf{K}}B_{\mathrm{DER}}(Q + R^{\mathrm{p}})^{-1}\hat{\mathbf{K}}^\top\hat{\mathbf{C}}^\top & \hat{\mathbf{C}}\hat{\mathbf{K}}A_{\mathrm{DER}} \end{bmatrix}$$

Remarks on the DN Model

Following Theorem 3.4.2, we assume that $\hat{\boldsymbol{\alpha}}$ is chosen such that the feedback closed loop DN system is stable. The model (4.20) describes the tracking of the distribution network to set-points in a closed loop. In the integration framework, we are only interested in the input-output behavior and, therefore, consider a minimal realization of the model (4.20) going forward. For brevity, we reuse the matrices A_d, B_d, and C_d with the understanding that they represent the minimal realization of the model in (4.20).

4.4 Extended TN Controller Design

In this section, we extend the TN controller design described in Section 4.2.1 by incorporating the minimal realization of the DN dynamic model (4.20) for the N_{DN} distribution networks. First, we define $\Delta P_{d,\mathrm{tot}}$ as the total power injection from the DNs into the TN system

$$\Delta P_{d,\mathrm{tot}} = \mathbb{1}^\top \Delta P_d \tag{4.21}$$

$$= \sum_{i=1}^{N_{\mathrm{DN}}} \Delta P_{d,i},$$

where $\Delta P_d = \mathsf{col}(\Delta P_{d,1}, \ldots, \Delta P_{d,N_{\mathrm{DN}}})$. Define $A_d = \mathsf{blkdiag}(A_{d,1}, \ldots, A_{d,N_{\mathrm{DN}}})$ and similarly for block diagonal B_d, C_d, and let $\mathbf{x}_d = \mathsf{col}(\mathbf{x}_{d,1}, \ldots, \mathbf{x}_{d,N_{\mathrm{DN}}})$. The combined DNs model can be written as

$$\mathbf{x}_d^+ = A_d\,\mathbf{x}_d + B_d\Delta P_d^{\mathrm{set}}, \tag{4.22}$$

$$\Delta P_d = C_d\mathbf{x}_d,$$

where $\Delta P_d^{\mathrm{set}} = \mathsf{col}(\Delta P_{d,1}^{\mathrm{set}}, \ldots, \Delta P_{d,N_{\mathrm{DN}}}^{\mathrm{set}})$.

We consider the case where the DN-DERs provide primary droop response with a droop constant R_d. Therefore, we drop the droop constant R_{IBR} from 4.1. Let $\xi = \mathsf{col}(\mathbf{x}_t, \Delta P_u, \mathbf{x}_d)$ denote the combined state vector for both (TN and DN), then the augmented system model can be described as

$$\xi^+ = A\xi + B\Delta P_d^{\mathrm{set}}, \tag{4.23}$$

$$y = \mathsf{col}(y_t, \Delta P_d) = C\xi,$$

where A_t, B_t, C_t, B_1 are as defined in Section 4.2.1, $C = \begin{bmatrix} C_t & \mathbb{0}^\top \end{bmatrix}$ for frequency measurements and

$$A = \begin{bmatrix} A_t & B_t & B_1 C_d \\ \mathbb{0}^\top & 1 & \mathbb{0}^\top \\ B_d R_d^{-1} C_t & \mathbb{0} & A_d \end{bmatrix}, \quad B = \begin{bmatrix} \mathbb{0} \\ 0 \\ B_d \end{bmatrix}.$$

The following result establishes that this extended model is detectable.

Lemma 4.4.1 (Detectability of augmented system (4.23)**)** *Consider the augmented system* (4.23)*, where* A_t, A_d *are Schur stable and assume* $\begin{bmatrix} A_t - I & B_t \\ C_t & 0 \end{bmatrix}$ *is full rank. Then for sufficiently large* R_d*,* (C,A) *is detectable.*

Proof of Lemma 4.4.1: Consider the PBH test [105], detectability of (C, A) is equivalent to $\mathsf{col}(A - \lambda I, C)$ having full column rank for all $\lambda \in \mathbb{C}$ with $|\lambda| \geq 1$. Then, A should not have unstable eigenvector in $\mathsf{null}(C)$.

Rewrite the augmented system by reordering the state vector as

$$\begin{bmatrix} \mathbf{x}_t^+ \\ \mathbf{x}_d^+ \\ \Delta P_u^+ \end{bmatrix} = \begin{bmatrix} A_t & B_1 C_d & B_t \\ \hline B_d R_d^{-1} C_t & A_d & \mathbb{0} \\ \hline \mathbb{0}^\top & \mathbb{0}^\top & 1 \end{bmatrix} \begin{bmatrix} \mathbf{x}_t \\ \mathbf{x}_d \\ \Delta P_u \end{bmatrix} + \begin{bmatrix} \mathbb{0} \\ B_d \\ 0 \end{bmatrix} \Delta P_d^{\text{set}}, \qquad (4.24)$$

$$\Delta \omega = \begin{bmatrix} C_t & \mathbb{0}^\top & 0 \end{bmatrix} \begin{bmatrix} \mathbf{x}_t \\ \mathbf{x}_d \\ \Delta P_u \end{bmatrix}.$$

Let A' denote the reordered A matrix, and accordingly define reordered B' and C'. The matrix A' is block upper triangular matrix with eigenvalues

$$\mathsf{eig}(A) = \mathsf{eig}\left(\begin{bmatrix} A_t & B_1 C_d \\ B_d R_d^{-1} C_t & A_d \end{bmatrix}\right) \cup \{1\}.$$

For the sufficiently large R_d, $\left|\mathsf{eig}\left(\begin{bmatrix} A_t & B_1 C_d \\ B_d R_d^{-1} C_t & A_d \end{bmatrix}\right)\right| < 1$. Then, for the unstable eigenvalue of 1, we examine $(A' - I)w = 0$

$$\begin{bmatrix} A_t - I & B_1 C_d & B_t \\ B_d R_d^{-1} C_t & A_d - I & \mathbb{0} \\ \mathbb{0}^\top & \mathbb{0} & 0 \end{bmatrix} \begin{bmatrix} w_1 \\ w_2 \\ w_3 \end{bmatrix}.$$

80

The third row implies $w_3 = \nu$ is a free variable. From the first row

$$w_1 = (A_t - I)^{-1} B_1 C_d w_2 + (A_t - I)^{-1} B_t \nu . \tag{4.25}$$

Using the second row and substituting (4.25) for w_1 yield

$$B_d R_d^{-1} C_t \left((A_t - I)^{-1} B_1 C_d w_2 + (A_t - I)^{-1} B_t \nu \right) + (A_d - I) w_2 = 0 . \tag{4.26}$$

We rewrite (4.26) as

$$w_2 = \mathcal{W}^{-1} B_d R_d^{-1} G_t(1) \nu, \tag{4.27}$$
$$\mathcal{W} \triangleq B_d R_d^{-1} C_t (A_t - I)^{-1} B_1 C_d + (A_d - I),$$
$$G_t(1) \triangleq C_t (A_t - I)^{-1} B_t .$$

Substituting (4.27) in (4.25)

$$w_1 = (A_t - I)^{-1} B_1 C_d \mathcal{W}^{-1} B_d R_d^{-1} G_t(1) \nu + (A_t - I)^{-1} B_t \nu . \tag{4.28}$$

Given $w = \mathsf{col}(w_1, w_2, w_3)$, $C' = \begin{bmatrix} C_t & \mathbb{0} & 0 \end{bmatrix}$, and $\nu = 1$, we examine $C'w$

$$C'w = C_t w_1 \tag{4.29}$$
$$= (1 + C_t (A_t - I)^{-1} B_1 C_d \mathcal{W}^{-1} B_d R_d^{-1}) G_t(1)$$

which for sufficiently large R_d, $C'w \approx G_t(1)$. But $G_t(1) \neq 0$ since $\begin{bmatrix} A_t - I & B_t \\ C_t & 0 \end{bmatrix}$ is full rank by assumption. Hence, (C, A) is detectable. $\qquad \square$

The rank assumption of $\begin{bmatrix} A_t - I & B_t \\ C_t & 0 \end{bmatrix}$ impose that the transfer function from ΔP_u to $\Delta \omega$ has no transmission zeros at $z = 1$. Then, following the TN controller design in Section 4.2.1, one can design an observer for the extended TN model as

$$\hat{\xi} = A\hat{\xi} + B\Delta P_d^{\text{set}} + L(C\hat{\xi} - y), \tag{4.30}$$
$$\Delta \hat{P}_u = \begin{bmatrix} 0 & 0 & 1 & \mathbb{0}^\top \end{bmatrix} \hat{\xi},$$

where L is the estimator gain matrix and A, B, C are defined in (4.23).

Remarks on the augmented model and the disturbance estimator

The framework presented here establishes a promising foundation for achieving perfect disturbance rejection in the augmented system with the observer (4.30). Leveraging the

established results of the TN controller in [32], this study suggests that the proposed approach holds potential for comparable performance.

By driving the total power contribution of the distribution networks, $\Delta P_{d,\text{tot}}$, towards the estimated disturbance $\Delta \hat{P}_u$ generated by the observer (4.30) using the power allocator described in Section 4.2.1, the DERs within the distribution networks effectively mitigate the disturbance. Future research will focus on formalizing these observations to establish a rigorous framework for achieving perfect disturbance rejection, and conducting closed-loop stability analysis.

In the following section, we evaluate the integration scheme developed against the requirements outlined in Section 2.3.1.

4.4.1 Evaluation of Proposed integration scheme Against Transmission & Distribution Coordination Requirements

In this section, we summarize the key aspects of the proposed integration scheme and evaluate it against the Transmission & Distribution Coordination Requirements (T.R1)-(T.R3) identified earlier.

Key Features and Benefits of the Integration Scheme

The proposed integration scheme embodies several critical features designed to enhance the coordination between TN and DN networks:

(i) **Separable Control:** The integration scheme results in a separable controller design for each layer (TN and DN). The DN controller is tuned independently, without interfering with the TN design process. The only information communicated to the TN layer for better estimating the disturbance is the linear DN model. This leads to faster response and settling times, enhancing grid stability and swiftly regulating frequency, as demonstrated in the simulations (Section 4.5).

(ii) **Real time operation:** The framework optimizes real-time control by focusing on timely coordination between the TN and DN controllers. It removes the burden of direct communication with DERs from the TN layer, to maintain fast communication channels, minimizing potential communication delays. The DN control structure, which has demonstrated fast response times to set-point adjustments provided by the TSO, ensures that the system can react swiftly to changes.

Evaluation Against Requirements

Now, we evaluate the proposed integration scheme against the Transmission & Distribution Coordination Requirements described in Section 2.3.1:

- **Minimize data sharing (T.R1):** The integration scheme minimizes data exchange among different stakeholders, controllers, and control layers to protect privacy and streamline communication. Proprietary information, detailed models, measurements, and the structure behind the meter remain confidential, safeguarding the privacy of DN controllers and DERs.

- **DN-DER Coordination Managed Separately from TN Controller (T.R2):** The scheme ensures the separation of control design, preventing TN actions from disrupting DN networks and vice versa. It allows for local optimization within each DN, ensuring that actions taken at the transmission level do not negatively impact the distribution level. This prevents local imbalances and inefficiencies that could destabilize the network.

- **Operate in Real-time and Coordinate within Seconds (T.R3):** The TN coordination framework with DN control structure operates in real time and successfully utilize the available DN-flexibility within seconds, as demonstrated in the simulations (Section 4.5). The ability to coordinate quickly ensures that the system can adapt to dynamic conditions and continue to operate in real-time.

The proposed controller architecture successfully meets the requirements set for Transmission & Distribution Coordination (T.R1)-(T.R3), offering an enhanced integration of DN-DERs into transmission network fast frequency control scheme. This evaluation underscores its effectiveness in optimizing grid performance while maintaining operational integrity and safeguarding privacy.

4.5   Case Studies

We validate the design illustrated above by applying it to IEEE 9-bus system [106], incorporating two IEEE-123 distribution feeders into the TN to demonstrate the coordination between transmission and distribution levels, see Figure 4.1. The distribution feeders utilize the hierarchical control structure discussed in Section 3.6.2, featuring 6 Control Areas (CAs)
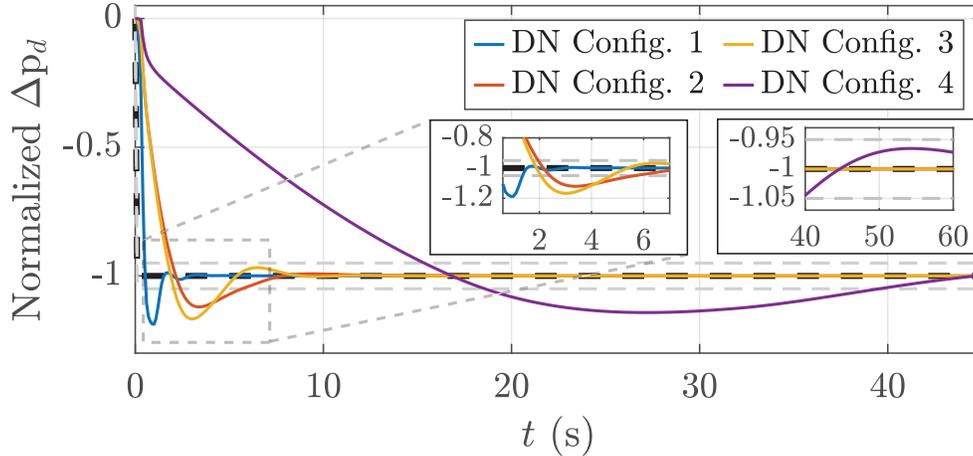
Figure 4.2: DN normalized response to 200kW step-change set-point at the interface bus for different configurations of the DN hierarchical control structure.

and 24 DERs (4 per CA), as depicted in Figure 3.14. We consider multiple tuning configurations of the DN controllers with different response speeds to represent diverse DN configurations.

When multiple stakeholders or operators manage the DN control areas, fine-tuning the controllers for fast response with minimal oscillations can be challenging. Therefore, we consider a variety of configurations, including those exhibiting slow and oscillatory behavior, reflecting situations where fine-tuning is not feasible due to lack of cooperation between involved parties, or technical limitations. The baseline for comparison is the TD coordination scenario without integrating DN dynamics into the TN disturbance estimator.

In our simulations, "Config. 1" represents an ideal scenario with well-tuned controllers optimized for fast response, akin to the performance demonstrated in Chapter 3, referred to as the best-case scenario. "Config. 2" introduces a cautious tuning approach with slower response characteristics, suitable when comprehensive controller tuning is challenging. We further explore "Config. 3", which exhibits a more aggressive response compared to Config. 2. Lastly, "Config. 4" represents a scenario where DN controllers are deliberately detuned.

Figure 4.2 illustrates the normalized response of the DN to a step-change set-point request at the interface bus for the different configurations described above. As expected, Config. 1, characterized by fast and well-tuned controllers, demonstrates the best performance with a settling time of only 1.39s, emphasizing the impact of controller tuning. Moving to Config. 2 and Config. 3, settling times degrade to 5.7s and 4.7s, respectively, due to slower and oscillatory responses. Config. 4, featuring a slow-responding DN controllers,

exhibits the longest settling time at 39.6s.

The TD-integration tests were conducted using MATLAB$^®$/Simulink, OpenDSS$^©$ V9.6.1.3, and MATDSS V0.94, which includes additional functions for the integration with Simulink. The IEEE 9-bus system was modeled in Simulink, incorporating a sixth-order synchronous generator with detailed turbine-governor, excitation, and power system stabilizer (PSS) models. The IEEE-123 feeders are simulated in OpenDSS$^©$using the provided script and configured through MATDSS Application. Detailed configurations of all the components are summarized in Appendix C. The integration of the two systems was achieved using a Level-2 MATLAB S-function, where the feeders' contribution at the transmission network level were modeled using Simscape Electrical components in Simulink. The DERs within the feeders were configured as shown in Table 3.3.

In the system depicted in Figure 4.1, generators and DN-DERs are configured with 5% droop control and the pre-disturbance generation/demand in the system is approximately 339MW. All loads within the TN are set as constant-PQ loads, while the loads within the feeders are kept at their original configurations within OpenDSS$^©$'s original script. A disturbance of 50MW at bus 9 is triggered at $t = 2$s, with the DN-DERs within the feeders being utilized to regulate the frequency.

The implemented disturbance estimator is based on the augmented system model (4.23).

The DERs are modeled as described in (4.17) with $\tau = 0.2$s for all. The internal DN measurements are not shared with the TN controller, except for total power draw (at the interface bus). The estimator gain L was tuned using standard linear-quadratic methods. Simulation tests were conducted with a controller sampling time of $T_s = 100$ms. When the disturbance at bus 9 is triggered, TN controller updates the estimated disturbance and DNs set-points.

In the following plots, we denote the setup with disturbance estimator not including DN dynamic model as "T-Observer", while "TD-Observer" indicates that DN dynamics are incorporated within the disturbance estimator design. The response of the four configurations described above is depicted in Figure 4.3. The TD-Observer setup demonstrated faster settling time for all the configurations. In Config. 1, the settling time for the TD-Observer was ~ 6.3s to be within ±0.001Hz, while T-Observer settling time was ~ 15.2s. In Config. 2 and Config. 3, the TD-Observer based TN controller ramps up the DN-DERs faster to regulate the frequency. In Config. 2, the TD-Observer based controller resulted in minimal oscillations. In both cases, the TD-Observer settling time was faster than T-Observer by ~ 20s and ~ 5s, respectively. In the last configuration, both controllers resulted in oscillatory response, indicating that TN controller needs to be tuned to slow it down for slow dynamic DN response.

When looking at the performance within the feeders, Figure 4.4a shows the response of DN-1 CAs to their set-points for Config. 1. The TD-observer coordination was able to promptly drive the controllers within the DN to provide the requested power as it estimated the disturbance faster than the T-Observer. Figure 4.4b shows the CAs performance for Config. 2. The oscillations observed in Config. 2 response resulted in oscillations within the feeder structure. Such cases could lead to instability within the feeders. Due to the presence of the low-pass filters within the feeder structure, these oscillations decreased within child areas.

4.6   Summary

We have proposed an integration scheme for Distribution Networks (DNs) and Transmission Networks (TNs) designed to meet operational requirements: minimizing data sharing, managing DN-DER coordination independently from TN controllers, and ensuring real-
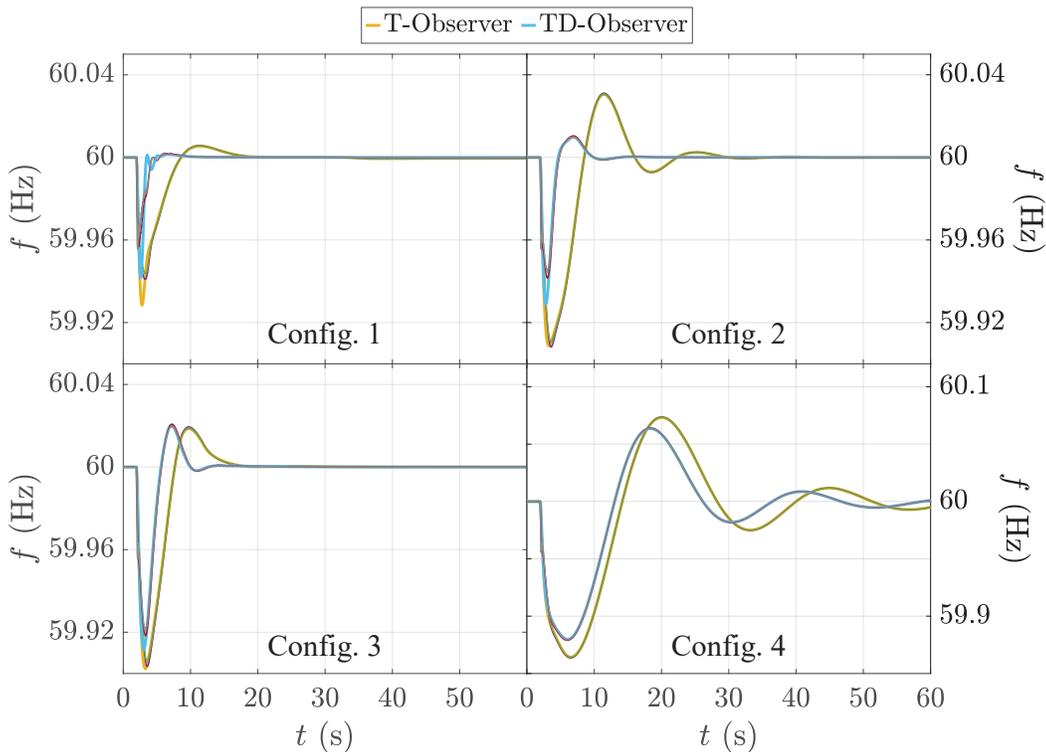
Figure 4.3: Frequency response to 50MW disturbance at bus 9 using the four DN configurations.

time responsiveness with coordination within seconds. Building upon the TN controller framework from [32], which includes a disturbance estimator and a power allocator, our approach enhances system performance by incorporating DN dynamics into the disturbance estimator. This integration improves disturbance estimation accuracy and enables faster, more stable and robust response to disturbances and frequency deviations.

Our methodology involves deriving a linear model of the centralized DN control structure using a simplified optimization problem of the DN controller. The DN dynamic model is then integrated into the disturbance estimator, extending the TN controller design, thereby enhancing its capability to accurately estimate disturbances. We validate the proposed integration scheme through simulations, where two DNs within IEEE 9 Bus TN were integrated. The simulations demonstrated that the proposed DN dynamics-aware TN controller design enhances system responsiveness and frequency regulation compared to the baseline, where DN dynamics are not considered.
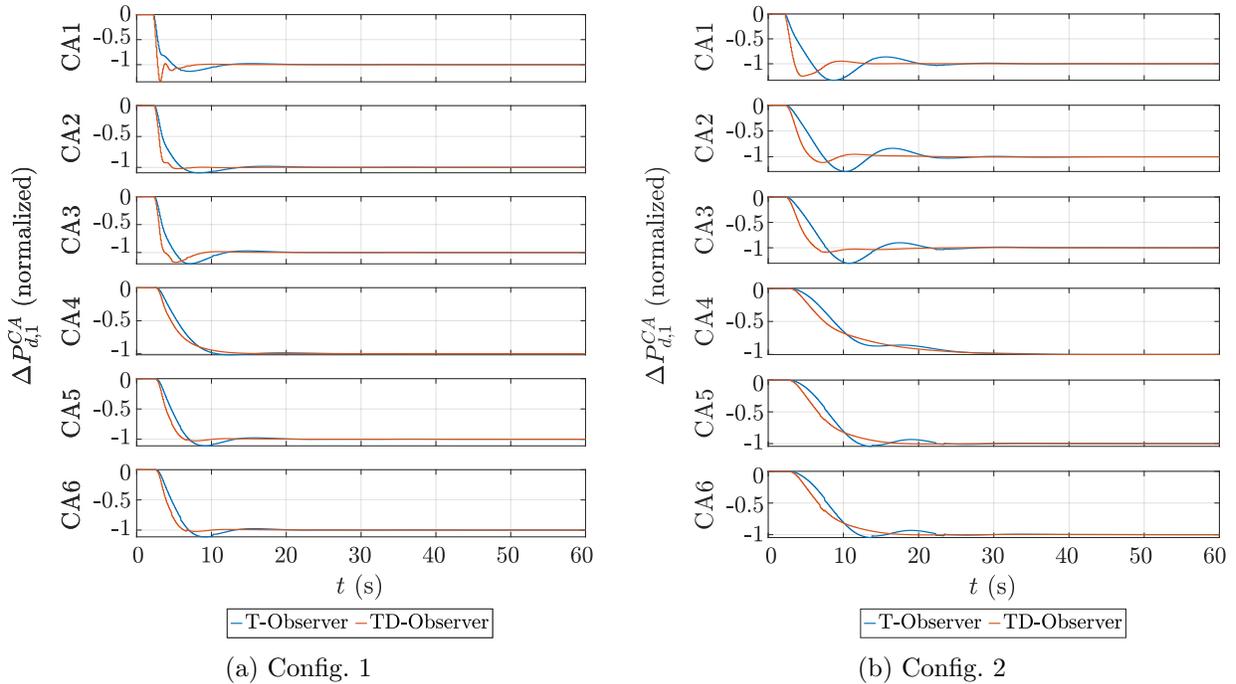
Figure 4.4: Comparison of CAs response in DN 1 for Config. 1 and Config. 2.

Chapter 5

Conclusions and Future Work

5.1   Summary

In this work, the main objective is to leverage controllable DERs within the distribution network to tack power set-points provided by the TSO at the Transmission Network (TN)-Distribution Network (DN) interface bus, while operational constraints are maintained throughout the DN and the DERs are used optimally. The key feature of the proposed work is that the design is subject to the constraint that information and management boundaries between different control areas must be respected. To achieve this objective, the work was divided to two main stages described below:

- Distribution network control architecture;

- Transmission-Distribution network integration framework

The first stage tackle the challenge in transmission-distribution coordination focusing on how to quickly and reliably coordinate DN-DERs to support the TN while ensuring operational constraints continue to be met within the DN. We develop a hierarchical feedback-based multi-area control architecture for coordination of DN-DERs, enabling the DN to quickly respond to power set-point requests from the TSO while maintaining local DN constraints. Our scheme allows for multiple independently-managed areas within the DN to optimize their local resources while coordinating to support the TN, and while maintaining data privacy. The proposed architecture minimizes communication requirements as it only requires inter-area communication between physically adjacent areas within the DN control

hierarchy. Analyzing the stability of the highly scalable control architecture yielded intuitive conditions for closed-loop stability, and we provide detailed tuning recommendations. The proposal is validated via case studies on multiple feeders, including IEEE-123 and IEEE-8500, using a custom MATLAB®-based application which integrates with OpenDSS©.

The second stage tackle the challenge of integrating the developed framework within the transmission network control scheme. This work focuses on incorporating the proposed DN hierarchical control within the broader TN control strategy. We considered a recently developed TN fast frequency controller design, where we consider integrating the DN hierarchical control structures developed in first stage within the TN framework. The novel contribution is the development of a linear model of DN dynamics that is integrated into the TN control design. The TN control design problem relies on a simplified model of the anticipated response of the DN-DERs based on the developed control structure in the first stage. This integrated design approach is validated through case studies on the IEEE 9-bus system. Each DN feeder is modeled using IEEE-123 distribution feeders with a hierarchical control structure consisting of multi-control areas. Various configurations and tuning of DN feeders are considered to assess the impact of different dynamics on the performance and stability of the integration process. The ground-up design approach enhances the responsiveness and stability of the system.

Combining the benefits of both stages —developing a scalable distribution network control architecture and integrating distribution network dynamics into transmission network control schemes—results in a comprehensive solution that enhances overall system stability and performance. The proposed architecture not only improves the system's response to dynamic disturbances but also ensures efficient coordination between control layers. By incorporating sensitivity matrices and simplified models, the transmission network control design can effectively manage DN-DERs' anticipated responses, leading to faster settling times, reduced oscillations, and better handling of varying DER dynamics and network conditions. This combined approach represents a valuable contribution to power system control and management, promoting the efficient and reliable operation of future grid systems in the face of increasing renewable integration and evolving energy demands.

The practical application of our framework is demonstrated through the MATDSS Application. MATDSS is a MATLAB®-based tool seamlessly integrated with OpenDSS©, a specialized application for simulating distribution networks. Utilizing a `COM` interface, it effectively communicates with OpenDSS© to model distribution network feeders using its solver engine. The software features a user-friendly GUI, allowing users to import existing feeders or create new ones via OpenDSS© scripts. Key features include modular functions for customizable DER and local controller behavior, partitioning feeders into control areas, and comprehensive simulation setup management. It provides real-time monitoring, customiz-

able plotting, and data export functionalities for simulation analysis. MATDSS enhances workflow efficiency and facilitates quick simulation initialization, making it highly usable for researchers and engineers working on complex distribution network control architectures and simulations.

5.2   future work

5.2.1   Distribution Network Control Architecture

Moving forward, there are several avenues to enhance the robustness and efficiency of the developed distribution network control architecture. Firstly, automating the tuning process for controller parameters and DERs' cost functions represents a critical step. This automation aims to streamline the optimization of controller settings to achieve desired time-domain responses effectively [107–109]. Additionally, integrating more realistic DER models into the architecture will improve the accuracy of simulations and enhance the predictive capabilities of the control system.

Explicitly accounting for the diverse dynamics of DERs is another pivotal area for future research. This includes developing strategies to coordinate both fast-responding and slow-responding DERs within the hierarchical control framework. Such coordination will optimize resource allocation and improve overall system stability under varying operating conditions.

To address practical challenges, the design should be made robust against communication delays and measurement errors. Implementing robust control mechanisms that can accommodate these uncertainties will ensure reliable operation in real-world scenarios. Furthermore, incorporating actual DERs data (e.g. power profiles for renewable sources) from field installations will provide valuable insights into system behavior and validate the effectiveness of the control strategies in diverse operational environments. As the scheme requires partitioning of the system into areas, investigating the impact of different partitioning on controller performance is also an important direction, as is exploring the extension of our approach to non-radial distribution topologies.

A related advance would be a formal stability analysis of the PID implementation from Section 3.6.1, and an extension of the stability analysis to include nonlinear feeder models and nonlinear loads. Further development is also required in addressing voltage regulation challenges, especially in scenarios where lower-level areas might become burdened in heavily loaded feeders; this will likely require improved coordination across areas, to ensure more

effective and fair voltage and current management. A promising direction involves leveraging data-driven approaches for sensitivity analysis. By utilizing real-time network measurements to estimate DERs' sensitivities, as discussed in [50, 110], the architecture can evolve towards a more adaptive and responsive control framework.

5.2.2 Transmission-Distribution Coordination Framework

Our near-term future work will focus on formally demonstrating perfect disturbance rejection for the integrated system. By analyzing closed-loop system dynamics with the observer-based control strategy, we aim to build a formal proof that will solidify the theoretical foundation for this approach.

Furthermore, we aim to extend the linear model of the DN to a hierarchical structure, making it more capable of relying on local model information within each CA. This includes exploring the possibility of CAs sharing models as transfer functions based on their internal sensitivities and DER capabilities to protect their privacy. In addition, examining the impact of communication delays and ensuring robustness against measurement errors are critical when integrating DN dynamics into the TN control scheme. We plan to investigate and develop methodologies to mitigate the impact of these factors to enhance system reliability and responsiveness.

Additionally, we plan to integrate the DN control structure into more complex TN control frameworks. This integration will allow DN resources to participate in providing ancillary services in addition to frequency support such as voltage support and black start.

References

[1] Matasci, Sara, "How solar panel cost and efficiency have changed over time", 2021, [Data retrieved - Aug 2021] link: https://news.energysage.com/solar-panel-efficiency-cost-over-time/.

[2] "Solar PV module prices", [Data retrieved - Aug 2021] link: https://ourworldindata.org/grapher/solar-pv-prices.

[3] Ministry of Energy, "Powering Ontario's Growth: Ontario's Plan for a Clean Energy Future," Goverment of Ontario, 2023. [Online]. Available: https://www.ontario.ca/page/powering-ontarios-growth

[4] A. Huque and E. Farantatos, *Grid Forming Inverters: EPRI Tutorial*, 2020. [Online]. Available: https://www.epri.com/research/products/000000003002018676

[5] Office of Energy Efficiency & Renewable Energy, *Solar Integration: Inverters and Grid Services Basics*, U.S. Department of Energy. [data retrieved - Oct. 2021] link: https://www.energy.gov/eere/solar/solar-integration-inverters-and-grid-services-basics.

[6] Electric Power Research Institute, Inc., *Impact of Inverter-Based Resources on Protection Schemes Based on Negative Sequence Components*, 2019. [Online]. Available: https://www.epri.com/research/products/000000003002016197

[7] A. Tuohy, P. Dattaray, E. Farantatos, A. Kelly, and E. Lannoye, *Implications of Reduced Inertia Levels on the Electricity System: Technical Report on the Challenges and Solutions for System Operations with Very High Penetrations of Non-Synchronous Resources*, 2019. [Online]. Available: https://www.epri.com/research/products/000000003002014970

[8] F. Milano, F. Dörfler, G. Hug, D. J. Hill, and G. Verbič, "Foundations and challenges of low-inertia systems (invited paper)," in *Power Syst. Computation Conf.*, 2018, pp. 1–25.

[9] International Energy Agency, "Snapshot of Global PV Markets-2021", [Data retrieved - Aug. 2021] link:https://iea-pvps.org/wp-content/uploads/2021/04/IEA_PVPS_Snapshot_2021-V3.pdf.

[10] J. Björk, K. H. Johansson, and F. Dörfler, "Dynamic virtual power plant design for fast frequency reserves: Coordinating hydro and wind," 2021.

[11] J. Alipoor, Y. Miura, and T. Ise, "Power system stabilization using virtual synchronous generator with alternating moment of inertia," *IEEE Journal of Emerging and Selected Topics in Power Electronics*, vol. 3, no. 2, pp. 451–458, 2015.

[12] Y. Qi, T. Yang, J. Fang, Y. Tang, K. R. R. Potti, and K. Rajashekara, "Grid inertia support enabled by smart loads," *IEEE Trans. Power Electron.*, vol. 36, no. 1, pp. 947–957, 2021.

[13] R. Yan, N.-A. Masood, T. Kumar Saha, F. Bai, and H. Gu, "The anatomy of the 2016 south australia blackout: A catastrophic event in a high renewable network," *IEEE Trans. Power Syst.*, vol. 33, no. 5, pp. 5374–5388, 2018.

[14] S. Sreekumar, D. S. Kumar, and J. Savier, "A case study on self healing of smart grid with islanding and inverter volt–var function," *IEEE Trans. Ind. Appl.*, vol. 56, no. 5, pp. 5408–5416, 2020.

[15] K. H. Abdul-Rahman, H. Alarian, M. Rothleder, P. Ristanovic, B. Vesovic, and B. Lu, "Enhanced system reliability using flexible ramp constraint in CAISO market," in *Proc. IEEE PESGM*, 2012, pp. 1–6.

[16] Y. Liu, J. Li, and L. Wu, "Coordinated optimal network reconfiguration and voltage regulator/der control for unbalanced distribution systems," *IEEE Trans. Smart Grid*, vol. 10, no. 3, pp. 2912–2922, 2019.

[17] R. Dobbe, O. Sondermeijer, D. Fridovich-Keil, D. Arnold, D. Callaway, and C. Tomlin, "Toward distributed energy services: Decentralizing optimal power flow with machine learning," *IEEE Trans. Smart Grid*, vol. 11, no. 2, pp. 1296–1306, 2020.

[18] A. Khurram, M. Amini, L. A. D. Espinosa, P. D. H. Hines, and M. R. Almassalkhi, "Real-time grid and der co-simulation platform for testing large-scale der coordination schemes," *IEEE Trans. Smart Grid*, vol. 13, no. 6, pp. 4367–4378, 2022.

[19] Federal Energy Regulatory Commission, "Participation of distributed energy resource aggregations in markets operated by regional transmission organizations

and independent system operators," Department of Energy, FERC Document 172 FERC 61,247, September 2020, docket No. RM18-9-000; Order No. 2222. [Online]. Available: https://www.ferc.gov/sites/default/files/2020-09/E-1_0.pdf

[20] A. Dubey, S. Paudyal *et al.*, "Distribution system optimization to manage distributed energy resources (ders) for grid services," *Foundations and Trends® in Electric Energy Systems*, vol. 6, no. 3-4, pp. 120–264, 2023.

[21] W. Liu and F. Ding, "Collaborative distribution system restoration planning and real-time dispatch considering behind-the-meter ders," *IEEE Trans. Power Syst.*, vol. 36, no. 4, pp. 3629–3644, 2021.

[22] J. Stekli, L. Bai, U. Cali, U. Halden, and M. F. Dynge, "Distributed energy resource participation in electricity markets: A review of approaches, modeling, and enabling information and communication technologies," *Energy Strategy Reviews*, vol. 43, p. 100940, 2022.

[23] B. Kellison, "The next five years will see massive distributed energy resource growth," Wood Mackenzie, 2020. [Online]. Available: https://www.woodmac.com/news/editorial/der-growth-united-states/

[24] J. S. John, "5 major trends driving the $110b us distributed energy resources market through 2025," Greentech Media, 2020. [Online]. Available: https://www.greentechmedia.com/articles/read/5-takeaways-on-the-future-of-the-u.s-distributed-energy-resources-market

[25] M. Miller, E. Martinot, S. Cox, B. Speer, O. Zinaman, S. Booth, R. Zissler, J. Cochran, S. Soonee, P. Audinet *et al.*, "Status report on power system transformation: A 21st century power partnership report," National Renewable Energy Lab.(NREL), Golden, CO (United States), Tech. Rep., 2015.

[26] H. Gerard, E. I. Rivero Puente, and D. Six, "Coordination between transmission and distribution system operators in the electricity sector: A conceptual framework," *Utilities Policy*, vol. 50, pp. 40–48, 2018.

[27] S. Xia, S. Bu, C. Wan, X. Lu, K. W. Chan, and B. Zhou, "A fully distributed hierarchical control framework for coordinated operation of ders in active distribution power networks," *IEEE Trans. Power Syst.*, vol. 34, no. 6, pp. 5184–5197, 2019.

[28] Z. Yuan and M. R. Hesamzadeh, "Hierarchical coordination of tso-dso economic dispatch considering large-scale integration of distributed energy resources," *Applied Energy*, vol. 195, pp. 600–615, 2017.

[29] North American Electric Reliability Corporation (NERC), *Glossary of Terms Used in NERC Reliability Standards*, 2024. [Online]. Available: https://www.nerc.com/pa/Stand/Glossary%20of%20Terms/Glossary_of_Terms.pdf

[30] Electric Power Research Institute, Inc., *Ancillary Services in the United States: Technical Requirements, Market Designs and Price Trends*, 2019. [Online]. Available: https://www.epri.com/research/products/000000003002015670

[31] I. Farhat, E. Ekomwenrenren, J. W. Simpson-Porco, E. Farantatos, M. Patel, and A. Haddadi, "A multi-area architecture for real-time feedback-based optimization of distribution grids," 2024.

[32] E. Ekomwenrenren, Z. Tang, J. W. Simpson-Porco, E. Farantatos, M. Patel, and H. Hooshyar, "Hierarchical coordinated fast frequency control using inverter-based resources," *IEEE Trans. Power Syst.*, vol. 36, no. 6, pp. 4992–5005, Nov. 2021.

[33] Z. Tang, E. Ekomwenrenren, J. W. Simpson-Porco, E. Farantatos, M. Patel, and H. Hooshyar, "Measurement-based fast coordinated voltage control for transmission grids," *IEEE Trans. Power Syst.*, vol. 36, no. 4, pp. 3416–3429, 2021.

[34] E. Ekomwenrenren, Z. Tang, J. W. Simpson-Porco, E. Farantatos, M. Patel, H. Hooshyar, and A. Haddadi, "An integrated frequency-voltage controller for next-generation power systems," Jul. 2022.

[35] R. Poudineh, C. Brandstätt, and F. Billimoria, *Electricity distribution networks in the decentralisation era: rethinking economics and regulation.* Springer Nature, 2022.

[36] S. P. Boyd and L. Vandenberghe, *Convex optimization.* Cambridge university press, 2004.

[37] A. Bernstein and E. Dall'Anese, "Real-time feedback-based optimization of distribution grids: A unified approach," *IEEE Trans. Control Net. Syst.*, vol. 6, no. 3, pp. 1197–1209, 2019.

[38] E. Dall'Anese and A. Simonetto, "Optimal power flow pursuit," *IEEE Trans. Smart Grid*, vol. 9, no. 2, pp. 942–952, 2018.

[39] R. R. Jha and A. Dubey, "Network-level optimization for unbalanced power distribution system: Approximation and relaxation," *IEEE Trans. Power Syst.*, vol. 36, no. 5, pp. 4126–4139, 2021.

[40] S. Karagiannopoulos, C. Mylonas, P. Aristidou, and G. Hug, "Active distribution grids providing voltage support: The swiss case," *IEEE Trans. Smart Grid*, vol. 12, no. 1, pp. 268–278, 2021.

[41] H. T. Nguyen and D.-H. Choi, "Decentralized distributionally robust coordination between distribution system and charging station operators in unbalanced distribution systems," *IEEE Trans. Smart Grid*, vol. 14, no. 3, pp. 2164–2177, 2023.

[42] R. Gupta, F. Sossan, and M. Paolone, "Grid-aware distributed model predictive control of heterogeneous resources in a distribution network: Theory and experimental validation," *IEEE Transactions on Energy Conversion*, vol. 36, no. 2, pp. 1392–1402, 2021.

[43] L. Wang, A. Dubey, A. H. Gebremedhin, A. K. Srivastava, and N. Schulz, "Mpc-based decentralized voltage control in power distribution systems with ev and pv coordination," *IEEE Trans. Smart Grid*, vol. 13, no. 4, pp. 2908–2919, 2022.

[44] X. Chen, E. Dall'Anese, C. Zhao, and N. Li, "Aggregate power flexibility in unbalanced distribution systems," *IEEE Trans. Smart Grid*, vol. 11, no. 1, pp. 258–269, 2020.

[45] X. Chen and N. Li, "Leveraging two-stage adaptive robust optimization for power flexibility aggregation," *IEEE Trans. Smart Grid*, vol. 12, no. 5, pp. 3954–3965, 2021.

[46] A. Ingalalli and S. Kamalasadan, "Decentralized state estimation-based optimal integral model predictive control of voltage and frequency in the distribution system microgrids," *IEEE Trans. Smart Grid*, vol. 14, no. 3, pp. 1790–1803, 2023.

[47] B. Fritz, H. Ipach, and C. Becker, "Hierarchical online-optimization for the control of flexible loads and generators in distribution grids," in *PESS 2021; Power and Energy Student Summit*, 2021, pp. 1–6.

[48] G. Cavraro, A. Bernstein, R. Carli, and S. Zampieri, "Feedback power cost optimization in power distribution networks with prosumers," *IEEE Trans. Control Net. Syst.*, vol. 9, no. 4, pp. 1633–1644, 2022.

[49] S. Fan, G. He, X. Zhou, and M. Cui, "Online optimization for networked distributed energy resources with time-coupling constraints," *IEEE Trans. Smart Grid*, vol. 12, no. 1, pp. 251–267, 2021.

[50] S. Nowak, Y. C. Chen, and L. Wang, "Measurement-based optimal der dispatch with a recursively estimated sensitivity model," *IEEE Trans. Power Syst.*, vol. 35, no. 6, pp. 4792–4802, 2020.

[51] M. Colombino, J. W. Simpson-Porco, and A. Bernstein, "Towards robustness guarantees for feedback-based optimization," in *Proc. IEEE CDC*, 2019, pp. 6207–6214.

[52] M. Colombino, E. Dall'Anese, and A. Bernstein, "Online optimization as a feedback controller: Stability and tracking," *IEEE Trans. Control Net. Syst.*, vol. 7, no. 1, pp. 422–432, 2019.

[53] L. S. P. Lawrence, J. W. Simpson-Porco, and E. Mallada, "Linear-convex optimal steady-state control," *IEEE Trans. Autom. Control*, vol. 66, no. 11, pp. 5377–5384, Nov. 2021.

[54] L. Ortmann, A. Hauswirth, I. Caduff, F. Dörfler, and S. Bolognani, "Experimental validation of feedback optimization in power distribution grids," *Electric Power Syst. Research*, vol. 189, p. 106782, 2020.

[55] E. Dall'Anese, S. V. Dhople, and G. B. Giannakis, "Regulation of dynamical systems to optimal solutions of semidefinite programs: Algorithms and applications to ac optimal power flow," in *Proc. ACC*, Chicago, IL, USA, July 2015, pp. 2087–2092.

[56] G. Bianchin, J. Cortés, J. I. Poveda, and E. Dall'Anese, "Time-varying optimization of LTI systems via projected primal-dual gradient flows," *IEEE Trans. Control Net. Syst.*, vol. 9, no. 1, pp. 474–486, 2022.

[57] A. Bernstein, J. Comden, Y. Chen, and J. Wang, "Time-varying feedback optimization for quadratic programs with heterogeneous gradient step sizes," 2023.

[58] Y. Zhang, E. Dall'Anese, and M. Hong, "Online proximal-admm for time-varying constrained convex optimization," *IEEE Trans. Signal Inf. Process. Netw.*, vol. 7, pp. 144–155, 2021.

[59] H. Laaksonen, C. Parthasarathy, H. Khajeh, M. Shafie-Khah, and N. Hatziargyriou, "Flexibility services provision by frequency-dependent control of on-load tap-changer and distributed energy resources," *IEEE Access*, vol. 9, pp. 45 587–45 599, 2021.

[60] A. M. Prostejovsky, M. Marinelli, M. Rezkalla, M. H. Syed, and E. Guillo-Sansano, "Tuningless load frequency control through active engagement of distributed resources," *IEEE Trans. Power Syst.*, vol. 33, no. 3, pp. 2929–2939, 2018.

[61] Q. Hong, M. Nedd, S. Norris, I. Abdulhadi, M. Karimi, V. Terzija, B. Marshall, K. Bell, and C. Booth, "Fast frequency response for effective frequency control in power systems with low inertia," *The Journal of Eng.*, vol. 2019, no. 16, pp. 1696–1702, 2019.

[62] V. Häberle, M. W. Fisher, E. Prieto-Araujo, and F. Dörfler, "Control design of dynamic virtual power plants: An adaptive divide-and-conquer approach," *IEEE Trans. Power Syst.*, vol. 37, no. 5, pp. 4040–4053, 2022.

[63] V. Häberle, A. Tayyebi, X. He, E. Prieto-Araujo, and F. Dörfler, "Grid-forming and spatially distributed control design of dynamic virtual power plants," *IEEE Trans. Smart Grid*, vol. 15, no. 2, pp. 1761–1777, 2024.

[64] H. Mavalizadeh, L. A. D. Espinosa, and M. R. Almassalkhi, "Improving frequency response with synthetic damping available from fleets of distributed energy resources," *IEEE Trans. Power Syst.*, vol. 39, no. 2, pp. 4498–4509, 2024.

[65] H. Mavalizadeh, L. A. Duffaut Espinosa, and M. R. Almassalkhi, "Decentralized frequency control using packet-based energy coordination," in *Proc. IEEE Conf. Smart Grid Comm.*, 2020, pp. 1–7.

[66] F. Sanniti, R. Benato, and F. Milano, "Participation of ders to the bottom-up power system frequency restoration processes," *IEEE Trans. Power Syst.*, vol. 38, no. 3, pp. 2630–2640, 2023.

[67] X. Han, A. M. Kosek, D. E. Morales Bondy, H. W. Bindner, S. You, D. V. Tackie, J. Mehmedalic, and F. Thordarson, "Assessment of distribution grid voltage control strategies in view of deployment," in *2014 IEEE International Workshop on Intelligent Energy Systems (IWIES)*, 2014, pp. 46–51.

[68] K. Utkarsh, F. Ding, X. Jin, M. Blonsky, H. Padullaparti, and S. P. Balamurugan, "A network-aware distributed energy resource aggregation framework for flexible, cost-optimal, and resilient operation," *IEEE Trans. Smart Grid*, vol. 13, no. 2, pp. 1213–1224, 2022.

[69] A. Maitra, L. Rogers, and R. Handa, "Program on technology innovation: Microgrid implementations: Literature review," *Palo Alto, California*, 2016.

[70] J. Ikäheimo, C. Evens, and S. Kärkkäinen, "Der aggregator business: the finnish case," *Technical Research Centre of Finland (VTT): Espoo, Finland*, 2010.

[71] E. Dall'Anese, H. Zhu, and G. B. Giannakis, "Distributed optimal power flow for smart microgrids," *IEEE Trans. Smart Grid*, vol. 4, no. 3, pp. 1464–1475, 2013.

[72] B. Morvaj, R. Evins, and J. Carmeliet, "Optimization framework for distributed energy systems with integrated electrical grid constraints," *Applied Energy*, vol. 171, pp. 296–313, 2016.

[73] I. De Mel, O. V. Klymenko, and M. Short, "Balancing accuracy and complexity in optimisation models of distributed energy systems and microgrids with optimal power flow: A review," *Sustainable Energy Technologies and Assessments*, vol. 52, p. 102066, 2022.

[74] N. Amjady, A. Attarha, S. Dehghan, and A. J. Conejo, "Adaptive robust expansion planning for a distribution network with ders," *IEEE Trans. Power Syst.*, vol. 33, no. 2, pp. 1698–1715, 2018.

[75] M. Silva, H. Morais, and Z. Vale, "An integrated approach for distributed energy resource short-term scheduling in smart grids considering realistic power system simulation," *Energy Conversion and Management*, vol. 64, pp. 273–288, 2012.

[76] Y. Riffonneau, S. Bacha, F. Barruel, and S. Ploix, "Optimal power flow management for grid connected pv systems with batteries," *IEEE Trans. Sust. Energy*, vol. 2, no. 3, pp. 309–320, 2011.

[77] M. D. Al-falahi, S. Jayasinghe, and H. Enshaei, "A review on recent size optimization methodologies for standalone solar and wind hybrid renewable energy system," *Energy Conversion and Management*, vol. 143, pp. 252–274, 2017.

[78] W. Lin and C. Zhao, "Cost functions over feasible power transfer regions of virtual power plants," *IEEE Systems Journal*, vol. 17, no. 2, pp. 2950–2960, 2023.

[79] A. Bernstein and E. Dall'Anese, "Linear power-flow models in multiphase distribution networks," in *IEEE PES Innov. Smart Grid Tech. Conf. Europe*, 2017, pp. 1–6.

[80] A. Bernstein, C. Wang, E. Dall'Anese, J.-Y. Le Boudec, and C. Zhao, "Load flow in multiphase distribution networks: Existence, uniqueness, non-singularity and linear models," *IEEE Trans. Power Syst.*, vol. 33, no. 6, pp. 5832–5843, 2018.

[81] V. I. Sumin and M. I. Sumin, "On the iterative regularization of the lagrange principle in convex optimal control problems for distributed systems of the volterra type with operator constraints," *Differential Equations*, vol. 58, no. 6, pp. 791–809, Jun 2022.

[82] B. Seal, "Understanding DERMS," *Electric Power Research Institute (EPRI) Technical Update (3002013049)*, vol. 2018, 2018. [Online]. Available: https://www.epri.com/research/products/000000003002013049

[83] B. Deaver, "Distribution management systems planning guide," *Electric Power Research Institute (EPRI), Technical Update (1024385)*, 2013. [Online]. Available: https://www.epri.com/research/products/1024385

[84] A. Pratt, S. Veda, A. Maitra, T. Hubert, J. Reilly, J. Wang, R. Singh, N. Kang, and X. Lu, "DMS advanced applications for accommodating high penetrations of DERs and microgrids," National Renewable Energy Lab.(NREL), Golden, CO (United States), Tech. Rep., 2017. [Online]. Available: https://www.nrel.gov/docs/fy17osti/67775.pdf

[85] P. Kundur, *Power System Stability And Control.* McGraw-Hill, 1994.

[86] J. D. Glover, T. J. Overbye, and M. S. Sarma, *Power system analysis & design.* Cengage Learning, 2017.

[87] J. J. Grainger and J. W. D. Stevenson, *Power system analysis.* McGraw-Hill, 1999.

[88] H. Saadat *et al.*, *Power system analysis.* McGraw-hill, 1999, vol. 2.

[89] A. Agarwal, J. W. Simpson-Porco, and L. Pavel, "Game-theoretic feedback-based optimization," *IFAC-PapersOnLine*, vol. 55, no. 13, pp. 174–179, 2022, iFAC NecSys Workshop.

[90] L. Pavel, *Game theory for control of optical networks.* Springer Science & Business Media, 2012.

[91] G. Belgioioso, D. Liao-McPherson, M. H. de Badyn, S. Bolognani, J. Lygeros, and F. Dörfler, "Sampled-data online feedback equilibrium seeking: Stability and tracking," in *Proc. IEEE CDC*, Austin, TX, USA, 2021, pp. 2702–2708.

[92] F. Facchinei and C. Kanzow, "Generalized nash equilibrium problems," *Annals of Operations Research*, vol. 175, no. 1, pp. 177–211, Mar 2010.

[93] A. Fischer, M. Herrich, and K. Schönefeld, "Generalized nash equilibrium problems - recent advances and challenges," *Pesquisa Operacional*, vol. 34, no. 3, p. 521–558, Sep 2014.

[94] X. Zhou, "On the Fenchel duality between strong convexity and lipschitz continuous gradient," 2018.

[95] F. Facchinei and J.-S. Pang, *Finite-dimensional variational inequalities and complementarity problems.* Springer, 2003, vol. 2.

[96] M. Colombino, J. W. Simpson-Porco, and A. Bernstein, "Towards robustness guarantees for feedback-based optimization," in *Proc. IEEE CDC*, 2019, pp. 6207–6214.

[97] G. Dileep, "A survey on smart grid technologies and applications," *Renewable Energy*, vol. 146, pp. 2589–2625, 2020.

[98] I. Ali and S. S. Hussain, "Control and management of distribution system with integrated ders via iec 61850 based communication," *Engineering Science and Technology, an International Journal*, vol. 20, no. 3, pp. 956–964, 2017.

[99] Electric Power Research Institute (EPRI), "Open Distribution System Simulator (OpenDSS - V9.6.1.3)," https://www.epri.com/pages/sa/opendss, 2023.

[100] I. Farhat, "MATDSS application v0.92." [Online]. Available: https://github.com/aldahabi27/MATDSS

[101] ——, "Supplementary online materials for "transmission and distribution networks coordination: A novel multi-layered control structure" manuscript." [Online]. Available: https://1drv.ms/b/s!AmH_VfOdVVKazYUpDEVplHjtvj-7ZA?e=oyfXD4

[102] P. Anderson and M. Mirheydar, "A low-order system frequency response model," *IEEE Trans. Power Syst.*, vol. 5, no. 3, pp. 720–729, 1990.

[103] H. Min, F. Paganini, and E. Mallada, "Accurate reduced order models for coherent synchronous generators," in *Allerton Conf on Comm, Ctrl & Comp*, 2019, pp. 316–317.

[104] W. S. Levine, *The control systems handbook: control system advanced methods.* CRC press, 2018.

[105] A. Isidori, *Lectures in feedback design for multivariable systems.* Springer, 2017.

[106] P. M. Anderson and A. A. Fouad, *Power system control and stability.* John Wiley & Sons, 2008.

[107] K. Åström and T. Hägglund, *Advanced PID Control.* ISA-The Instrumentation, Systems, and Automation Society; Research Triangle Park, NC 27709, 2006.

[108] V. Häberle, L. Huang, X. He, E. Prieto-Araujo, and F. Dörfler, "Dynamic ancillary services: From grid codes to transfer function-based converter control," 2023.

[109] J. Comden, J. Wang, and A. Bernstein, "Adaptive primal-dual control for distributed energy resource management," 2023.

[110] Z. Tang, E. Ekomwenrenren, J. W. Simpson-Porco, E. Farantatos, M. Patel, A. Haddadi, and H. Hooshyar, "Data-driven extension of "measurement-based fast coordinated voltage control for transmission grids"," *IEEE Trans. Power Syst.*, 2022.

APPENDICES

Appendix A

Distribution Network Model and DERs' sensitivity matrices (A, B, M, H)

In this appendix, we develop the modified sensitivity matrices discussed in Section 3.2.2. We rely on the same DN circuit model and introduce some parameters that are necessary for the development of these matrices.

A.1 Distribution Network Model

We adopt the multi-phase distribution model presented in [79,80]. Within each control area, we consider the same model. For the ith CA, we let $\overline{\mathcal{N}}_i = \{0\} \cup \mathcal{N}_i$ with $\mathcal{N}_i := \{1, 2, \ldots, N_i\}$ denote the set of buses, where the interface bus of the CA is given the node "0". We consider a general setup where each bus is potentially multi-phase, with up to three phases. In the annotations below, we show the derivations and relationships for three phases, where for any configurations with less than three phases, the corresponding components can be set to zero. Also, we drop the control area indexing 'i' with the understanding that all parameters and variables belong to the ith CA.

In addition, we recall that $\mathcal{M}_v$ denotes the set of monitored and controlled bus voltages and $\mathcal{M}_i$ denotes the set of monitored and controlled branch currents. For more details about those sets and structure details, refer to Section 3.2.2.

We define $\mathbf{Y}$ as the three-phase admittance matrix for the distribution network as

$$\mathbf{Y} := \begin{bmatrix} \mathbf{Y}_{00} & \mathbf{Y}_{0L} \\ \mathbf{Y}_{L0} & \mathbf{Y}_{LL} \end{bmatrix} \in \mathbb{C}^{3(N+1)\times 3(N+1)} \tag{A.1}$$

where $\mathbf{Y}_{00} \in \mathbb{C}^{3\times3}$, $\mathbf{Y}_{L0} \in \mathbb{C}^{3N\times3}$, $\mathbf{Y}_{0L} \in \mathbb{C}^{3\times3N}$ and $\mathbf{Y}_{LL} \in \mathbb{C}^{3N\times3N}$ when considering an all 3-phase buses. In addition, we define $\mathbf{G}$ as $3N \times 3N$ block diagonal matrix that is considered as *phase-to-ground* to *phase-to-phase* (3-phase) voltage conversion matrix.

$$\mathbf{G} := \begin{bmatrix} \boldsymbol{\Gamma} & & \\ & \ddots & \\ & & \boldsymbol{\Gamma} \end{bmatrix}, \qquad \boldsymbol{\Gamma} := \begin{bmatrix} 1 & -1 & 0 \\ 0 & 1 & -1 \\ -1 & 0 & 1 \end{bmatrix} \tag{A.2}$$

In [79, 80], the linear models for voltages, currents and interface bus powers that capture active sources or DERs sensitivities are developed for wye and delta connected devices separately. We show next the main results from [79, 80], where Table A.1 lists the main parameters used in their linear model.

Table A.1: Distribution network model parameters

Parameter	Description	Parameter	Description
$\mathbf{x}^Y$	Active and reactive powers for wye-connected sources and devices	$\hat{\mathbf{v}}$	Voltage profile of the network (for linearization purposes)
$\mathbf{x}^\Delta$	Active and reactive powers for delta-connected sources and devices	$\mathbf{w}$	Zero-load voltage profile
$\bar{c}$	denotes conjugate of c		

A.1.1 Linear models for $\mathbf{v}, \mathbf{i}$ and $\mathbf{s}_0$

Voltage Phasor : The voltage profile phasor is linearly modeled as a function of wye and delta powers of devices as

$$\tilde{\mathbf{v}} = \mathbf{M}^Y \mathbf{x}^Y + \mathbf{M}^\Delta \mathbf{x}^\Delta + \mathbf{a} \tag{A.3a}$$

where

$$\mathbf{M}^Y = \left[\mathbf{Y}_{LL}^{-1} \mathsf{diag}(\overline{\hat{\mathbf{v}}})^{-1}, -\jmath \mathbf{Y}_{LL}^{-1} \mathsf{diag}(\overline{\hat{\mathbf{v}}})^{-1} \right], \tag{A.3b}$$

$$\mathbf{M}^\Delta = \left[\mathbf{Y}_{LL}^{-1} \mathbf{G}^\top \mathsf{diag}\left(\mathbf{G}\overline{\hat{\mathbf{v}}} \right)^{-1}, -\jmath \mathbf{Y}_{LL}^{-1} \mathbf{G}^\top \mathsf{diag}\left(\mathbf{G}\overline{\hat{\mathbf{v}}} \right)^{-1} \right], \tag{A.3c}$$

$$\mathbf{a} = \mathbf{w}. \tag{A.3d}$$

Voltage magnitude : The voltage profile magnitude is obtained from the phasor profile described in (A.3) as

$$|\tilde{\mathbf{v}}| = \mathbf{K}^Y \mathbf{x}^Y + \mathbf{K}^\Delta \mathbf{x}^\Delta + \mathbf{b} \tag{A.4a}$$

where

$$\mathbf{W} = \mathsf{diag}(\mathbf{w}), \tag{A.4b}$$

$$\mathbf{K}^Y = |\mathbf{W}| \ \mathsf{Re}\{\mathbf{W}^{-1}\mathbf{M}^Y\}, \tag{A.4c}$$

$$\mathbf{K}^\Delta = |\mathbf{W}| \ \mathsf{Re}\{\mathbf{W}^{-1}\mathbf{M}^\Delta\}, \tag{A.4d}$$

$$\mathbf{b} = |\mathbf{w}|. \tag{A.4e}$$

Power flow at the interface bus : The complex power flow model at the interface bus is given by

$$\tilde{\mathbf{s}}_0 = \mathbf{G}^Y \mathbf{x}^Y + \mathbf{G}^\Delta \mathbf{x}^\Delta + \mathbf{c} \tag{A.5a}$$

where

$$\mathbf{G}^Y = \mathsf{diag}(\mathbf{v}_0)\overline{\mathbf{Y}}_{0L}\overline{\mathbf{M}}^Y, \tag{A.5b}$$

$$\mathbf{G}^\Delta = \mathsf{diag}(\mathbf{v}_0)\overline{\mathbf{Y}}_{0L}\overline{\mathbf{M}}^\Delta, \tag{A.5c}$$

$$\mathbf{c} = \mathsf{diag}(\mathbf{v}_0)\left(\overline{\mathbf{Y}}_{00}\overline{\mathbf{v}}_0 + \overline{\mathbf{Y}}_{0L}\overline{\mathbf{a}}\right). \tag{A.5d}$$

Branch currents : The current flowing in the line connecting buses i & j is given by

$$\tilde{\mathbf{i}}_{ij} = \mathbf{J}_{ij}^Y \mathbf{x}^Y + \mathbf{J}_{ij}^\Delta \mathbf{x}^\Delta + \mathbf{c}_{ij} \tag{A.6a}$$

where

$$\mathbf{Z}_{ij} \in \mathbb{C}^{3\times 3} \text{ phase impedance matrix of line } (i,j), \tag{A.6b}$$

$$\mathbf{Y}_{ij}^{(s)} \in \mathbb{C}^{3\times 3} \text{ shunt admittance matrix of line } (i,j), \tag{A.6c}$$

$$\mathbf{E}_i = \left[\mathbf{0}_{3\times 3(i-1)}, \mathbf{I}_3, \mathbf{0}_{3\times 3(N-i)}\right], \tag{A.6d}$$

$$\mathbf{J}_{ij}^Y = \left[\left(\mathbf{Y}_{ij}^{(s)} + \mathbf{Z}_{ij}^{-1}\right)\mathbf{E}_i - \mathbf{Z}_{ij}^{-1}\mathbf{E}_j\right]\mathbf{M}^Y, \tag{A.6e}$$

$$\mathbf{J}_{ij}^\Delta = \left[\left(\mathbf{Y}_{ij}^{(s)} + \mathbf{Z}_{ij}^{-1}\right)\mathbf{E}_i - \mathbf{Z}_{ij}^{-1}\mathbf{E}_j\right]\mathbf{M}^\Delta, \tag{A.6f}$$

$$\mathbf{c}_{ij} = \left[\left(\mathbf{Y}_{ij}^{(s)} + \mathbf{Z}_{ij}^{-1}\right)\mathbf{E}_i - \mathbf{Z}_{ij}^{-1}\mathbf{E}_j\right]\mathbf{w}. \tag{A.6g}$$

Following the main results, we note the following:

- The linear models shown above considers the wye and delta devices separately. However, in our control architecture, we aim to control all DERs according to their cost functions and utilize them to track power requests and maintain circuit constraints without explicitly separating them to: wye/delta or *1-/2-/3-* phases connected devices.

- Therefore, we aim to capture their connection type and number of phases effects within a unified sensitivity matrices that implicitly capture these information.

- In the following section, we regroup the DERs and develop a unified sensitivity matrices that map the DERs accordingly.

A.2   Modified Equations of distribution network model

Following the main results of [79, 80], we now derive a linearized model for the distribution network that groups wye and delta DERs to obtain a linear model of the form

$$\text{(voltage magnitude)} \quad \tilde{\mathbf{v}}_{\mathcal{M}_v}(\mathbf{x}_i) = \sum_{j \in \mathcal{D}_i} A_j x_j + a_j \qquad = \mathbf{A}_i \mathbf{x}_i + \mathbf{a}_i \qquad \text{(A.7a)}$$

$$\text{(current magnitude)} \quad \tilde{\mathbf{i}}_{L,\mathcal{M}_i}(\mathbf{x}_i) = \sum_{j \in \mathcal{D}_i} B_j x_j + b_j \qquad = \mathbf{B}_i \mathbf{x}_i + \mathbf{b}_i \qquad \text{(A.7b)}$$

$$\tilde{\mathbf{p}}_0(\mathbf{x}_i) = \sum_{j \in \mathcal{D}_i} M_j x_j + m_j \qquad = \mathbf{M}_i \mathbf{x}_i + \mathbf{m}_i \qquad \text{(A.7c)}$$

$$\tilde{\mathbf{q}}_0(\mathbf{x}_i) = \sum_{j \in \mathcal{D}_i} H_j x_j + h_j \qquad = \mathbf{H}_i \mathbf{x}_i + \mathbf{h}_i \qquad \text{(A.7d)}$$

where $\mathbf{x}_i = \mathsf{col}(x_1, \ldots, x_{D_i})$ is the vector of all DER/DER-aggregator set-points where $D_i = |\mathcal{D}_i|$ denotes the number of DERs within the control area and "$\sim$" indicates that the obtained variables are the linear modeled values. We recall that $x_1 = \mathsf{col}(p_1, q_1)$.

Mapping $\mathbf{A}, \mathbf{B}, \mathbf{M}, \mathbf{H}, \mathbf{a}, \mathbf{b}, \mathbf{m}$ & $\mathbf{h}$ to multi-phase distribution network model matrices (Eqs. A.4a, A.5a & A.6a)

In the work below, we drop the control area indexing "i" with the understanding that these calculations are done per control area. To simplify the derivations, we consider that all buses consists of three phases. However, the same logic applies for buses with 1 or 2 phases, where the missing phases are simply omitted from the vectors and matrices.

A.2.1 A matrix

When building the matrix $\mathbf{A}$, we construct it by considering one DER at a time. Then, we combine all individual DERs A matrices together to obtain a unified sensitivity matrix for all DERs that can address all DERs at once. To begin with, we have from Eq. A.4a that

$$
\begin{aligned}
|\tilde{\mathbf{v}}| &= \mathbf{K}^Y \mathbf{x}^Y + \mathbf{K}^\Delta \mathbf{x}^\Delta + \mathbf{b} \\
&= \begin{bmatrix} \mathbf{K}^Y & \mathbf{K}^\Delta \end{bmatrix} \begin{bmatrix} \mathbf{x}^Y \\ \mathbf{x}^\Delta \end{bmatrix} + \mathbf{b} \\
&= \underbrace{\begin{bmatrix} \mathbf{K}^Y & \mathbf{K}^\Delta \end{bmatrix}}_{3N \times 12N} \underbrace{\begin{bmatrix} \mathbf{p}^Y \\ \mathbf{q}^Y \\ \mathbf{p}^\Delta \\ \mathbf{q}^\Delta \end{bmatrix}}_{12N \times 1} + \mathbf{b}
\end{aligned} \tag{A.8}
$$

To extract only the measured values $|\mathbf{v}_{\mathcal{M}_\mathbf{v}}|$ out of $|\tilde{\mathbf{v}}|$, and to express the right-hand side as a function only of the DER point setpoints $\mathbf{x}$, we do the following manipulations. First, we split the powers $\mathbf{p}$ and $\mathbf{q}$ to DER and none-DER components, and then, we extract the required components. To do this, let $\mathbf{Q}_L^v \in \mathbb{R}^{3r_v \times 3N}$ select the desired measured voltages from the vector of all voltages, where the ij component is given by

$$
(Q_L^v)_{ij} = \begin{cases} 1 & \text{if the } i\text{th voltage measurement is from bus } j \\ 0 & \text{otherwise} \end{cases}
$$

and then set $\mathbf{Q}_L^v = Q_L^v \otimes I_3$. With this notation, we have that

$$
|\tilde{\mathbf{v}}_{\mathcal{M}_v}| = \mathbf{Q}_L^v |\tilde{\mathbf{v}}|.
$$

Next, we wish to express $|\tilde{\mathbf{v}}|$ in terms of $\mathbf{x}$. We define a matrix $\mathbf{Q}_R$ such that

$$
\begin{bmatrix} \mathbf{p}^Y \\ \mathbf{q}^Y \\ \mathbf{p}^\Delta \\ \mathbf{q}^\Delta \end{bmatrix} = \mathbf{Q}_R \mathbf{x} + \mathbf{c}
$$

Here, $\mathbf{Q}_R$ places DER powers at the correct phases and locations within the vector of wye and delta powers, accounting for their method of interconnection:

For the jth DER connected at bus i (here $e_j \in \mathbb{R}^{2D}$ is a zero vector with 1 at the jth component)

⋄ Y-connected balanced DER (3-phases)

$$\begin{bmatrix} \mathbf{Q}_{R,\text{rows}(i:i+2)} \\ \mathbf{Q}_{R,\text{rows}(3N+i:3N+i+2)} \end{bmatrix} = \begin{bmatrix} \frac{1}{3}\mathbb{1}_3 e_{2j-1}^\top \\ \frac{1}{3}\mathbb{1}_3 e_{2j}^\top \end{bmatrix} \tag{A.9a}$$

⋄ Single-phase connected DER

$$\begin{bmatrix} \mathbf{Q}_{R,\text{rows}(i:i+2)} \\ \mathbf{Q}_{R,\text{rows}(3N+i:3N+i+2)} \end{bmatrix} = \begin{cases} \begin{bmatrix} e_{2j-1} & \mathbb{0} & \mathbb{0} & e_{2j} & \mathbb{0} & \mathbb{0} \end{bmatrix}^\top & , \text{if connected at phase } a \\ \begin{bmatrix} \mathbb{0} & e_{2j-1} & \mathbb{0} & \mathbb{0} & e_{2j} & \mathbb{0} \end{bmatrix}^\top & , \text{if connected at phase } b \\ \begin{bmatrix} \mathbb{0} & \mathbb{0} & e_{2j-1} & \mathbb{0} & \mathbb{0} & e_{2j} \end{bmatrix}^\top & , \text{if connected at phase } c \end{cases} \tag{A.9b}$$

⋄ Δ-connected balanced DER (3-phases)

$$\begin{bmatrix} \mathbf{Q}_{R,\text{rows}(6N+i:6N+i+2)} \\ \mathbf{Q}_{R,\text{rows}(9N+i:9N+i+2)} \end{bmatrix} = \begin{bmatrix} \frac{1}{3}\mathbb{1}_3 e_{2j-1}^\top \\ \frac{1}{3}\mathbb{1}_3 e_{2j}^\top \end{bmatrix} \tag{A.9c}$$

⋄ phase-to-phase connected DER

$$\begin{bmatrix} \mathbf{Q}_{R,\text{rows}(6N+i:6N+i+2)} \\ \mathbf{Q}_{R,\text{rows}(9N+i:9N+i+2)} \end{bmatrix} = \begin{cases} \begin{bmatrix} e_{2j-1} & \mathbb{0} & \mathbb{0} & e_{2j} & \mathbb{0} & \mathbb{0} \end{bmatrix}^\top & , \text{if } ab\text{-phase connected} \\ \begin{bmatrix} \mathbb{0} & e_{2j-1} & \mathbb{0} & \mathbb{0} & e_{2j} & \mathbb{0} \end{bmatrix}^\top & , \text{if } bc\text{-phase connected} \\ \begin{bmatrix} \mathbb{0} & \mathbb{0} & e_{2j-1} & \mathbb{0} & \mathbb{0} & e_{2j} \end{bmatrix}^\top & , \text{if } ca\text{-phase connected} \end{cases} \tag{A.9d}$$

⋄ Other connections - treat similarly to what presented here. One can have two phase-to-phase, or phase-to-ground connected DERs ("ab" and "bc", or "a" and "b" for example). In both cases, we consider their corresponding e_j vectors, and we scale them by $1/2$ (for balanced response).

With the defined $\mathbf{Q}_R$ rows above, we have

109

$$\underbrace{|\mathbf{v}_{\mathcal{M}_v}|}_{3r_v \times 1} = \overbrace{\underbrace{\mathbf{Q}_L^v}_{3r_v \times 3N} \underbrace{\left[\mathbf{K}^Y \quad \mathbf{K}^\Delta\right]}_{3N \times 12N} \underbrace{\mathbf{Q}_R}_{12N \times 2D}}^{\mathbf{A}} \underbrace{\begin{bmatrix} p_1 \\ q_1 \\ \vdots \\ p_D \\ q_D \end{bmatrix}}_{2D \times 1} + \overbrace{\mathbf{Q}_L^v \left(\left[\mathbf{K}^Y \quad \mathbf{K}^\Delta\right] \begin{bmatrix} \mathbf{p}^Y_{\text{none}-\text{DER}} \\ \mathbf{q}^Y_{\text{none}-\text{DER}} \\ \mathbf{p}^\Delta_{\text{none}-\text{DER}} \\ \mathbf{q}^\Delta_{\text{none}-\text{DER}} \end{bmatrix} + \mathbf{b} \right)}^{\mathbf{a}} \tag{A.10}$$

One can define the matrix $\mathbf{A}$ by defining the sensitivity matrices $\mathbf{A}_1$, $\mathbf{A}_2, \ldots$, $\mathbf{A}_D$ as shown above then combine them to get

$$\mathbf{A} = \begin{bmatrix} \mathbf{A}_1 & \cdots & \mathbf{A}_D \end{bmatrix} \tag{A.11}$$

where $\mathbf{A}_i \in \mathbb{R}^{3r_v \times 2}, \forall i \in \{1, \ldots, D\}$. Note that both, $\mathbf{Q}_L^v$ and $\mathbf{Q}_R$ are "unitless". Therefore, the unit of $\mathbf{A}$ is the same as $\mathbf{K}^Y$ and $\mathbf{K}^\Delta = \frac{V}{W}$.

A.2.2   B matrix

Following a similar approach, we start with Eq. A.6a.

$$\tilde{\mathbf{i}}_{ij} = \mathbf{J}^Y_{ij} \mathbf{x}^Y + \mathbf{J}^\Delta_{ij} \mathbf{x}^\Delta + \mathbf{c}_{ij} \tag{A.12}$$

Let the line ij map to the branch $k \in \mathcal{M}_i$. Then, we combine the J matrices, and collect all constants in new $\mathbf{b}$ vector, to get the updated equation of $\tilde{\mathbf{i}}_k$

$$\tilde{\mathbf{i}}_k = \tilde{\mathbf{i}}_{ij} = \begin{bmatrix} \mathbf{J}^Y_{ij} & \mathbf{J}^\Delta_{ij} \end{bmatrix} \begin{bmatrix} \mathbf{x}^Y \\ \mathbf{x}^\Delta \end{bmatrix} + \mathbf{c}_{ij} \tag{A.13a}$$

$$\tilde{\mathbf{i}}_k = \overbrace{\begin{bmatrix} \mathbf{J}^Y_{ij} & \mathbf{J}^\Delta_{ij} \end{bmatrix} \mathbf{Q}_R}^{\overline{\mathbf{B}}_k} \underbrace{\begin{bmatrix} p_1 \\ q_1 \\ \vdots \\ p_D \\ q_D \end{bmatrix}}_{\mathbf{x}} + \overbrace{\begin{bmatrix} \mathbf{J}^Y_{ij} & \mathbf{J}^\Delta_{ij} \end{bmatrix} \begin{bmatrix} \mathbf{p}^Y_{\text{none}-\text{DER}} \\ \mathbf{q}^Y_{\text{none}-\text{DER}} \\ \mathbf{p}^\Delta_{\text{none}-\text{DER}} \\ \mathbf{q}^\Delta_{\text{none}-\text{DER}} \end{bmatrix} + \mathbf{c}_{ij}}^{\overline{\mathbf{b}}_k} \tag{A.13b}$$

where $\overline{\mathbf{B}}_k \in \mathbb{R}^{3 \times 2D}$. To calculate the current in all branches (similar to how we calculate the voltage), we can stack $\overline{\mathbf{B}}_k$ matrices next to each other to form a new $\mathbf{B} = \begin{bmatrix} \overline{\mathbf{B}}_1^\top & \cdots & \overline{\mathbf{B}}_{r_i}^\top \end{bmatrix}^\top$. We then can re-partition $\mathbf{B}$ per DER device (rather than per branch) as follows: $\mathbf{B} = \begin{bmatrix} \mathbf{B}_1 & \cdots & \mathbf{B}_{|\mathcal{D}|} \end{bmatrix}$, where $\mathbf{B}_i \in \mathbb{R}^{3r_i \times 2}$.

The unit of $\mathbf{B}$ is the same as $\mathbf{J}^Y$ and $\mathbf{J}^\Delta = \frac{A}{W}$.

A.2.3 M & H matrices

We start with Eq. A.5a.

$$\tilde{\mathbf{s}}_0 = \mathbf{G}^Y \mathbf{x}^Y + \mathbf{G}^\Delta \mathbf{x}^\Delta + \mathbf{c} \tag{A.14}$$

We then combine G matrices and collect all constants in $\mathbf{g}$ as follows:

$$\tilde{\mathbf{s}}_0 = \begin{bmatrix} \mathbf{G}^Y & \mathbf{G}^\Delta \end{bmatrix} \begin{bmatrix} \mathbf{x}^Y \\ \mathbf{x}^\Delta \end{bmatrix} + \mathbf{c} \tag{A.15a}$$

$$\tilde{\mathbf{s}}_0 = \overbrace{\begin{bmatrix} \mathbf{G}^Y & \mathbf{G}^\Delta \end{bmatrix} \mathbf{Q}_R}^{\overline{\mathbf{G}}} \overbrace{\begin{bmatrix} p_1 \\ q_1 \\ \vdots \\ p_D \\ q_D \end{bmatrix}}^{\mathbf{x}} + \overbrace{\begin{bmatrix} \mathbf{G}^Y & \mathbf{G}^\Delta \end{bmatrix} \begin{bmatrix} \mathbf{p}_{\text{none-DER}}^Y \\ \mathbf{q}_{\text{none-DER}}^Y \\ \mathbf{p}_{\text{none-DER}}^\Delta \\ \mathbf{q}_{\text{none-DER}}^\Delta \end{bmatrix} + \mathbf{c}}^{\mathbf{g}} \tag{A.15b}$$

$$\tag{A.15c}$$

We then define $\mathbf{M}, \mathbf{H}, \mathbf{m}$ & $\mathbf{h}$ based on $\overline{\mathbf{G}}$ and $\mathbf{g}$ as follows:

$$\mathbf{M} = \text{Re}(\overline{\mathbf{G}}) \tag{A.15d}$$

$$\mathbf{H} = \text{Im}(\overline{\mathbf{G}}) \tag{A.15e}$$

$$\mathbf{m} = \text{Re}(\mathbf{g}) \tag{A.15f}$$

$$\mathbf{h} = \text{Im}(\mathbf{g}) \tag{A.15g}$$

The units of $\mathbf{M}$ & $\mathbf{H}$ are the same of $\overline{\mathbf{G}}$. $\overline{\mathbf{G}}$ has the same unit of $\mathbf{G}^Y$ and $\mathbf{G}^\Delta$, which are "unitless".

With this, we have obtained the new sensitivity matrices that embed the DERs wye and delta configuration within.

111

Appendix B

MATDSS Related Setup and Configurations

B.1 DER Device Parameters & Model within MATDSS

In this section, we briefly summarize the first-order dynamical model used in the simulations in Section B.2, and explain the different parameters used to control the response of DERs.

B.1.1 DER Parameters

Active and reactive powers - x_i & x_i^{set}

Each DER device has an active and reactive power values ($x_i = \begin{bmatrix} p_i & q_i \end{bmatrix}^{\mathsf{T}}$) and set-points ($x_i^{\mathsf{set}} = \begin{bmatrix} p_i^{\mathsf{set}} & q_i^{\mathsf{set}} \end{bmatrix}^{\mathsf{T}}$). The controllers within MATDSS will assign different x_i^{set} values following the outcome of the optimization problem, and the DERs would respond accordingly. The units for active and reactive powers are W and Var, respectively.

Active and reactive power constraints set - $\mathcal{X}_i$

The set $\mathcal{X}_i$ represents the set of possible x_i that can be set for the ith DER. In the implementations we show, we have considered a box constraint $\mathcal{X}_i = [\underline{x}_i, \overline{x}_i]$, and we project the updated x_i^{set} on $\mathcal{X}_i$.

DER Cost function - $f_i(x_i)$

In the simulations, quadratic DERs cost functions were considered. The general form of a quadratic cost function is shown below.

$$f_i(x_i) = x_i^\mathsf{T} C_i'' x_i + x_i^\mathsf{T} C_i', \tag{B.1}$$

where $C_i'' \succ 0$ is a diagonal 2×2 matrix and $C_i' \in \mathbb{R}^2$.

B.1.2 DER 1$^{\text{st}}$ order model

The DERs are modeled within MATDSS as a 1$^{\text{st}}$ order differential equation; where the DERs are assumed to have decoupled active and reactive power controls. The general transfer function of the ith DER is given by

$$T_i(s) = \begin{bmatrix} \frac{1}{\tau_{p,i}s+1} & 0 \\ 0 & \frac{1}{\tau_{q,i}s+1} \end{bmatrix} \tag{B.2}$$

where $\tau_{p,i}$ and $\tau_{q,i}$ are the time-constants that represent how fast the DER responds to input signals (x_i^{set}). In the simulations, we consider the same time constant for active and reactive responses.

For more advanced and realistic models of DERs, one can change the dynamic simulation code (`MATDSS_DERUpdate` function) in MATDSS.

B.2 Simulations

In this section, we describe the configurations used for the simulations presented in Section 3.6. In addition, we discuss the changes made to the original feeder files in OpenDSS for IEEE-123 and IEEE-8500 feeders.

The Tables B.1-B.3 summarize the configurations used for simulation time, DERs and VDER for all simulations.

Table B.1: MATDSS simulation time settings for all test cases and circuits.

Parameter	Value
Duration*	[15s, 60s]
Simulation Time Step**	100ms
Controller Time Step	100ms
Measurement Time Step	100ms
Measurement Delay	0ms
Stabilization Time	0s

* Duration of 15s were used for step-change simulations while 60s were used for ramp-change simulations.
** For smaller circuits 10ms were used to have smoother curves (DERs' dynamics).

Table B.2: DER configurations in MATDSS for all test cases and circuits.

Parameter	Value
τ	0.2s
DER Type	PV
Mode	DSS_load
$\underline{x}_j$	$(-10^6 \text{W}, -10^6 \text{Var})$
$\overline{x}_j$	$(10^6 \text{W}, 10^6 \text{Var})$
(ax, cx)	$(1, 1)$

*** This is not used in dynamic simulation, but is used to define the variable in MATLAB struct.

B.2.1 Low-pass filter and PID Controller setup

As discussed in the Section 3.6.1, we found that the performance is improved by integrating a low-pass filter and proportional-derivative controller with the integral controller. The

114

Table B.3: VDER configurations in MATDSS for all test cases and circuits.

Parameter	Value
τ^{***}	10^{-6}
DER Mode***	DSS_load
$(P(x), Q(x))$	follow equation (3.11)

low-pass filter is applied to the VDERs set-points where it mainly works on smoothing the set-point curve (minimizing oscillations). The proportional controller is used to boost the initial response of DERs when a disturbance occur or a switching in set-point is requested at the interface bus. The derivative controller is used to additionally boost the response initially for the VDERs to get additional response from lower-level DERs that are behind the VDER bus. This process resulted in speeding up the participation of lower-level DERs and achieve more stable response from the feeder when tracking the interface bus set-points. The effective gain for each parameters is the multiplication of the parameter coefficient (κ) with the main controller gain (K). Table B.4 summarizes LPF-PID parameters used for all feeders.

Table B.4: Low-pass filter and PID Control Configurations

| | | Feeder | | |
		5-bus	IEEE-123	IEEE-8500
LPF	T_c	0.9	1	1
	Applied to	VDERs Only	VDERs Only	VDERs Only
P - Controller Configuration	K_p	850	1500	1000
	$\kappa_{p,\lambda}$	0.001	0.001	0.002
	$\kappa_{p,\mu}$	0.001	0.001	0.002
	$\kappa_{p,\eta}$	0.0005	0.001	5e-6
	$\kappa_{p,\psi}$	0.0005	0.001	5e-6
	$\kappa_{p,\gamma}$	1e-12	1e-12	1e-12
	$\kappa_{p,\nu}$	1e-12	1e-12	1e-12
	$\kappa_{p,\zeta}$	1e-7	1e-7	1e-7
	Applied to	DERs & VDERs	DERs & VDERs	DERs & VDERs
D - Controller Configuration	K_d	330	1500	5
	$\kappa_{d,\lambda}$	0.001	0.001	0.001
	$\kappa_{d,\mu}$	0.001	0.001	0.001
	$\kappa_{d,\eta}$	0.001	0.001	1e-6
	$\kappa_{d,\psi}$	0.001	0.001	1e-6
	$\kappa_{d,\gamma}$	1e-12	1e-12	1e-12
	$\kappa_{d,\nu}$	1e-12	1e-12	1e-12
	$\kappa_{d,\zeta}$	1e-7	1e-7	1e-7
	D-Signal	Measurements (Y)	Measurements (Y)	Measurements (Y)
	Applied to	VDERs Only	VDERs Only	VDERs Only

B.2.2 5-Bus Feeder

The 5 bus feeder circuit used is based on the '4Bus-DY-Bal' IEEE test case in OpenDSS. The circuit has been modified by changing the loads powers and adding line 3 (L3) and load 2. The final OpenDSS code used to run 5-bus feeder is shown below (Code 1).

```
clear
! IEEE 5-bus test case D-Y Stepdown Balanced based on IEEE 4-bus test case in OpenDSS (
    D-Y Stepdown Balanced)
new circuit.5busDYBal basekV=12.47 phases=3
~ mvasc3=200000 200000
! **** DEFINE WIRE DATA
new wiredata.conductor Runits=mi Rac=0.306 GMRunits=ft GMRac=0.0244 Radunits=in Diam
    =0.721
new wiredata.neutral Runits=mi Rac=0.592 GMRunits=ft GMRac=0.00814 Radunits=in Diam
    =0.563
! **** DEFINE LINE GEOMETRY; REDUCE OUT THE NEUTRAL
new linegeometry.4wire nconds=4 nphases=3 reduce=yes
~ cond=1 wire=conductor units=ft x=-4 h=28
~ cond=2 wire=conductor units=ft x=-1.5 h=28
~ cond=3 wire=conductor units=ft x=3 h=28
~ cond=4 wire=neutral units=ft x=0  h=24
! **** 12.47 KV LINE
new line.L1 geometry=4wire length=2000 units=ft bus1=sourcebus bus2=n2
! **** 3-PHASE STEP-DOWN TRANSFORMER 12.47/4.16 KV Delta-Ygrd
new transformer.t1 xhl=6
~ wdg=1 bus=n2 conn=delta kV=12.47 kVA=6000 %r=0.5
~ wdg=2 bus=n3 conn=wye kV=4.16 kVA=6000 %r=0.5
! **** 4.16 KV LINE
new line.L2 bus1=n3 bus2=n4 geometry=4wire length=2500 units=ft !NormAmps=990
new line.L3 bus1=n4 bus2=n5 geometry=4wire length=2500 units=ft NormAmps=123

! **** WYE-CONNECTED LOADS
new load.load1 phases=3 bus1=n4 conn=wye kV=4.16 kW=400 pf=0.9 model=1
new load.load2 phases=3 bus1=n5 conn=wye kV=4.16 kW=770 pf=0.9 model=1
~ vminpu=0.75   ! model will remain const p,q down to 0.75 pu voltage
set voltagebases=[12.47, 4.16]
calcvoltagebases   ! **** let DSS compute voltage bases
```

Code 1: 5-bus feeder OpenDSS code.

Controllers configurations

Table B.5: 5-bus feeder Controllers configurations

	1CA	2CAs		2CAs$_{\text{LPF-PID}}$	
# Control Area	1	1	2	1	2
Controller Type*	l2c	l2c	llc	l2c	llc
alpha	0.002	0.002	0.002	0.003	0.003
r_p	1e-4	1e-4	1e-4	1e-4	1e-4
$\bar{r}_d$	1e-3	1e-3	1e-3	1e-3	1e-3
E	1e2	1e2	1e2	1e2	1e2
v_{ul}	1.05	1.05	1.05	1.05	1.05
v_{ll}	0.95	0.95	0.95	0.95	0.95
i_{ul}	Specified in DSS File				
a_ρ^{**}	1	1	1	1	1
a_σ^{**}	1	1	1	1	1
a_λ	5e3	1e3	5e3	1e3	5e3
a_μ	5e3	1e3	5e3	1e3	5e3
a_η	1e3	1e3	1e3	1e3	1e3
a_ψ	1e3	1e3	1e3	1e3	1e3
a_γ	1e12	1e12	1e12	1e12	1e12
a_ν	1e12	1e12	1e12	1e12	1e12
a_ζ	1e7	1e7	1e7	1e7	1e7
c_ρ^{**}	1	1	1	1	1
c_σ^{**}	1	1	1	1	1
c_λ	1e-3	1e-3	1e-3	1e-3	1e-3
c_μ	1e-3	1e-3	1e-3	1e-3	1e-3
c_η	1e-3	1e-3	1e-3	1e-3	1e-3
c_ψ	1e-3	1e-3	1e-3	1e-3	1e-3
c_γ	1e-12	1e-12	1e-12	1e-12	1e-12
c_ν	1e-12	1e-12	1e-12	1e-12	1e-12
c_ζ	1e-7	1e-7	1e-7	1e-7	1e-7

* l2c indicates that the controller is tracking P_0^{set} and llc indicates the controller is tracking P_0^{set} and Q_0^{set}.
** Those parameters are not used in the simulation, but were introduced at early stages of development. They are not considered in the current implementation and their values are not used.

B.2.3 IEEE-123 Feeder

For IEEE-123 feeder, the OpenDSS circuit named `IEEE123Master.dss`' is considered where we modified the following:

- Renamed bus '`150`' to '`sourcebus`' due to how MATDSS is developed.

- Updated all defined '`Lines`' to have '`NormAmps=900`' to avoid any current violation when analyzing power tracking performance.

- The same current limit is added to the 'switches' since they are defined as lines in OpenDSS (to maintain compatibility with MATDSS).

The controllers configurations for the tests shown in Chapter 3 are summarized in Table B.7.

Controllers configurations

Table B.6: IEEE-123 feeder Controllers configurations

	Step Change			Stepped-Ramp Change		
	1CA	6CAs		1CA	6CAs	
# CA	1	1	{2,3,4,5,6}	1	1	{2,3,4,5,6}
Controller Type*	l2c	l2c	llc	l2c	l2c	llc
α	0.001	9.6e-4	4.32e-4	0.001	9.6e-4	4.32e-4
r_p	1e-4	1e-4	1e-4	1e-4	1e-4	1e-4
$\overline{r}_d$	1e-3	1e-3	1e-3	1e-3	1e-3	1e-3
E	1e2	1e2	1e2	1e2	1e2	1e2
v_{ul}	1.05	1.05	1.05	1.05	1.05	1.05
v_{ll}	0.95	0.95	0.95	0.95	0.95	0.95
i_{ul}	Specified in DSS File					
a_ρ^{**}	1	1	1	1	1	1
a_σ^{**}	1	1	1	1	1	1
a_λ	2e3	5e3	1e3	2e3	5e3	1e3
a_μ	2e3	5e3	1e3	2e3	5e3	1e3
a_η	1e3	1e3	1e3	1e3	1e3	1e3
a_ψ	1e3	1e3	1e3	1e3	1e3	1e3
a_γ	1e12	1e12	1e12	1e12	1e12	1e12
a_ν	1e12	1e12	1e12	1e12	1e12	1e12
a_ζ	1e8	1e8	1e8	1e8	1e8	1e8
c_ρ^{**}	1	1	1	1	1	1
c_σ^{**}	1	1	1	1	1	1
c_λ	1e-3	1e-3	1e-3	1e-3	1e-3	1e-3
c_μ	1e-3	1e-3	1e-3	1e-3	1e-3	1e-3
c_η	1e-3	1e-3	1e-3	1e-3	1e-3	1e-3
c_ψ	1e-3	1e-3	1e-3	1e-3	1e-3	1e-3
c_γ	1e-12	1e-12	1e-12	1e-12	1e-12	1e-12
c_ν	1e-12	1e-12	1e-12	1e-12	1e-12	1e-12
c_ζ	1e-8	1e-8	1e-8	1e-8	1e-8	1e-8

* l2c indicates that the controller is tracking P_0^{set} and llc indicates the controller is tracking P_0^{set} and Q_0^{set}.
** Those parameters are not used in the simulation, but were introduced at early stages of development. They are not considered in the current implementation and their values are not used.

B.2.4   IEEE-8500 Feeder

In this simulation, we consider the IEEE-8500 Feeder defined in OpenDSS '`Master.dss`' in the folder '`8500-Node`'. In our implementation, we have disabled the following internal switches:

- '`Line.WD701_48332_sw`'

- '`Line.V7995_48332_sw`'

- '`Line.WG127_48332_sw`'

- '`Line.WF856_48332_sw`'

- '`Line.WF586_48332_sw`'

In addition, we have partitioned the feeder into 49 control areas. To partition the feeder into these areas, we have considered all main and load buses ('`m`' and '`l`'). The control areas were defined to obtain a nested control areas that are interfaced through these buses.

Table B.7: IEEE-8500 feeder Controllers configurations

| | Stepped-Ramp Change | | |
| | 1CA | 49CAs | |
# CA	1	1	{2:49}
Controller Type*	l2c	l2c	llc
α	0.0015	4e-4	2e-4
r_p	1e-4	1e-4	1e-4
$\bar{r}_d$	1e-3	1e-3	1e-3
E	1e2	1e2	1e2
v_{ul}	1.05	1.05	1.05
v_{ll}	0.95	0.95	0.95
i_{ul}	Specified in DSS File		
a_ρ^{**}	1	1	1
a_σ^{**}	1	1	1
a_λ	20	5e3	1e3
a_μ	20	5e3	1e3
a_η	20	5e3	1e3
a_ψ	20	5e3	1e3
a_γ^{***}	0	0	0
a_ν^{***}	0	0	0
a_ζ^{***}	0	0	0
c_ρ^{**}	1	1	1
c_σ^{**}	1	1	1
c_λ	1e-3	1e-3	1e-3
c_μ	1e-3	1e-3	1e-3
c_η	1e-3	1e-3	1e-3
c_ψ	1e-3	1e-3	1e-3
c_γ	1e-12	1e-12	1e-12
c_ν	1e-12	1e-12	1e-12
c_ζ	1e-8	1e-8	1e-8

* l2c indicates that the controller is tracking P_0^{set} and llc indicates the controller is tracking P_0^{set} and Q_0^{set}.
** Those parameters are not used in the simulation, but were introduced at early stages of development. They are not considered in the current implementation and their values are not used.
*** To focus on power tracking performance, voltage and current control is disabled.

Appendix C

Transmission and Distribution Coordination Simulations Configurations and Setup

In Chapter 4, the derived linear model of the DN controller models the whole feeder as a single CA. Below, we attempt to modify the centralized model parameters, to incorporate the impact of multi-CAs on DERs set-points. We introduce the concept of effective sensitivities to map the sensitivities from lower level areas to feeder head power measurements.

C.1   Hierarchical DN Linear Model

The linear model in (4.20) describes the response of a single DN when managed by a central controller overseeing all DERs. Here, we extend this concept to incorporate the hierarchical structure within the central controller framework, leveraging the concepts of VDERs and effective sensitivities. Constructing the matrix $\mathbf{K}$ in hierarchical structures can be challenging without sharing a circuit model between the control areas. We demonstrate a method to approximate the centralized sensitivity matrix $\mathbf{K}$ using the VDERs and CAs sensitivities.

Consider an area i within the DN structure, where the jth DER is a VDER associated with area ℓ (i.e., area i is the parent of area ℓ), as illustrated in Figure C.1. The sensitivity matrix $\mathbf{K}_{ij}$ maps changes in VDER powers to the measurements within area i. Recall that VDER powers reflect changes in the DERs of the child area ℓ and its sub-areas.
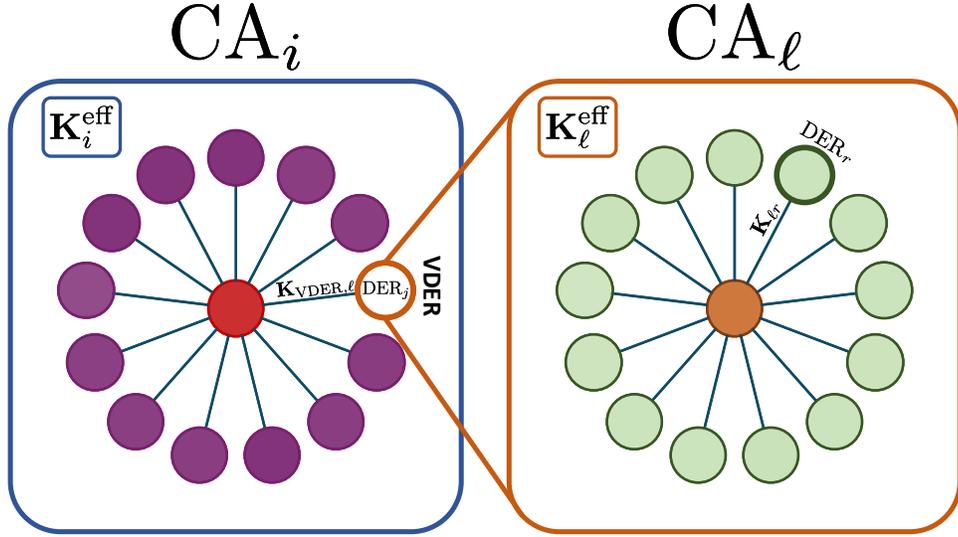
Figure C.1: Block diagram illustrating the relationship between parent area i and child area ℓ interfaced through a VDER.

Let $\mathbf{K}_{\text{VDER},\ell} = \mathbf{K}_{ij}$ denote the sensitivities of the VDER corresponding to area ℓ, and let $\mathbf{K}_\ell$ denote the local sensitivities of DERs and VDERs within area ℓ. Note that $\mathbf{K}_{\text{VDER},\ell}$ maps the sensitivities to the interface bus measurements of area i, while $\mathbf{K}_\ell$ maps the sensitivities to the interface bus measurements of area ℓ.

For a three phase VDER, we have $\mathbf{K}_{\text{VDER},\ell} \in \mathbb{R}^{3 \times 2}$, and let $\overline{\mathbf{K}}_{\text{VDER},\ell} \in \mathbb{R}^{1 \times 2}$ denotes its column sum. Since VDERs power is summed over all the phases, we can obtain the effective sensitivities of the rth DER in area ℓ to the measurements in area i as

$$\mathbf{K}_{\ell r}^{\text{eff}} = \mathbf{K}_{\ell r} \, \overline{\mathbf{K}}_{\text{VDER},\ell}^\top. \tag{C.1}$$

Then for the ℓth area-wide sensitivities, we construct $\overline{\mathbf{K}}_\ell^{\text{eff}}$

$$\overline{\mathbf{K}}_\ell^{\text{eff}} = \begin{bmatrix} \mathbf{K}_{\ell 1}^{\text{eff}} & \cdots & \mathbf{K}_{\ell|D_\ell|}^{\text{eff}} \end{bmatrix} = \mathbf{K}_\ell \begin{bmatrix} \overline{\mathbf{K}}_{\text{VDER},\ell}^\top \\ \vdots \\ \overline{\mathbf{K}}_{\text{VDER},\ell}^\top \end{bmatrix}. \tag{C.2}$$

Note that for nested areas, VDER sensitivities need to be adjusted for child areas before carrying out the calculations. In other words, one should start by scaling the effective sensitivities from parent areas to child areas. This ensures that effective sensitivities are used for child VDERs in (C.2).

124

Once all effective sensitivities are obtained, we construct the matrix $\mathbf{K}_\ell^{\text{eff}}$ by removing teh columns corresponding to the VDERs from $\overline{\mathbf{K}}_\ell^{\text{eff}}$, and then concatenate them to form the full DN sensitivity matrix $\mathbf{K}^{\text{eff}}$ as

$$\mathbf{K}^{\text{eff}} = \begin{bmatrix} \mathbf{K}_1^{\text{eff}} & \cdots & \mathbf{K}_{N_{\text{CA}}}^{\text{eff}} \end{bmatrix}. \tag{C.3}$$

The matrix $\mathbf{K}^{\text{eff}}$ approximates the actual sensitivities of all DERs to the power measurements at the DN interface bus.

C.2 Simulations

In this section, we report the modifications to the DN controllers configurations in Appendix B.2. For the IEEE-123 feeders in TD-integration simulations, the Configurations Config. 1 - Config. 4 has the following modified parameters:

Table C.1: IEEE-123 feeder Controllers configurations for TD integration simulations

	Config. 1		Config. 2		Config. 3		Config. 4	
# CA	1	{2,3,4,5,6}	1	{2,3,4,5,6}	1	{2,3,4,5,6}	1	{2,3,4,5,6}
α	0.001	5e-4	2.4e-4	1.2e-4	2.4e-4	1.2e-4	1.2e-4	1.2e-4
a_λ	5e3	1e3	5e3	3e3	5e3	5e3	3e3	1e3
a_μ	5e3	1e3	5e3	3e3	5e3	5e3	3e3	1e3